2-P(MIX)

NASA CR-134653

IMPROVED COATINGS FOR SILICA FIBER BASED CERAMIC REUSABLE SURFACE INSULATION (CRSI)

by Thomas J. Ormiston

GENERAL ELECTRIC COMPANY
RE-ENTRY AND ENVIRONMENTAL SYSTEMS DIVISION

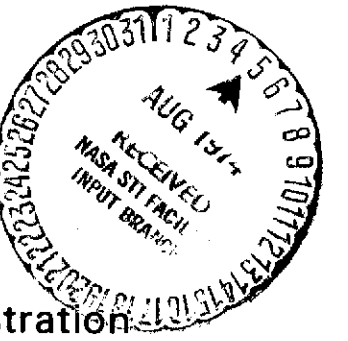

Prepared for

National Aeronautics and Space Administration
Lewis Research Center
Contract NAS3-17793
J.P. Merutka, Project Manager

94

94

1. Report No.	2. Government Accession No.	3. Recipient's Catalog No.

4. Title and Subtitle	5. Report Date
Improved Coatings for Silica Fiber Based Ceramic Reusable Surface Insulation	April 1974
	6. Performing Organization Code
7. Author(s)	8. Performing Organization Report No.
Thomas J. Ormiston	
9. Performing Organization Name and Address	10. Work Unit No.
General Electric Company - RESD P.O. Box 7722 Philadelphia, Pa. 19101	11. Contract or Grant No. NAS 3-17793
12. Sponsoring Agency Name and Address	13. Type of Report and Period Covered Contractor Report
National Aeronautics and Space Administration Washington, D.C. 20546	14. Sponsoring Agency Code

15. Supplementary Notes

Project Manager - John P. Merutka, Surface Protection Group, NASA Lewis Research Center, Cleveland, Ohio

16. Abstract

A series of coatings was developed for the Space Shuttle type silica fiber insulation system and characterized for optical and physical properties. Re-entry simulation tests were run using a radiant panel and also using a hypersonic plasma arc. The coatings produced had improved physical and optical properties as well as greater reuse capability over the GE version of the JSC-0042 coating.

17. Key Words (Suggested by Author(s))	18. Distribution Statement
Reusable Surface Insulation Silica Fibers Ceramic Coatings	

19. Security Classif. (of this report)	20. Security Classif. (of this page)	21. No. of Pages	22. Price*
Unclassified	Unclassified	100	$3.75

* For sale by the National Technical Information Service, Springfield, Virginia 22151

FOREWORD

This report was prepared by the Re-entry and Environmental Systems Division (RESD) of the General Electric Company, Philadelphia, Pennsylvania, under NASA Contract NAS3-17793. The work was administered under the direction of the Lewis Research Center, Cleveland, Ohio, with Mr. J. P. Merutka acting as Contract Manager.

This report covers the work conducted from July 1, 1973, through December 31, 1973, at the RESD's Advanced Materials Development Laboratory. Mr. T. J. Ormiston acted as Project Manager and edited the final report.

Special thanks is given to Dr. D. Deadmore of NASA-Lewis for many helpful suggestions and data which added significantly to the program.

TABLE OF CONTENTS

LIST OF ILLUSTRATIONS

LIST OF ILLUSTRATIONS (Cont'd)

LIST OF ILLUSTRATIONS (Cont'd)

LIST OF TABLES

SECTION 1

SUMMARY AND INTRODUCTION

1.1 SUMMARY

The purpose of this program was to advance the state-of-the-art on refractory coatings compatible with fused silica fiber-based reusable surface insulation. The specific objectives were to develop a coating with the following optical properties: an emittance of 0.8 or more at 1260° C, a solar absorption of 0.4 or less and a ratio of solar absorptance to low temperature (40° C) emittance of 0.5 or less. Additional objectives were a coating weight of .024 g/cm^2 or less with an impact strength of .18 Kg-M or more. The coating was to be able to withstand 100 simulated re-entry cycles in a plasma arc facility without cracking or loss of waterproofness.

A series of ceramic coatings were developed based on either SiO_2-B_2O_3-BPO_4 system or a combination of devitrification resistance commercial glasses. Pigments were developed and incorporated into the coatings to optimize the solar reflectance for orbital conditions and the high temperature emittance for re-entry conditions.

The identities, chemical composition and pertinent properties of these coatings is summarized in Table I. This data is compared to the properties of the GE produced JSC-0042 coating presently considered baseline. These coatings were subjected to a series of thermal aging, cyclic heating, and high temperature plasma cycling to evaluate their stability and potential service life. The coatings were characterized before and after re-entry cycling and their properties evaluated.

Two coatings from this study showed a number of improvements over the present baseline coating. These coatings, DD-3 and PB-1, both survived 100 re-entry cycles in a plasma arc simulator at 1100° C. These coatings had better than twice the impact strength and about twice the tensile strength of present systems. The PB-1 coating had improved optical properties to meet both the orbital and re-entry conditions. The high temperature emittance of PB-1 was .68 while its solar a solar absorptance was only .38 with a room temperature absorptance to emittance ratio of 0.540.

This study has identified methods for controlling the devitrification of fused silica. A series of highly devitrification resistant coatings has been successfully applied. Pigments which can successfully control the optical properties and cause little or no degradation of properties have been identified. Re-entry simulation tests have shown measurable improvements over baseline coatings.

TABLE I. COATING SUMMARY

	Program Objective	JSC 0042 Baseline Coating	31D	31D HE	31D LA	DD-3	PB-1
Composition		19 parts Vycor* 1 part Pyrex* 1 part SiC	86 parts SiO_2 9 parts BPO_4 5 parts B_2O_3	86 parts SiO_2 9 parts BPO_4 5 parts B_2O_3 10 parts CeO_2 1 part SiC	86 parts SiO_2 9 parts BPO_4 5 parts B_2O_3 10 parts HfB_2	19 parts Vycor 1 part Pyrex 1 part HfB_2	95 parts Vycor 5 parts Pyrex 5 parts CeO_2 2 parts HfB_2
Coating Weight	24 mg/cm (.05 lbs/ ft^2)	39-59 (.08-.12)	29 (.06)	29 (.06)	29 (.06)	44 (.09)	44 (.09)
Emittance	.8 or more	.73	.48	.69	.57	.69	.68
Solar Absorptance	.4 or less	.74	.18	.49	.34	.73	.38
Number of Re-entry Cycles in G.E. Re-entry Simulator	Not Defined	5	20-40	—	—	20-40	40-60
Number of Re-entry Cycles in Plasma Arc	100	Not Tested	—	—	29	100	100

1.2 INTRODUCTION

The space shuttle heat shield will consist of a matrix of lightweight ceramic tiles made of rigidized silica fibers. A coating is required on these tiles that is waterproof and capable of withstanding the thermal and acoustical conditions found during a vehicle re-entry. In addition to merely surviving the re-entry environment, this coating can play an active role in cooling the vehicle. A coating with a high emittance could make a difference of several hundred degrees during a re-entry where the heat flux caused by aerodynamic heating exceeds 25 BTU's/ft^2-sec. An added benefit sought for the coating would be a high reflectance of the solar heat load encountered while in orbit. If the coating reflected most of the sun's heat and had a high infrared emittance to re-radiate most of the heat that it did absorb, the temperature of the vehicle would be substantially cooler at the beginning of the re-entry.

Specific objectives of this program were to develop 5 to 10 coatings for rigidized silica which would have increased strength and half the weight of the present baseline coating. These coatings were to have a high temperature emittance of 0.8 or higher and a solar absorptance/low temperature emittance of 0.5 or less. The coatings were to be stable in a re-entry environment of 1260° C and capable of withstanding one overshoot conditions of 1480° C. The coatings were required to be thermally aged, tested in a plasma arc to prove 100 re-entry cycle capability. This contract covered a 6 month effort during which all development and test work was completed.

The baseline material which much of the data reported refers to is the Johnson Space Center-0042 coating. This material is based on a mixture of devitrification resistant commercial glasses which form a glaze over the tile. An addition of 5% silicon carbide is used in the JSC-0042 coating to give it a favorable high temperature emittance with limited improvement in its solar reflectance properties. Tests at GE have shown that the JSC-0042 coating, when produced by GE to the JSC specification, tends to crack after a few cycles to 1260° C in the GE re-entry simulator. The cracking is a result of the amorphous glaze crystallizing into a beta cristobalite structure which undergoes a catastrophic inversion at about 240° C. Here its crystal structure goes through a discontinuous change accompanied by a 20% change in volume. This inversion begins to crack the coatings whenever the volume percentage of cristobalite in the coating exceeds about 20%.

SECTION 2

COATING DEVELOPMENT

2.1 COATING DEVELOPMENT LOGIC

The logic chart shown in Figure 1 shows the straightforward planning which was used for organizing and scheduling this program to develop the coatings. Although this chart is sufficient for costing and scheduling, it does not provide a rational flow diagram for the actual materials development. A more detailed logic diagram, shown in Figure 2 takes into account the fact that several iterations are necessary to perfect a coating and its application technique. This iteration procedure, or learning cycle accounts for the closed loops found in this second chart.

The basic approach to the problem was as follows:

1. A series of pigments was developed which had a high emittance at 1100°C and a low solar absorbence to emittance ratio at 40°C.

2. A series of coatings were developed based on the SiO_2-B_2O_3-P_2O_5 ternary system having very high resistance to devitrification.

3. The pigments were combined with the coatings to marry these favorable properties into a series of candidate coatings.

4. These candidate coatings were then characterized before and after thermal aging and re-entry simulation in a vacuum simulator.

5. A second series of coatings was then derived and subjected to characterization studies before and after re-entry simulation in a plasma arc.

2.2 COATING DEVELOPMENT STAGES

The initial coating development program consisted of four stages. The first was a detailed study of the SiO_2-B_2O_3-P_2O_5 phase diagram to determine what materials in this system were the most resistant to devitrification. Then, using this information a coating was designed which consisted of the desired stoichiometry made from those precursor materials which yielded the highest devitrification resistance. Meanwhile, several pigments were evaluated which were expected to have a high emittance at 1100°C and a low solar absorbence/low temperature emittance ratio. Finally the

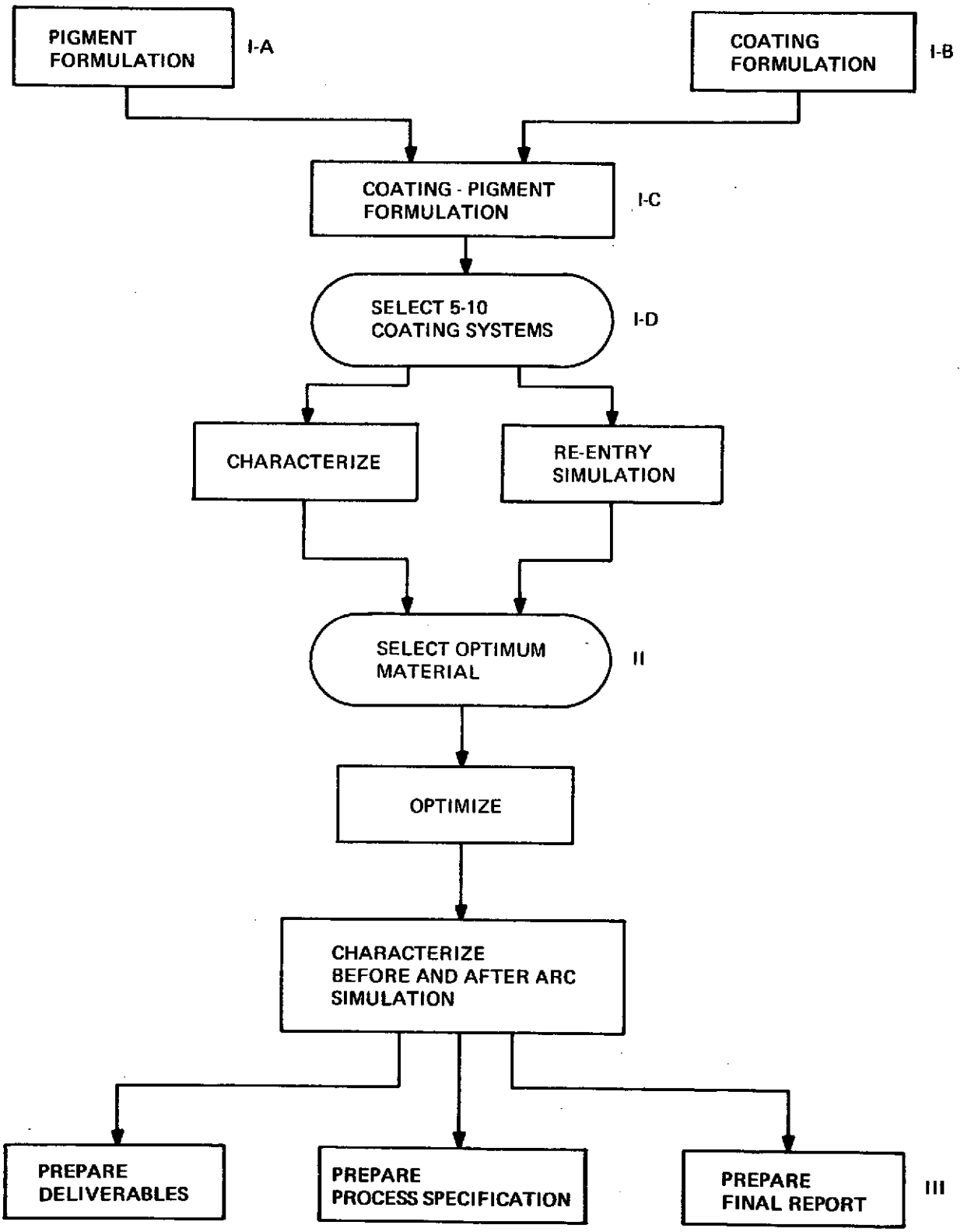

Figure 1. Program Logic

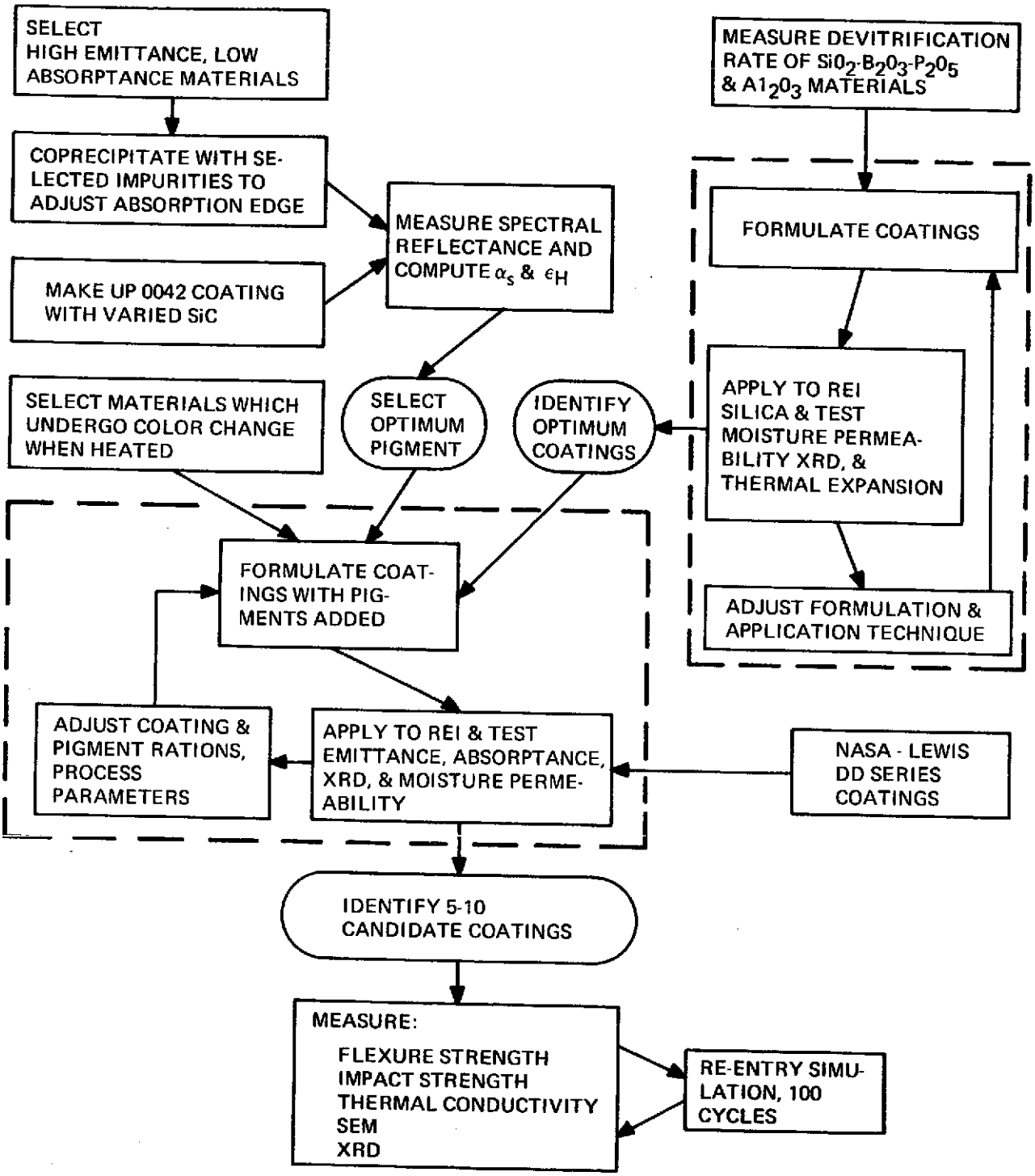

Figure 2. Coating Development Logic Chart

pigments were added to the coatings using a variety of techniques, to combine the desired optical properties with the high thermal stability of the coatings.

2.3 PHASE STABILITY STUDY OF THE SYSTEM SiO_2-B_2O_3-P_2O_5

High silica content specimens with varying amounts of boron trioxide and phosphorous pentoxide were subjected to long term thermal exposure cycles at 1260°C and 1370°C to determine their phase stability. Small amounts of alumina were added to some specimens to evaluate the inevitable contamination of an eventual coating mix from the ball milling operation.

The specimens were made from two initial sources of silica. The first was Corning's Code 7940* fused silica - a high purity synthetic silica formed by reacting high purity precursor chemicals in a vapor phase and depositing on a heated boule. The second source was GE's SR350 silicone resin, an extremely pure methyl silanol monomer which, when cured and pyrolyzed, yields a high purity amorphous silica. All specimens using Corning 7940 glass as the fused silica precursor were made by simple mixtures of the oxides. Specimens using SR-350 silicone resin as the silica precursor were made in a methanol solution using $AlCl_3$, B_2O_3, and H_3PO_4 as the soluble precursor form of the oxides where required. All mixtures (organic and inorganic) were fired to 540°C prior to crystallization rate testing.

The specimen composites and crystalline content after exposure are shown in Table II. (Following Figure 1-9.)

Most of the specimens were made using Boron Phosphate instead of the free oxides since early crystallization data from specimens 8, 9, 15, and 22 indicated that the presence of free P_2O_5 resulted in rapid devitrification of the mixtures.

Using a standard criteria of 20% cristobalite as being an acceptable upper limit the approximate stable area of the phase diagram is indicated in Figure 3 by the dashed lines.

The data given in Table 1 provides some interesting insight into the effects of various oxides on the devitrification rate of fused silica when plotted in the following figures. Figure 4 shows the devitrification rate of two forms of high purity silica; Corning 7940 glass and the silica formed from the decomposition of SR-350. Chemical analysis of these two forms of silica is given in Table II indicating the relative purity of the two forms. From Figure 4 it is obvious that increased purity does significantly decrease the initial devitrification rate of silica. It is also apparent, however, that once the extremely high purity material begins to crystallize it takes place very rapidly.

*Corning Glass Works, Corning, N.Y.

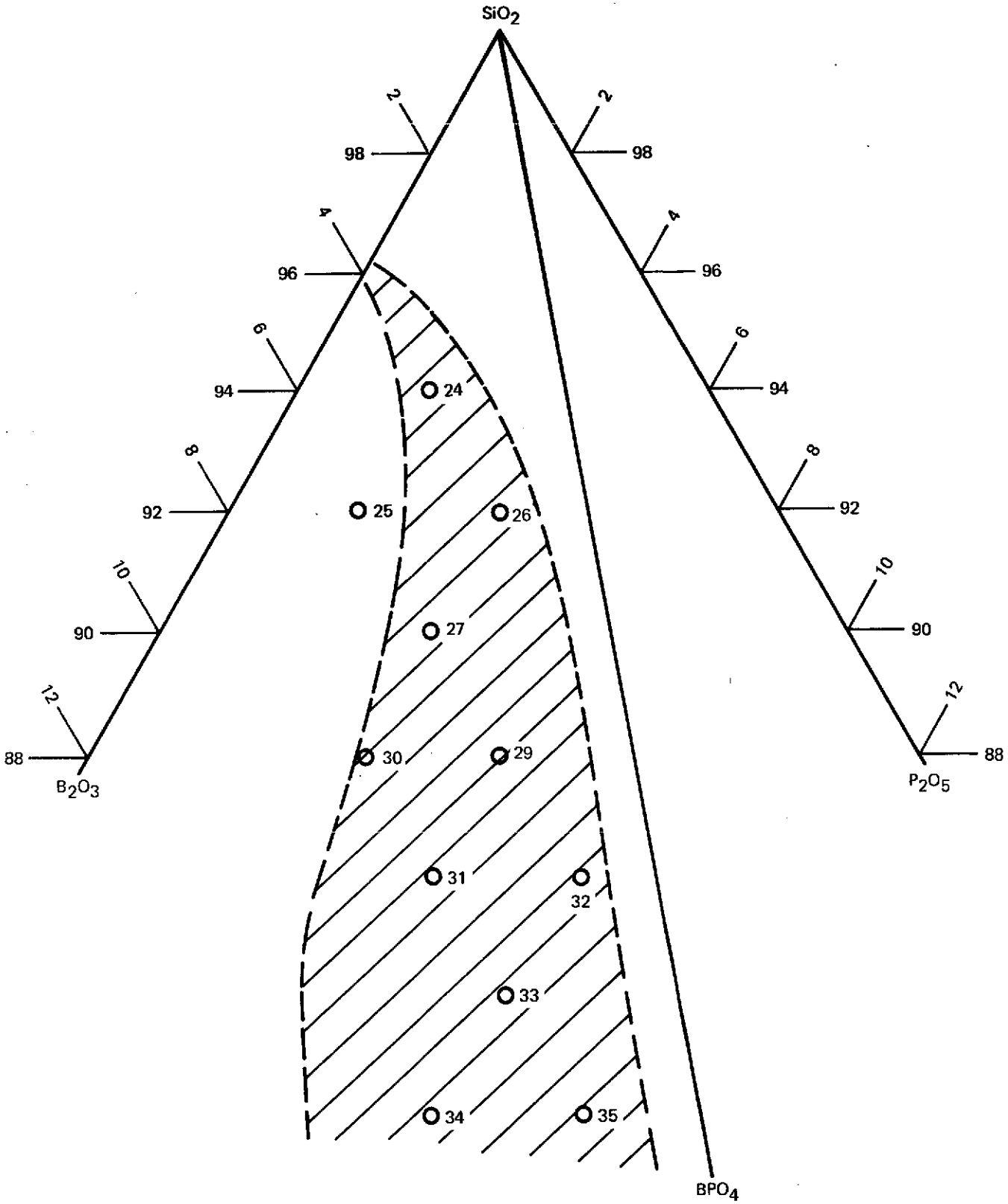

Figure 3. Shaded Area Shows Compounds with High Resistance to Devitrification

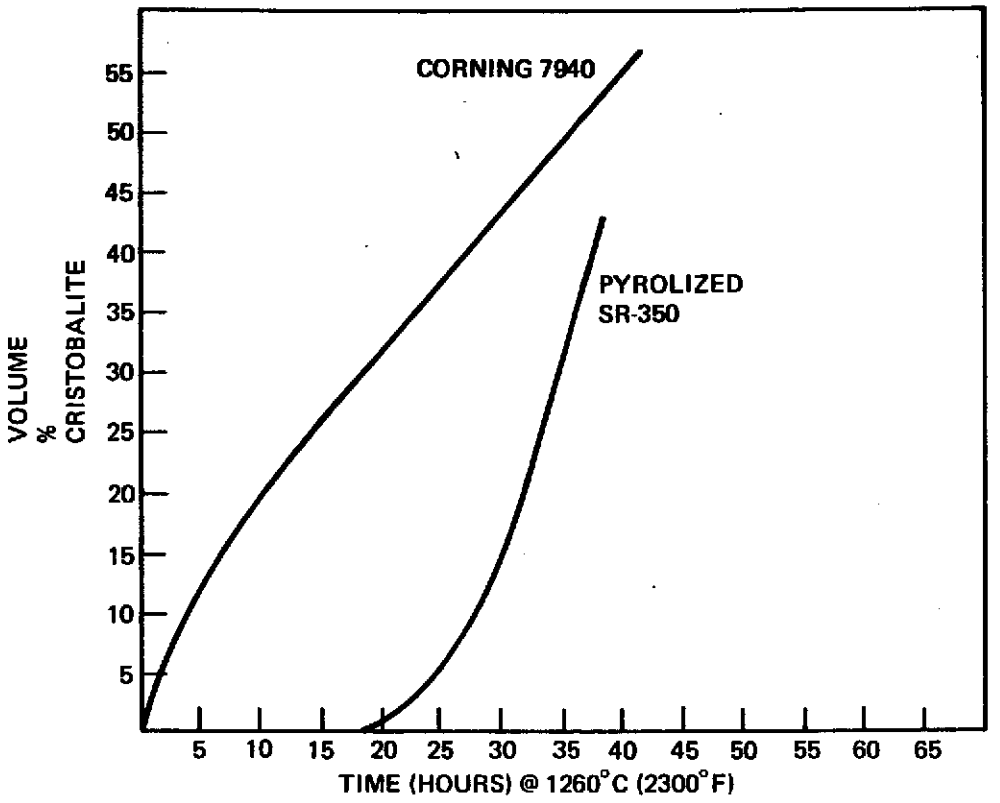

Figure 4. Devitrification of 7940 Fused Silica and Pyrolized SR-350 Resin

The effect of boron trioxide addition on the devitrification rate of 7940 fused silica and Vycor is shown in Figure 5. Increasing the concentration of B_2O_5 up to 4 mole % (4.6 wt.%) decreases the rate significantly, however, a further increase appears to create a negative effect.

Figure 6 shows the effect of BPO_4 addition on the devitrification of 7940 glass. Concentrations up to 4 to 6 mole % appear to initially increase the rates, while concentrations above 8 mole % drastically reduce the rate. Specimens at 12 mole % BPO_4 plus 2 mole % B_2O_3 are very highly resistant to devitrification forming very stable glasses even when exposed to 1370°C (see Table I).

Figure 7 shows the effect of small amounts of Al_2O_3 on the devitrification rate of BPO_4/7940 Silica mixtures. Comparison to Figure 6 indicates that small amounts of Al_2O_3 which might be added to a coating system during ball milling operations does not significantly affect the crystallization rate of the BPO_4/silica mixture.

Figure 8 also shows this by indicating the effect of alumina on the devitrification rates of 7940 and SR-350 type silicas.

TABLE II. PHASE STABILITY OF SiO_2, B_2O_3, P_2O_5, AND Al_2O_3 MIXTURES, % CRISTOBALITE

Specimen	No.	1100°C	1260°C				1370°C		
		18 hrs.	4 hrs.	18 hrs.	40 hrs.	66 hrs.	15 min.	4 hrs.	16 hrs.
100% 7940	1	0	10%	30%	56%	35%	2%	39%	
100% SR-350, Pryolized	2	0	0	Tr	50%	34%	Tr	39%	
97.7% 7940, 2.3% B_2O_3	3		Tr	Tr			Tr		
95.4% 7940, 4.6% B_2O_3	4	0	0	Tr	9%	11%	Tr	0	5%
100% Vycor Glass	5	Tr	5%	14%	15%	24%	Tr	4%	
95.4% SR-350, 4.6% B_2O_3	6	0	0	2%	45%	39%	Tr	39%	
94.3% 7940, 5.7 B_2O_3	7		0	16%			Tr		
93.2% 7940, 6.8% P_2O_5	8		33%	32%			Tr		
93.2% SR-350, 6.8% P_2O_5	9		30%	31%			0		
96.4% 7940, 3.5% BPO_4	10		40%	40%			5%		
93.2% 7940, 6.8% BPO_4	11		28%	28%			Tr		
86.7% 7940, 13.3% BPO_4	12		8%	11%			Tr		
80.6% 7940, 19.4% BPO_4	13	0	0	3%	2%	Tr	Tr	Tr	3%
78.6% 7940, 2.1% B_2O_3, 19.3% BPO_4	14	Tr	0	Tr	Tr	Tr	Tr	0	2%
78.6% SR-350, 2.1% B_2O_3, 19.3% BPO_4	15		17%	45%			Tr		
99.8% 7940, 0.2% Al_2O_3	16		5%	44%			Tr		
99.2% 7940, 0.8% Al_2O_3	17		17%	35%			Tr		

TABLE II. PHASE STABILITY OF SiO_2, B_2O_3, P_2O_5, AND Al_2O_3 MIXTURES, % CRISTOBALITE (Continued)

Specimen	No.	1100°C	1260°C				1370°C		
		18 hrs.	4 hrs.	18 hrs.	40 hrs.	66 hrs.	15 min.	4 hrs.	16 hrs.
98.3% 7940, 1.7% Al_2O_3	18		17%	35%			0		
98.3% SR-350, 1.7% Al_2O_3	19		0	4%	41%		Tr		
89.1% 7940, 0.8% Al_2O_3, 10.1% BPO_4	20		12%	20%			Tr		
79.3% 7940, 0.5% Al_2O_3, 19.2% BPO_4	21	Tr	Tr	2%	4%	4%	0	5%	Tr
78.6% SR-350, 2.1% B_2O_3, 19.3% BPO_4	22				5%				
79.3% SR-350, 0.5% Al_2O3, 19.2% BPO_4	23		30%	30%			6%		
94% 7940, 3% B_2O_3, 3% BPO_4	24				24%				
92% 7940, 5% B_2O_3, 3% BPO_4	25				23%				
92% 7940, 2% B_2O_3, 6% BPO_4	26				18%				21%
90% 7940, 4% B_2O_3, 6% BPO_4	27				18%				11%
90% 7940, 1.1% B_2O_3, 8.9% BPO_4	28				15%				12%
88% 7940, 3.1% B_2O_3, 8.9% BPO_4	29				10%				11%
88% 7940, 6% B_2O_3, 6% BPO_4	30				12%				10%
86% 7940, 5.1% B_2O_3, 8.9% BPO_4	31				6%				6%
86% 7940, 2.1% B_2O_3, 11.8% BPO_4	32				13%				9%
84% 7940, 4.1% B_2O_3, 11.9% BPO_4	33				5%				6%
82% 7940, 6.1% B_2O_3, 11.9% BPO_4	34				3%				3%
82% 7940, 3.1% B_2O_3, 14.9% BPO_4	35				Tr				3%

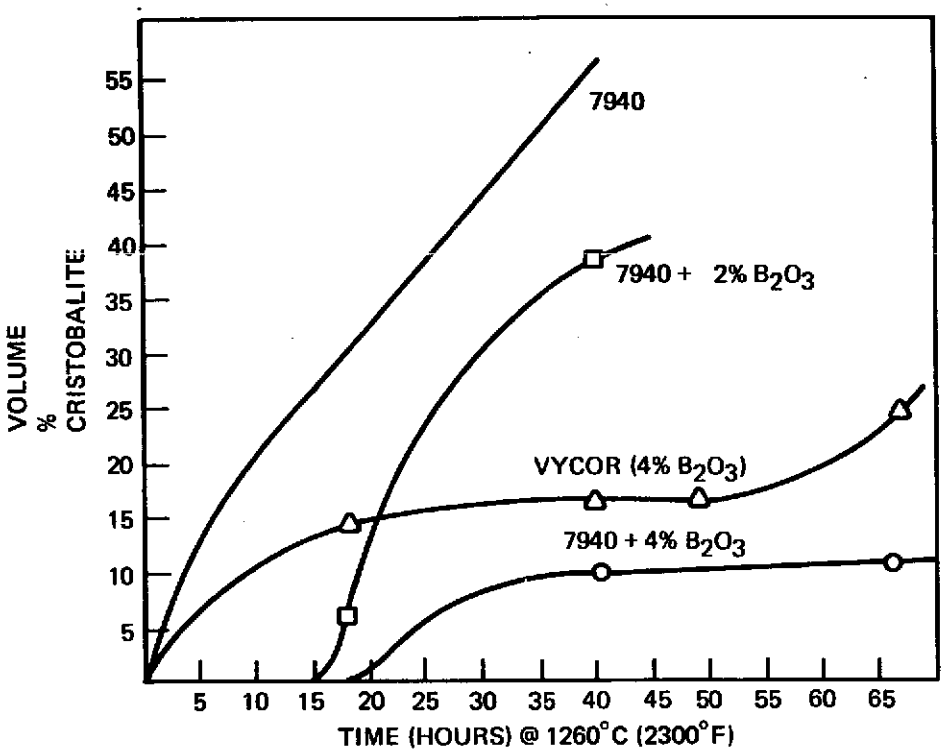

Figure 5. The Effect of B_2O_3 on the Devitrification of 7940 Fused Silica and Vycor ®

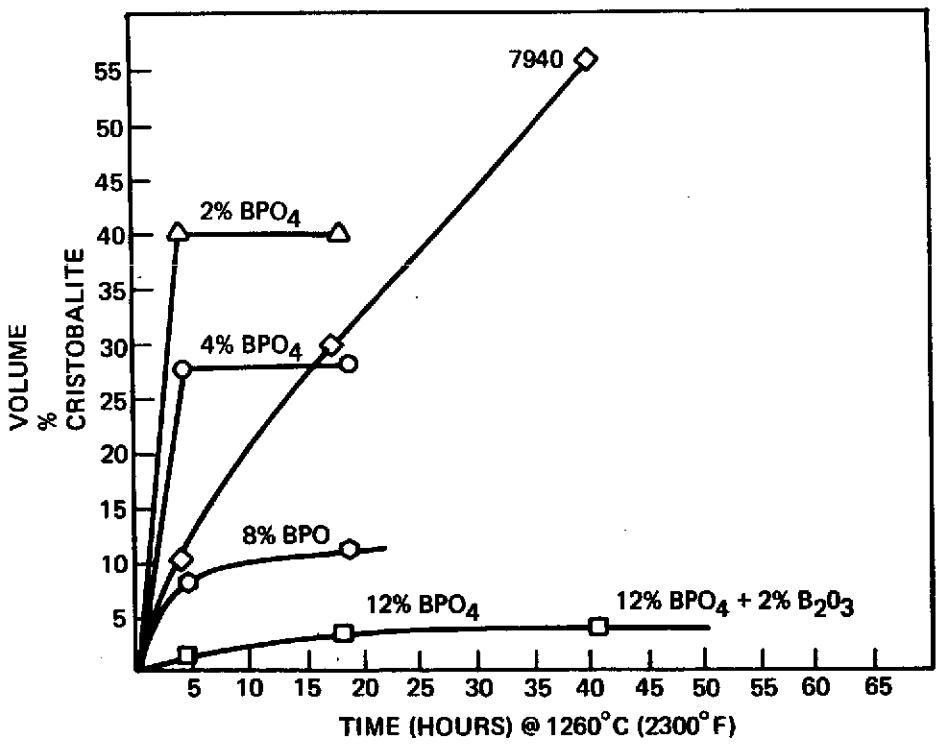

Figure 6. The Effect of BPO_4 on the Devitrification of 7940 Fused Silica

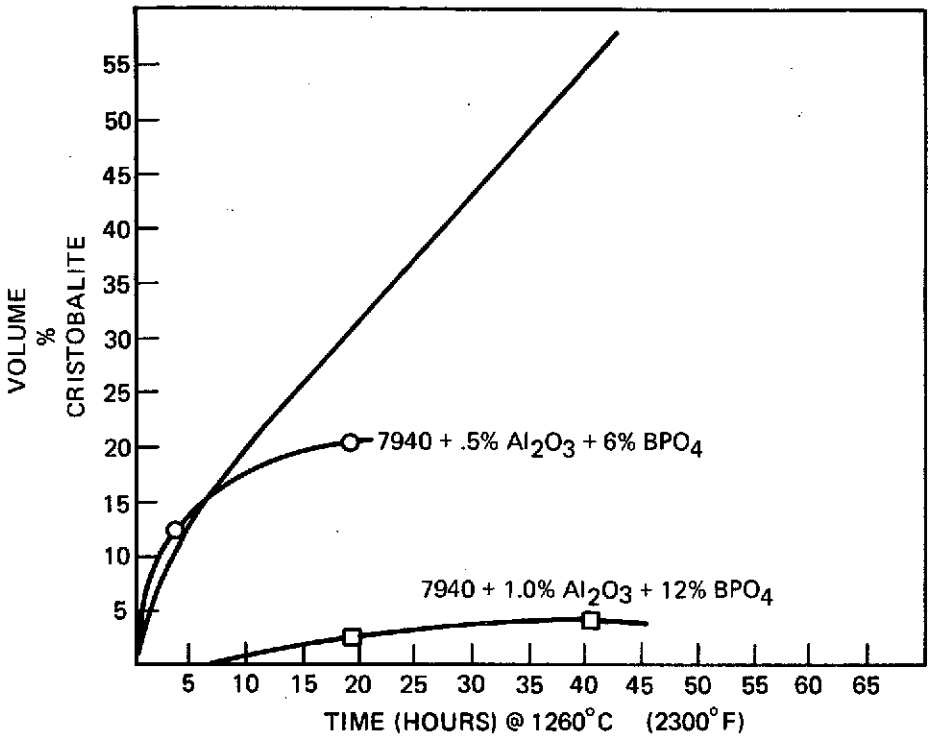

Figure 7. The Effect of Al_2O_3 and BPO_4 on the Devitrification Rate of 7940 Fused Silica

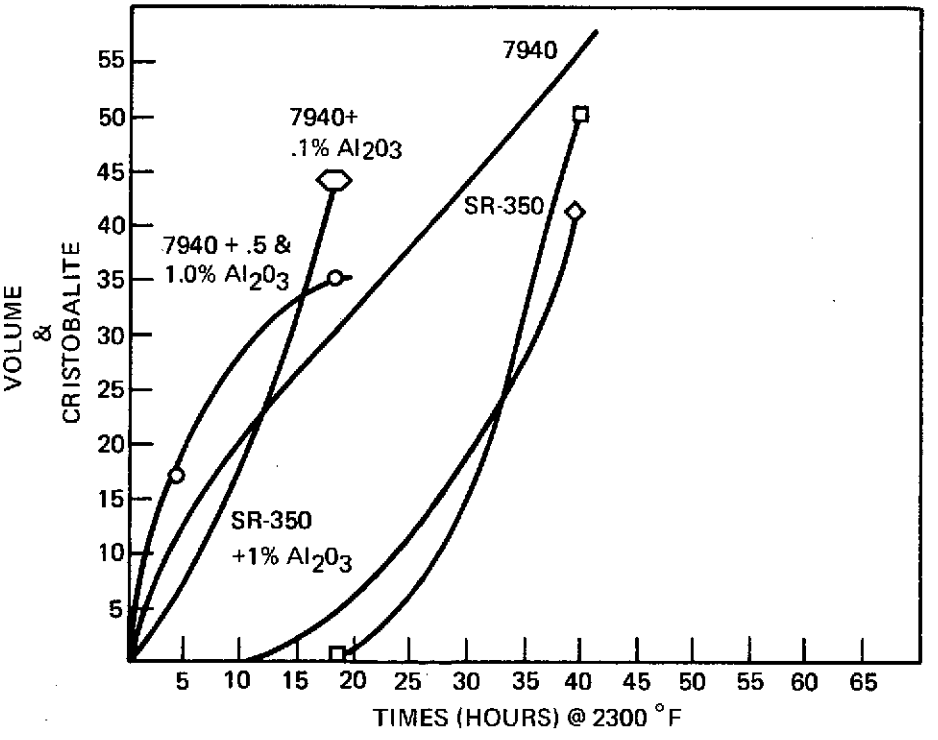

Figure 8. Effect of Al_2O_3 on the Devitrification Rate of Two Forms of Silica (7940 and SR-350)

Figure 9 shows the effect of various oxides on the devitrification rate of SR-350 produced silica. All specimens except the one labeled by the asterisk were made from solution. The asterisked specimen was made by addition of BPO_4 and B_2O_3 to pyrolyzed SR-350 powder.

It can be seen that preparing the specimens from solution in most cases did not result in lower crystallization rates compared to the SR-350 silica alone. In all cases where P_2O_5 were added (by the addition of reagent grade orthophosphoric acid) the specimens crystallized much faster than the silica alone. In the single cases where the BPO_4 and B_2O_3 were added as powders the composition thus formed was very resistant to crystallization. It was, however, slightly less resistant than the same composition fabricated using 7940 glass as the silica source (Figure 6).

Since the specimens with the highest resistance to devitrification appeared less refractory than the materials which devitrified more readily, it appeared possible that some of these materials were simply at equilibrium in a molten state. Several of these specimens were aged for 18 hours at 1100°C and analyzed to see if they would devitrify rapidly at this lower temperature. Table I shows that this is apparently not the case and that the materials are, in fact, stable.

2.4 COATING FORMULATION

The formulation of a coating from the precursor materials selected from the phase stability studies was a complex iterative procedure. A detailed logic circuit is shown in Figure 10. The baseline approach to applying the coatings was to mix the precursor powders (7940 fused silica, B_2O_3, and BPO_4) in a urethane-lined ball mill with an equal weight of distilled water and 0.5% methocell binder. This mixture was ball milled 16 hours using high purity alumina grinding balls, and sprayed on the tile directly, dried, and fired at 1370°C for 15 minutes. The above procedure was tried on materials 26, 27, 29, 30 and 31 from the phase diagram shown in Figure 3.

A general observation from these initial trials was that the coating had to be applied very sparingly and dried very carefully to keep from cracking. The B_2O_3 and BPO_4 are both water soluble and form complexes with water which shrink as the water is driven off.

A second approach was then tried on formulations 26, 30 and 31 in which the mixtures were ball milled for only four hours and brush coated on the surface. These coatings could be dried fairly rapidly but were not waterproof after firing. A sealer coat made up of silicon tetrachloride, B_2O_3, and BPO_4 dissolved in isopropynol was applied by brushing. The sealer coat was then dried at 120°C, prefired at 540°C for 15 minutes and then fired at 1370°C for 15 minutes. Although waterproof, the two firings required to apply these coatings caused the silica title to shrink badly. This was corrected by prefiring the coating to 1100°C for 15 minutes, applying the sealer coat, and firing

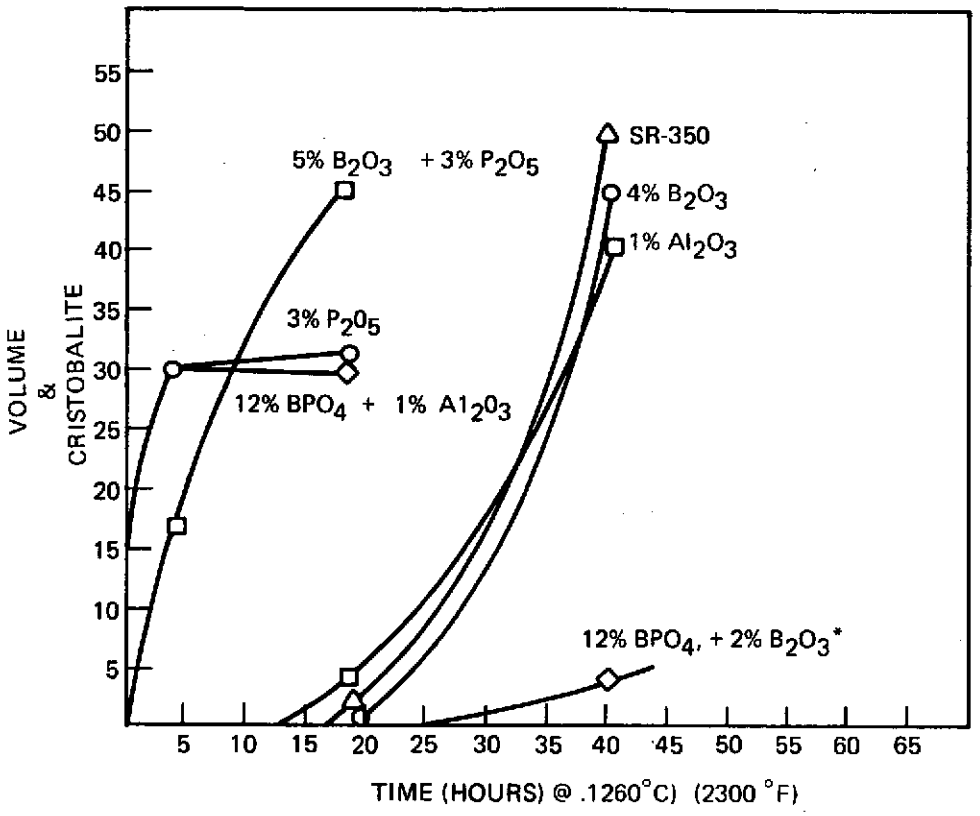

Figure 9. Effect of Various Oxides on the Devitrification Rate of Silica Made by the Decomposition of SR-350 Resin

the coating and sealer in one step at 1370°C for 10 minutes. These coatings were lightweight and waterproof, but had an uneven gloss due to the difficulty in controlling the amount of sealer which was applied to the porous substrate coating.

In order to alleviate the severe drying cracking experienced with water-based coatings, several non-aqueous carrier systems were tried with the coating powders. The first was a mixture of 5% Lucite-30 in acetone which was unsuccessful due to the extremely rapid evaporation of the carrier solvent which did not allow for a smooth spray application. Next, methylene chloride was mixed with 5% Lucite and an equal weight of powders was added. This mixture did form a smooth spraying slip after ball milling for 16 hours. The coating, however, still had a tendency to crack on drying.

Another approach which was used to apply the coatings was to melt a frit containing a high concentration of both B_2O_3 and BPO_4 and use this as a binder with pur silica. The following formulations were melted at 1565°C in high purity silica crucibles and water quenched:

1. 100 parts SiO_2
   22 parts B_2O_3
   51 parts BPO_4

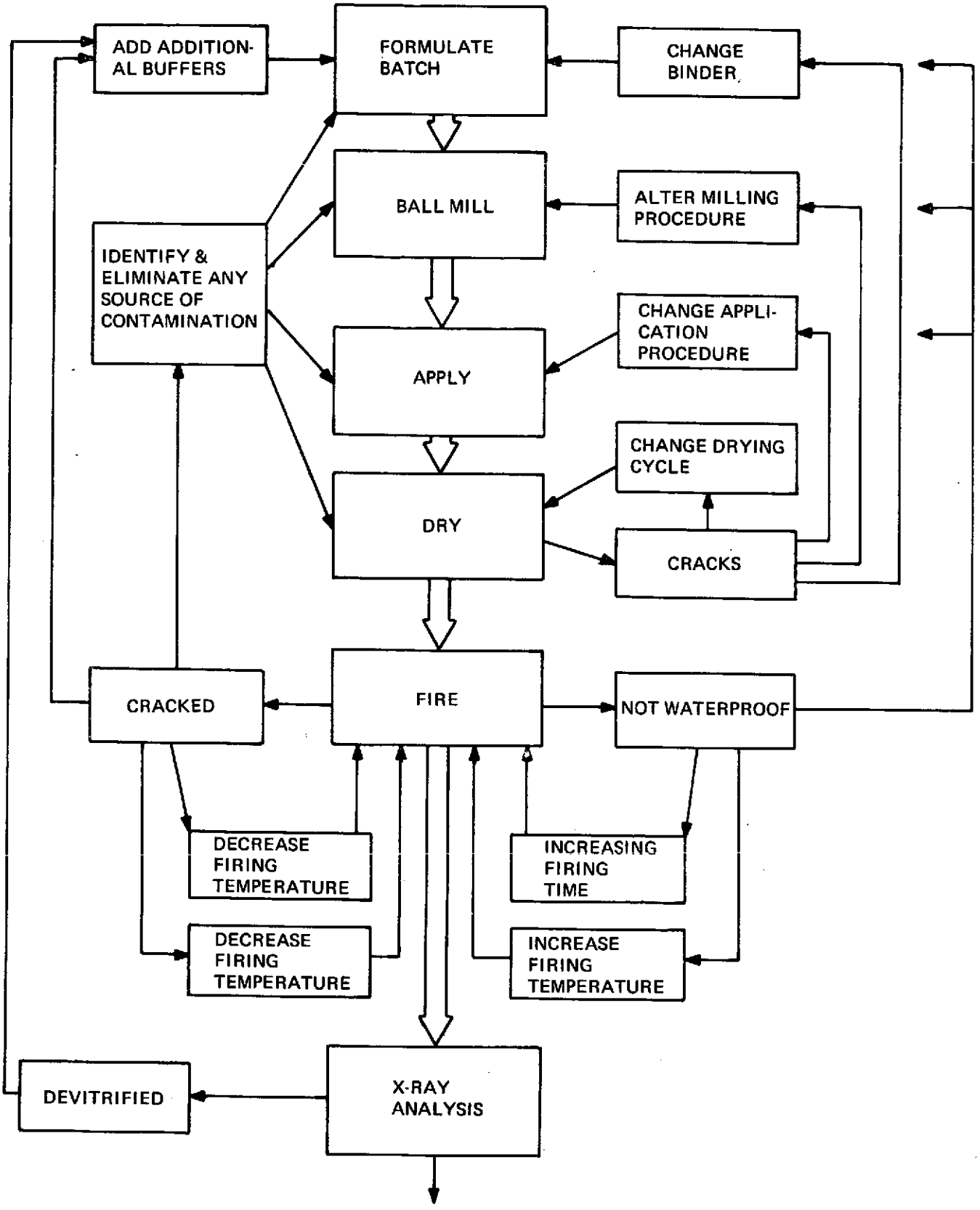

Figure 10. Logic Circuit for Base Coating Development

2. 80 parts SiO_2
   20 parts BPO_4

3. 79 parts SiO_2
   2 parts B_2O_3
   19 parts BPO_4

4. 82 parts SiO_2
   6 parts B_2O_3
   12 parts BPO_4

These frits were then ground to -100 mesh and mixed with either pure fused silica or Vycor plus water and methyl cellulose binder to form a coating slip. These slips were ball milled for 16 hours using high purity alumina grinding balls and then sprayed on 2" x 5" silica CRSI tiles. These specimens were dried at 80°C for 4 hours and fired at 1370°C for 15 minutes. Table III shows the formulation of the various coating slips prepared. Although these premelted frits should have been less soluble in water than free B_2O_3 and BPO_4 it was found that drying cracks were still a problem. As Table III shows only a few mixes actually produced smooth coatings and all of these contained at least 20% cristobalite.

Since the drying cracks in all of the coatings apparently resulted from the volume shrinkage of hydrated B_2O_3, and BPO_4 complexes it appeared that a possible approach to prevent cracking would be to use a flexible binder. This would allow the individual particles to shrink and move within a continuous matrix. Polyvinyl butyral (PVB) was chosen as a suitable candidate as it has an extremely high elongation to failure and does not char when burned. A solution of 10% PVB was dissolved in isopropynol and then mixed with an equal weight of formulation #31 powder. This mixture was ball-milled 16 hours in a urethane lined ball mill. This mixture was far too thick for spray application so it was diluted 50% with more PVB-isopropynol solution. While spraying this mixture it was observed that the material was being fiberized rather than atomized by the spray gun. The mixture was cut another 30% with toluene to finally give a smooth, sprayable slip.

The PVB bound coating could be easily dried at 80°C for two hours and either fired with the binder still intact or prefired at 760°C for ten minutes to remove the binder prior to firing. A firing time of 10 minutes at 1370°C produced a smooth, uniform coating. This was called the 31-D coating.

The above procedure was then tried on formulations #26, 27, 29, and 30 and with the exception of #26, all formed smooth, continuous coatings on 2" x 5" substrate samples. Attempts were then made to coat 6" x 6" samples with the 31-D material. It was found that some skill had to be exercised when applying the coating to prevent the slip from skinning over and blistering. This could be prevented best by spraying two light coats of slip on the sample. Best results were obtained if the binder was burned out of the first coat prior to the application of the second.

TABLE III. EMISSION SPECTOGRAPHIC ANALYSIS OF TWO FORMS OF HIGH PURITY SILICA

IMPURITIES PPM		
ELEMENT	CORNING 7941	SR-350
Sodium	30	5
Lithium	10	1
Potassium	30	2
Magnesium	30	1
Calcium	20	3
Strontium	1	1
Aluminum	1000	5
Lead	20	20
Iron	100	20
Copper	30	5
Nickel	100	10
Titanium	30	1
Zirconium	Not Detected	10
Boron	200	30

an x-ray diffraction analysis was then run on the 27B and 31D coatings to see if any critobalite was present. These results showed that the coating - fiber interface had, indeed, begun to devitrify.

Since the fibers were still high purity silica, the impurities from the coating, which had begun to diffuse, created an unfavorable stoichiometry at this interface which precipitated some devitrification. To rectify this situation a densifier slip was added. This slip contained 200 parts distilled water, 96 parts silica and 4 parts B_2O_3 by weight. The slip was brushed on the surface of the tile, dried 1/2-hour at 120° C, and fired at 1100° C for 15 minutes prior to coating the tile. Although this operation reduced the amount of devitrification, it did not eliminate it.

One additional operation had to be added to the process to eliminate the devitrification. This operation consisted of pretreating the tile surface with a boric acid solution prior to densification. A balance had to be established between the loss of refractoriness caused by adding too much boric acid and a loss of thermal stability of not adding enough. It was found that 30 grams of 3% boric acid per square foot of the tile surface was sufficient to retard devitrification during coating firing.

The two coating systems which were chosen for further evaluation with various pigments were the 31-D system and the 27B system. The 27B coating had the highest silica content of all the coatings which could be applied consistently to give a smooth waterproof surface. It was, therefore, the most refractory coating and had the lowest thermal expansion rate. The 31D coating had the greatest resistance to devitrification and was expected to be the most stable in the re-entry simulation tests.

Having developed the advanced tile pretreatment and densification procedure, an experiment was run in which a clear coating similar to the JSC-0042 material was sprayed over a tile which had been treated with boric acid and densified in the same manner as with the 31-D coating process described above. This produced a coating with no sign of devitrification at the coating-fiber interface as well.

This was considered significant as all previous attempts to apply the JSC-0042 coating to silica CRSI at GE had resulted in some traces of cristobalite.

2.5 PIGMENT FORMULATION

Three approaches were pursued to optimize the optical properties of the coatings. The first was to vary the content and particle size of silicon carbide in the JSC-0042 coating system to establish a credible baseline for comparing advanced systems. The second, was to attempt to adjust the optical spectrum of a white pigment so that it would have a high emittance (absorptance) in the near infrared. The third approach was to find a combination of materials that become darker at elevated temperatures so they would have a high emittance at 1100°C and yet have a low solar absorptance at room temperature.

2.5.1 OPTIMIZATION OF SILICON CARBIDE

Commercial, abrasive grade silicon carbide was separated into size fractions of 0-5, 5-10, 10-20, and 20-30 micron sizes in a water settling column. These various size fractions were then mixed by hand into unpigmented batches of JSC-0042 coating in concentrations of 2, 5, and 8 percent. The coatings were then applied to 2" x 2" specimens of REI silica and processed according to the JSC-0042 specification. The emittance and absorptance of these specimens was measured to obtain the curves shown in Figure 11.

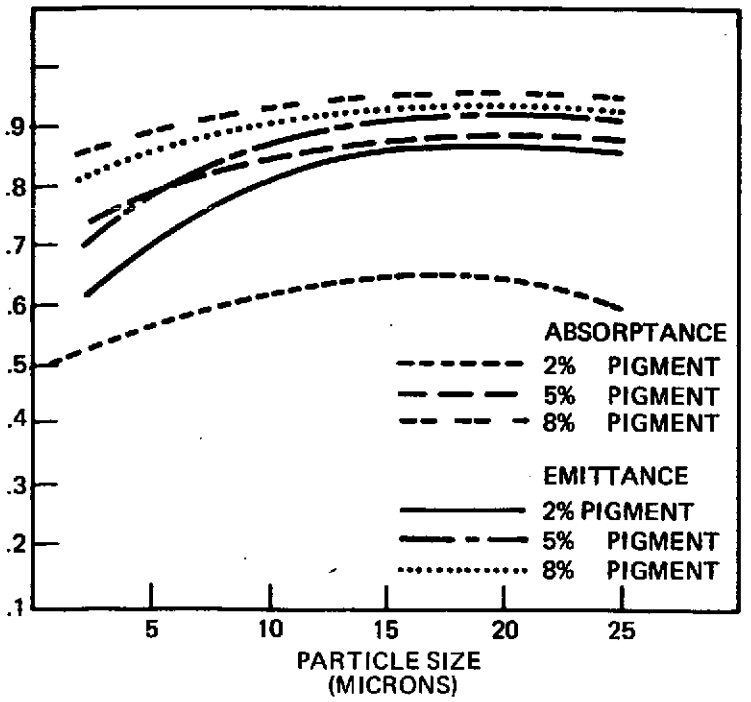

Figure 11. Optical Properties of Various JSC-0042 - SiC Mixtures

As the curves show, it is not possible to obtain a truly high emittance, low absorptance coating within the matrix tested. The best optical properties obtained within this matrix had an emittance of .8, a solar absorptance of 0.73 and an $\alpha_s/\epsilon_{H40°C}$ ratio of 0.93.

2.5.2 HAFNIA PIGMENTS

Theoretical analysis has shown that a material with a high reflectance in the visible spectrum and a high absorptance in the near infrared spectrum would be ideally suited for temperature control on the space shuttle orbiter. Figure 12 shows the radiant energy distribution from the sun along with a blackbody spectrum at 1100° C and one at 40°C. If a sharp cut-off exists at about 1.0 to 1.5 microns where the material changes from a reflector to an absorber the material would be able to meet the three proposed requirements.

Hafnium oxide meets the orbital requirements of high visible reflectance and high emittance at 40°C but it has a high reflectance in the 1.0 to 4.0 micron range as well, making it a poor emitter at 1100°C. Attempts were made to shift the optical absorption edge of hafnium oxide to a shorter wavelength by substituting zirconium and titanium ions into the lattice. By substituting these lighter ions into the hafnia lattice without decreasing the lattice constant the vibrational frequency of the lattice could be increased.

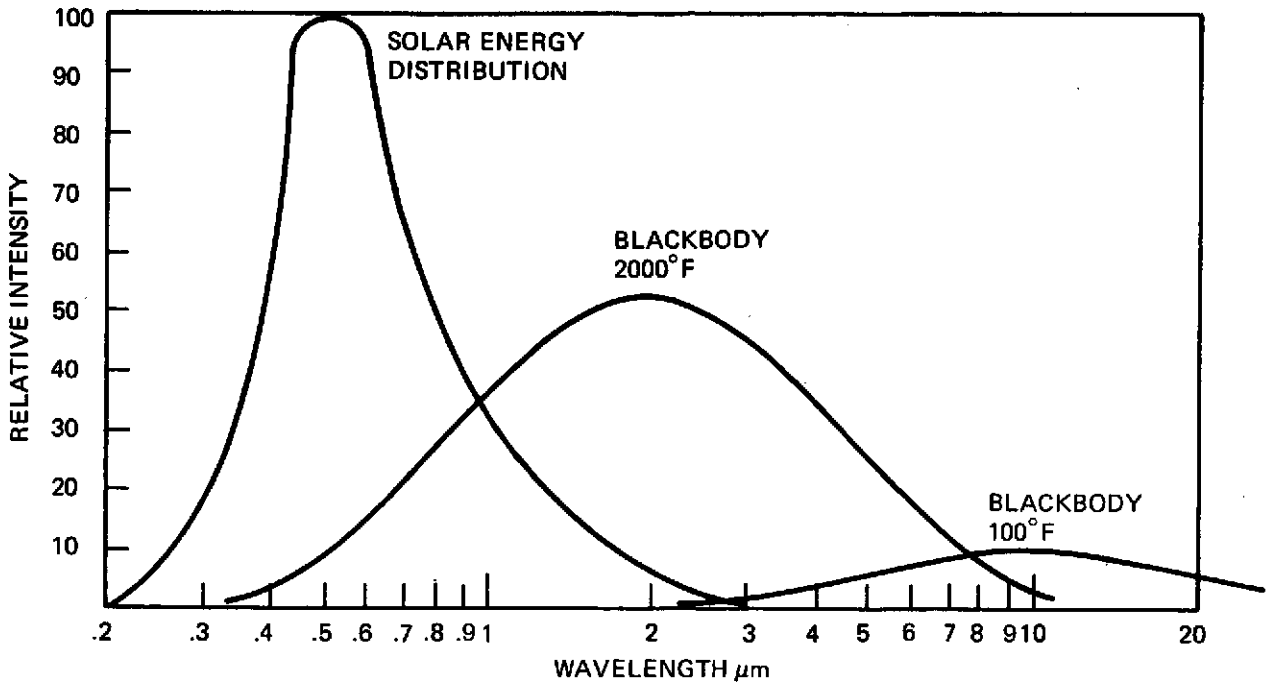

Figure 12. Energy Distributions Used for Designing Pigments

Extremely fine intimately mixed powders of Hafnia-zirconia, hafnia-titania, hafnia-zirconia-titania, and hafnium silicate-ceria, were produced by dissolving the metal chlorides in isopropynol in the proper ratios and then adding ammonia drop by drop while stirring vigorously to precipitate the metal hydrates. The gelatinous mass which resulted was filtered and washed on a buchner funnel using clean isopropynol to wash the material. The gels were then dried for 16 hours at 120°C and calcined at 540°C for one hour.

After calcining, the powders were crushed in a mortar and pestle to eliminate any segregation of the constituents which may have occurred. They were then placed in a platinum crucible and fired at 1425°C for 2 hours.

The reflectance spectrum for these powders is shown in Figure 13. Note that the optical absorption edge has indeed been shifted on all of these materials. Most of the treated hafnia powders had an absorption edge of 2-3 microns. Additional attempts at shifting the edge to even shorter wavelengths were unsuccessful as concentrations of ZrO_2 or TiO_2 higher than 10 mole % would simply shift the absorption edge back out toward longer wavelengths.

As is, these pigments would produce a solar absorptance of around 0.3 and a room temperature emittance of 0.7 to 0.8. The emittance at 1100°C would be about 0.6.

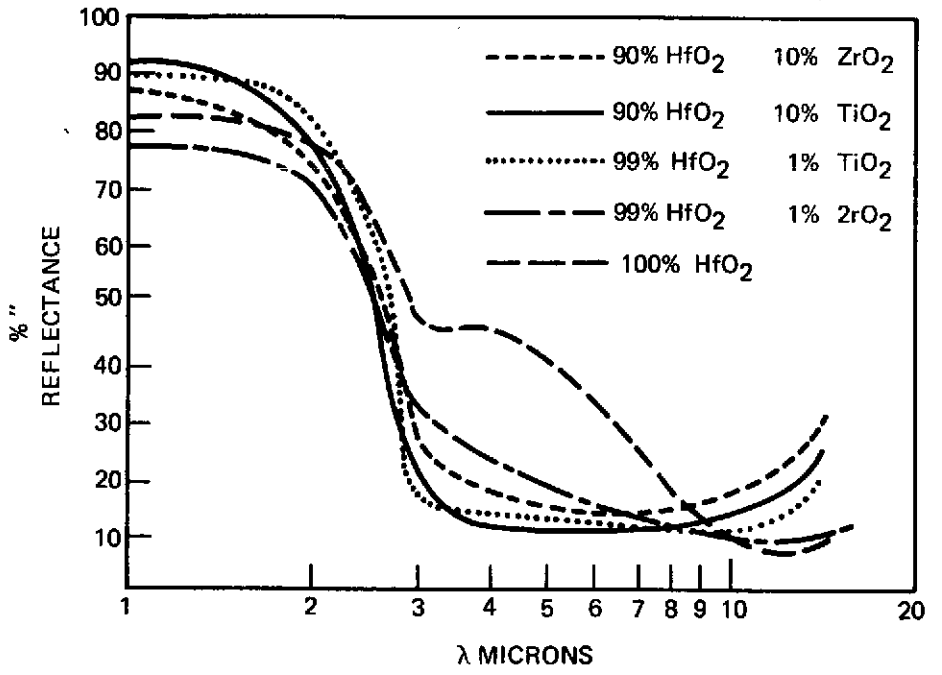

Figure 13. Reflectance Curves for HfO_2-ZrO_2-TiO_2 Compounds

2.5.3 CERIUM-OXIDE BASED PIGMENTS

Certain oxides, in combination with other materials, change color when heated. This is especially true with cerium oxide which is used to brighten the illumination of gas lantern mantles and was found to be ideally suitedfor tailoring the optical properties of G.E.'s mullite based REI coatings.

Mixtures of CeO_2 and various refractory oxides including HfO_2, ThO_2, and Y_2O_3 were made by dissolving the chlorides of the parent metals in isopropynol and precipitating the hydroxides with ammonia. The precipitates were then filtered, washed, dried, calcined at 540°C for one hour, and fired at 1425°C for 2 hours in a platinum crucible.

Cerium oxide was also combined with silica and germania by this same process. An intimate mixture of CeO_2 and B_2O_3 was made by mixing -325 mesh powders and melting in a high purity silica crucible at 760°C for 4 hours. This mixture was then crushed to -200 mesh.

The reflectance spectra for these materials shown in Figure 14 show that the HfO_2-CeO_2, and B_2O_3-CeO_2 combinations have favorable optical properties to meet the orbital requirement . Since the high temperature emittance of these materials would probably

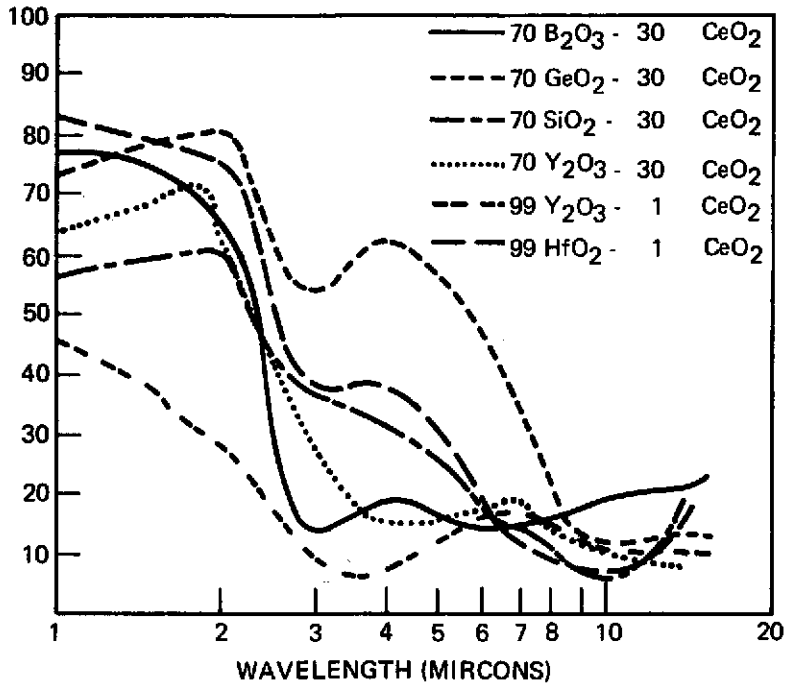

Figure 14. Reflectance Spectra for Cerium-Doped Pigments

be different from the predicted values at room termperature, these pigments were later combined in a coating to measure their effects at 1160°C.

2.6 COATING-PIGMENT COMBINATIONS

An initial series of screening tests was run in which the various pigments were mixed with the 31-D coating slip in concentrations of 5% and 10% by weight. The high temperature emittance and room temperature absorptance of these combinations was then run to give the data shown in Table IV. These data showed that the hafnia based pigments could not produce the high emittance desired even though their room temperature absorptance to emittance ratios were low. The generally low emittance of most of the pigments tried indicated that the addition of a darkening agent would be necessary to obtain the high emittance desired.

At the suggestion of Dr. D. Deadmore of NASA/Lewis, a second series of coating-pigment combinations based on the JSC-0042 coating system were also tried. These coatings, designated DD-1, DD-2, and DD-3 all had a high emittance but also had a high absorptance. The coatings used a combination of white pigments with a high α_s/ϵ H40 ratio ($ZrSiO_4$ + Y_2O_3) and dark pigments with a high emittance (HfB_2 & SiC). Of special interest with these coatings was the HfB_2 darkener which gave the coatings a high emittance and yet did not affect the texture of the coating as SiC has been observed to do.

TABLE IV. COATINGS MADE WITH PREMELTED FRITS

Coating No.	Frit No.	Composition (Parts by Weight)				Result
		Frit	Silica	Water	Methyl Cellulose	
F-27-1	1	23	77*	100	0.5	Difficult to Dry Without Cracking
13-F-1	2	44	56	100	0.5	Not Waterproof
13-F-2	2	39	61	100	0.5	Not Waterproof
13-F-3	2	54	46	100	0.5	Smooth & Waterproof - Devitrified
14-F-1	3	50	50	100	0.5	Difficult to Dry Without Cracking
14-F-2	3	40	60	100	0.5	Not Waterproof
14-F-3	3	60	40	100	0.5	Smooth & Waterproof - Devitrified
14-F-4	3	68	32	100	0.5	Smooth & Waterproof - Devitrified
F-27-2	4	66	34	100	0.5	Difficult to Dry - Not Waterproof

*Vycor (Corning Code 7913) was used instead of 7940.

A second matrix of coating-pigment combinations was tried with the more promising pigments from both the 31-D and DD series coatings. The high temperature emittance and absorptance of these coatings is shown in Table V. The total hemispherical reflectance curves for the DD-3 Mod. 2 and PB-1 coatings are shown in Figure 15.

The more promising of these coatings were then optimized through the logic chart shown in Figure 16. Five coating systems evolved from this study which were selected for arc test evaluation. A description of these coatings follow:

31-D Unpigmented

The 31-D coating was selected because of the high resistance of this formulation to devitrification and so that pigmented versions of this coating could be compared to a common baseline.

31-D-LA

This coating is the same as 31-D except that ten percent hafnium diboride (HfB_2) was added to control the emittance. This coating has an emittance at 1100°C of 0.57 and an absorptance of 0.34.

DD-3 Mod. 2

This coating is essentially the JSC-0042 coating with the following modifications: 1) the densifier used is that developed for the 31-D system, i.e., surface treated with boric acid solution and densified with a slip of 96% SiO_2, 4% B_2O_3, 2) Hafnium diboride is used as a pigment instead of the silicon carbide used in the JSC-0042 coating. The emittance of this coating is 0.71 and the absorptance is 0.73.

31-D-HE

This coating has a surface layer sprayed over a base coating slip of 31-D. The surface layer consists of 31-D slip with 17% cerium oxide (CeO_2) and 0.9% silicon carbide (SiC). This material has an emittance at 1100°C of 0.69 and an absorptance of 0.44.

PB-1

This coating was an attempt at combining a high emittance-low absorptance pigment with a JSC-0042 - based coating. The tile was densified in the same manner as the 31-D samples and was then coated with a 0042 slip which contained 5% cerium oxide and 2% hafnium diboride. The 1100°C emittance of this coating is 0.68 with a solar absorptance of 0.384.

TABLE V. PROPERTIES OF VARIOUS PIGMENTS WITH THE 31-D COATING SYSTEM

Pigment #	Formulation	Wt. % Added To Coating	α_s	$\epsilon_{H_{1100°C}}$
1	No Pigment	---	0.18	0.48
2	90% HfO_2	5%		0.43
	10% CeO_2	10%	0.19	0.44
3	90% HfO_2	5%		0.44
	10% TiO_2	10%	0.23	0.47
4	90% $ZrSiO_2$	5%	0.45	0.59
	10% SiC	10%	0.51	0.60
5	98% $HfSiO_4$	5%	0.25	0.46
	2% CeO_2	10%	0.23	0.46
6	90% CeO_2	10%	0.44	0.60
	10% SiC			
7	HfB_2	10%	0.34	0.57
8	60% HfO_2	10%	0.24	0.44
	7% SiC			
	33% HfB_2			

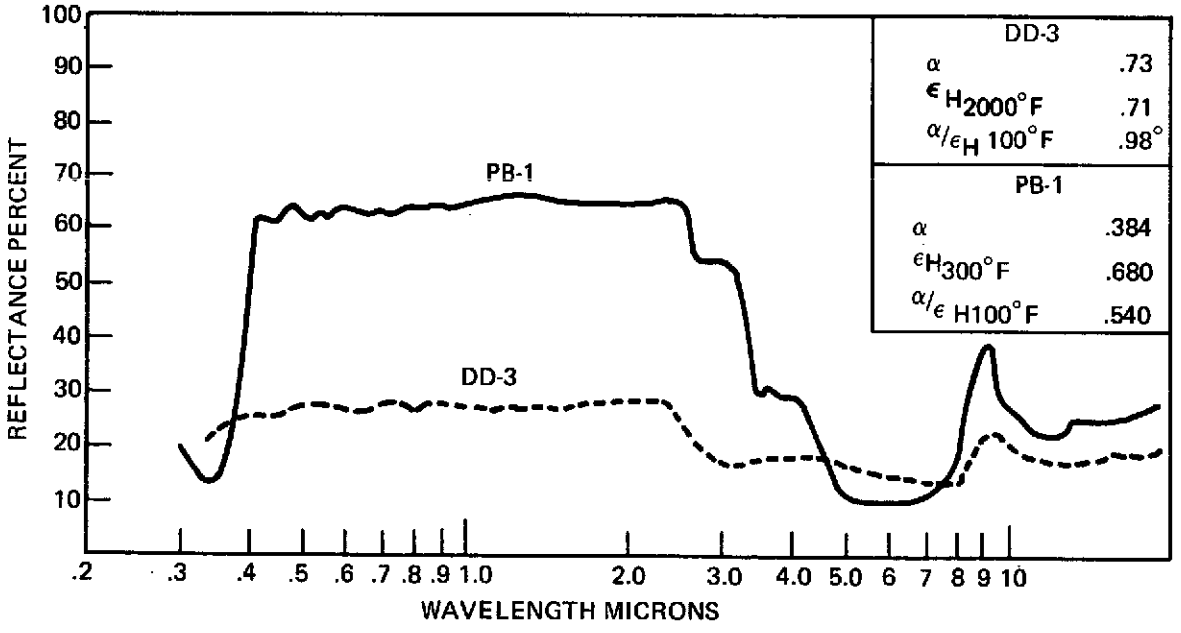

Figure 15. Reflectance Spectra for DD-3 and PB-1 Coatings

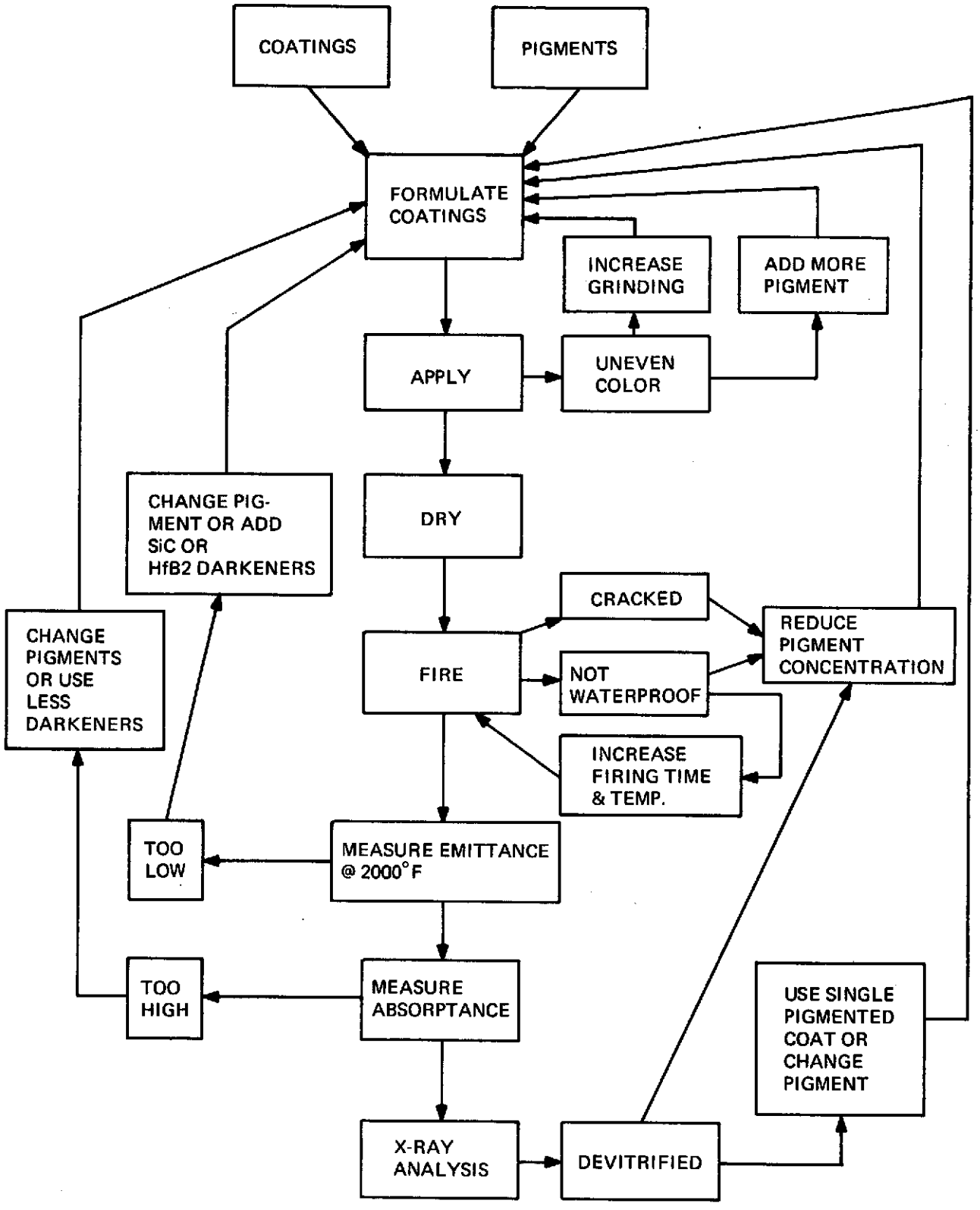

Figure 16. Logic Chart for Coating Optimization

2.7 ALTERNATE COATING PIGMENT COMBINATION CONCEPTS

Two attempts were made to disperse the pigments on the surface of the coating. One of these was to microencapsulate the pigment particles in SR-350 resin, spray over an unpigmented coating, and pyrolize and fire the resin in-situ. The microencapsulation technique was as follows:

Twenty grams of coprecipitated 90% HfO-10% TiO_2 powder was placed in a round bottom flask and purged with nitrogen which had been bubbled through trichloromethyl silane. This treatment made the surface of the powders totally non-poplar and extremely hydrophobic. The treated powder was then added to 500 ml distilled water and agitated vigorously with a teflon stirring bar to disperse the particles. A 10 ml solution of 5% SR-350 in freon was then added slowly to the mixture while stirring rapidly. The non-polar surface of the particles rapidly adsorbed the resin. The water was then heated to a boil while still stirring to remove the freon and cure the resin. The powder was then filtered and dried.

The powder was applied to the coating surface by wetting the surface with 1-4 dioxane and spraying the powder with an atomizer to disperse it uniformly over the surface. This was then dried 30 minutes at 120°C, pyrolized at 760°C for 15 minutes, and fired at 1370°C for 5 minutes. The surface produced in this way, was very matte and dull. It was waterproof, however, water droplets tended to spread out but were held on the surface of the coating. The fact that the pryolized SR-350 resin devitrified quite readily in contact with other contaminants prevented any further testing or development of this process.

Another method of dispersing the pigment on the surface was to apply a heavily pigment-loaded slip in a thin coat over an unpigmented coating. A delicate balance had to be reached in order to maximize the optical effects of the pigment while minimizing the effect on mechanical strength, waterproofness, thermal expansion and thermal stability of the base coating. After adding concentrations of 40 wt.%, 20 wt.%, and 10 wt. % of the ceria, silicon carbide, and Hafnium oxide pigments to the 31-D coating slip. It was found that up to 20% pigment could be tolerated without cracking or loss of waterproofness in these mixtures. This concept was used for producing the 31-D-HE coating.

TABLE VI. OPTICAL CHARACTERISTICS OF EXPERIMENTAL COATINGS

Coating Number	Designation	Base Coating	Pigment (s)	$\epsilon_{H\ 1100°C}$	α_s
1	JSC-0042	95% Vycor 5% Pyrex	5 wt. % SiC	0.72	0.73
2	31-D	86% SiO_2 5.1% B_2O_3 8.9% BPO_4	None	0.48	0.18
3	Black Standard	95% CoO 5% $AlPO_4$		0.80	---
4	31D-HE	86% SiO_2 5.1% B_2O_3 8.9% BPO_4	17.7% CeO_2 0.9% SiC	0.68	0.45
5		86% SiO_2 5.1% B_2O_3 8.9% BPO_4	18.6% $BaTiO_2$	0.48	0.30
6		86% SiO_2 5.1% B_2O_3 8.9% BPO_4	5% B_2O_3 5% CeO_2 2% SiC	0.69	0.72
7		86% SiO_2 5.1% B_2O_3 8.9% BPO_4	9.5% B_2O_3 9.5% CeO_2	0.55	0.27
8		86% SiO_2 5.1% B_2O_3 8.9% BPO_4	18.6% CeO_2	0.55	0.32
9	NASA Lewis DD-1	100% Vycor	5% SiC 5% $ZrSiO_4$	0.74	0.68
10	NASA Lewis DD-2	100% Vycor	5% Y_2O_3 5% SiC	0.69	0.62
11	NASA Lewis DD-3	100% Vycor	5% HfB_2 5% $ZrSiO_2$	0.71	0.73
12	DD-3 Mod. 2	95% Vycor 5% Pyrex	5% HfB_2	0.73	0.75
13	PB-1	95% Vycor	5% CeO_2 2% HfB_2	0.68	0.38
14	31-D-LA	86% SiO_2 5.1% B_2O_3 8.9% BPO_4	10% HfB_2	0.58	0.34

SECTION 3

RE-ENTRY SIMULATION

Two series of tests were run in which coatings were exposed in simulated re-entry cycling and characterized before and after this exposure. The first test series was run on the 31-D and 27B coating systems in which the coatings were cycled in a radiant heating facility. The second series was run on various combinations of pigments and coatings in a hypersonic plasma arc facility. From the arc test the two coatings which finally survived the entire 100 mission exposure (DD3 and PB1) were submitted to further characterization in the radiant heating facility.

3.1 PRELIMINARY TESTING OF 27B and 31D COATINGS

3.1.1 DESCRIPTION OF THE G. E. RADIANT PANEL SIMULATOR

A schematic drawing of the G. E. Radiant Panel Simulator is shown in Figure 17. The simulator consists of a bank of 16 silicon carbide resistance heating elements (Glo-bars) enclosed in a foamed silica frame. The heating elements are encased in fused silica tubes to prevent contamination of the models by the heating elements. The test models are fitted into a foamed silica model holder and held approximately 1-1/2 inches from the heating elements. Figure 18 shows the simulator with one side closed to show the positioning of the models and heaters in the operational mode.

The temperature is controlled by a platinum rhodium thermocouple imbedded into the surface of a dummy model made of the same materials as the test models. Up to four 6" x 6" models can be tested at one time since the models can be placed on both sides of the heater bank. The back face of the models is supported by a water-cooled copper plate.

The radiant heater is installed in a 6 foot diameter high vacuum chamber shown in Figure 19. The temperature of the system is programmed into an automatic controller which is monitored by the thermocouple in the dummy model. Once the system is set up it will cycle automatically for as many cycles as desired. The pressure in the chamber is controlled manually with a controlled leak valve.

This simulator has been used to characterize all of the previous G. E. REI type coatings and was also used for evaluating development of the G. E. version of the 0042 coating.

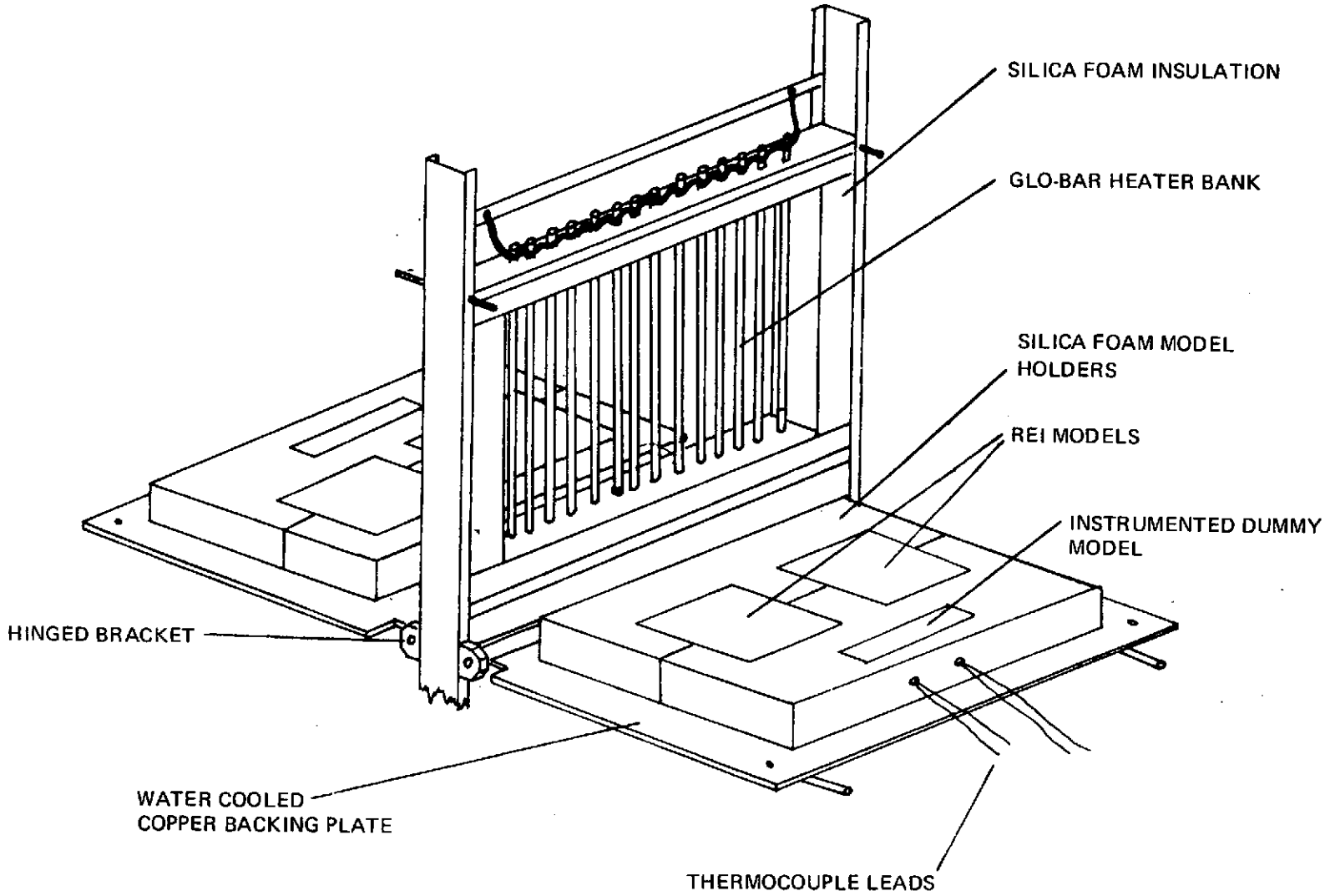

Figure 17. Re-entry Simulator Configuration

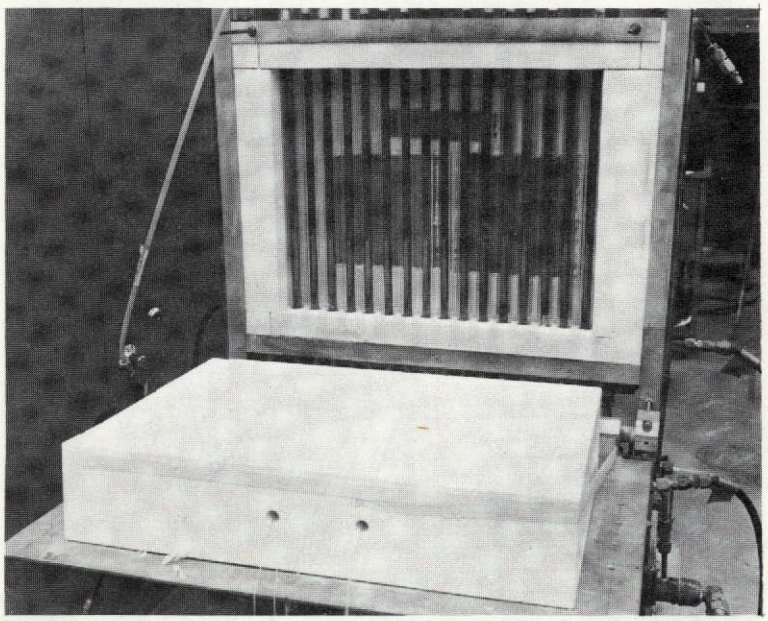

Figure 18. Radiant Heater for GE Simulator

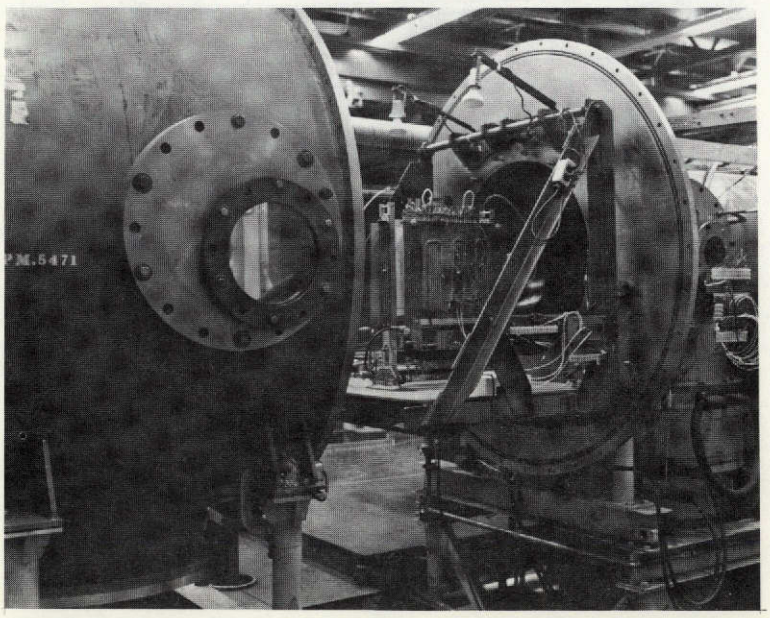

Figure 19. High Vacuum Chamber with Heater and Models Installed

3.1.2 TEST CONDITIONS

The first series of G. E. 's re-entry simulation tests were run on the 31D coating and the 27B coating. Since an optimum pigment system had not yet been determined, the coatings were applied without pigment and with a 3% addition of silicon carbide. The following nomenclature is used to identify the coatings:

31D-U	31D coating with no pigment
31D-P	31D coating with 3% SiC
27B-U	27B coating with no pigment
27B-P	27B coating with 3% SiC

A 6" x 6" x 2" model of REI silica was coated with each of the above coatings and installed in the simulator. The simulator was set to follow the time temperature profile shown in Figure 20 at a constant pressure of 7 torr. After every twenty cycles the simulator was opened and the models inspected and photographed. Once a crack or loss of waterproofness was observed, the model was removed and replaced.

A set of test specimens for impact strength and tensile strength were made up at the same time as the GE re-entry simulator models. These specimens were thermally aged in a vacuum furnace at 1260°C for two hours. A controlled atmosphere of nitrogen at 7 torr pressure was passed over the specimens during the thermal aging.

3.1.3 RESULTS

Table VII shows the results of the initial GE re-entry simulator test. These results were encouraging as previous coatings evaluated in this manner rarely survived 20 cycles. The white, unpigmented coatings are shown in Figures 21 and 22 before and after simulated exposure. The water droplets indicate that the as-fabricated coatings are waterproof. The coatings were treated after test with a dilute solution of india ink to make the crack patterns more visible. The crack patterns are typical of coatings which fail due to devitrification. The pigmented coatings shown in Figures 23 and 24 could not be treated with the ink due to their greater surface roughness. The crack patterns in both of these were not as severe as the unpigmented coatings.

Scanning electron photomicrographs (SEM's) of all four coatings are shown in Figures 25 through 28. All of these show that the failure occurs at the coating-fiber interface and works up to the surface. Note that the unpigmented coatings appear more dense than the pigmented coatings. The bubbles in the pigmented coating are apparently caused by decomposition of the SiC pigment and become worse as the coatings are aged.

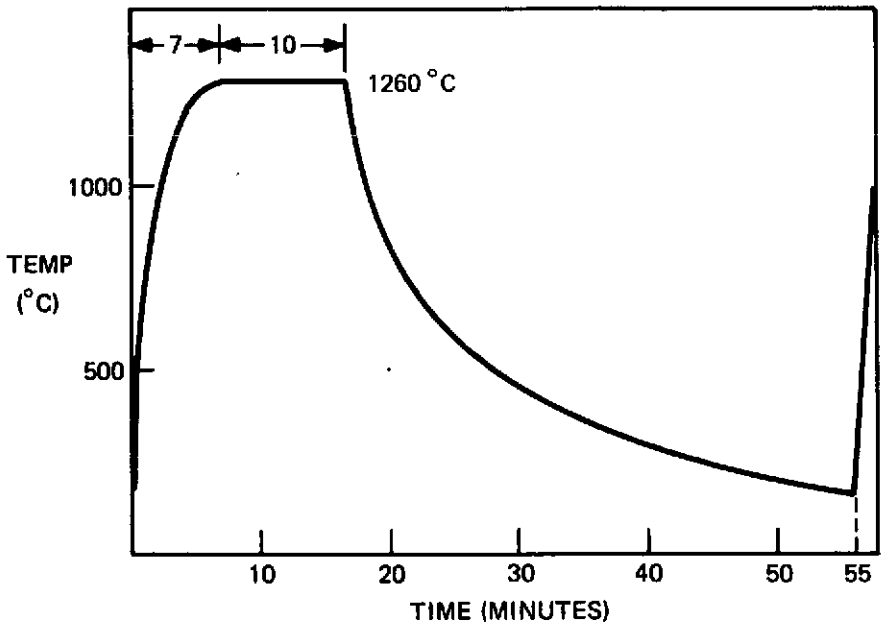

Figure 20. Time-Temperature Profile of GE Re-entry Simulator

TABLE VII. RE-ENTRY SIMULATOR RESULTS ON 27B & 31D COATINGS

Coatings	Results
27B	Cracked after 20 cycles
27B	Cracked after 20 cycles
27B + 3% SiC	Cracked after 40 cycles
31D	Cracked after 40 cycles
31D	Cracked after 40 cycles
31D + 3% SiC	Cracked after 60 cycles

Table VIII shows the results of the characterization testing before and after simulation exposure. The impact tests do not indicate any particular change, however, the tensile properties indicate a definite degradation of the coatings. The degradation correlates fairly well with the formation of cristobalite indicated by the x-ray diffraction data.

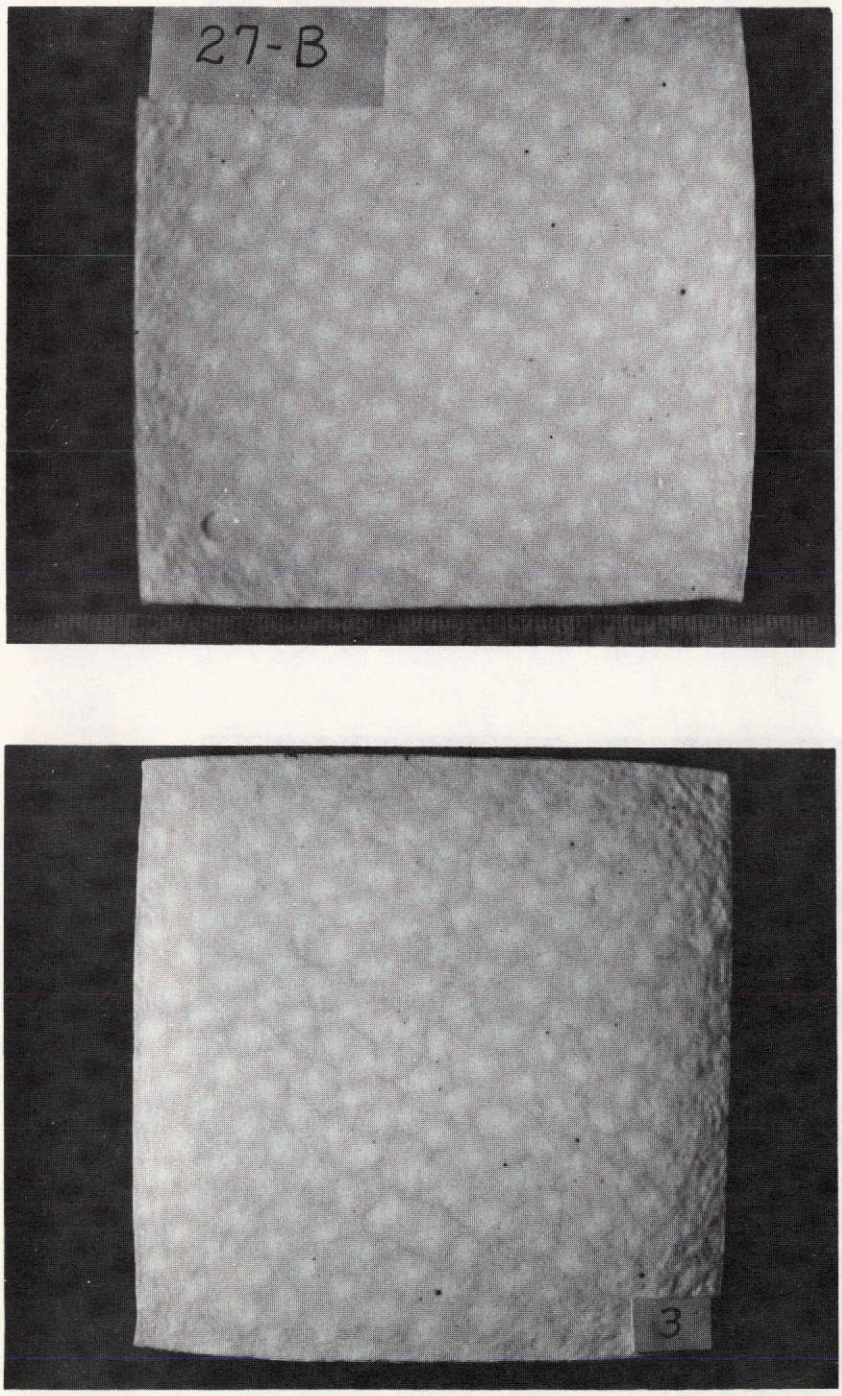

Figure 21. 27B-U Surface of Re-entry Model No. 2 without Pigment, before and after G. E. Re-entry Simulator Exposure

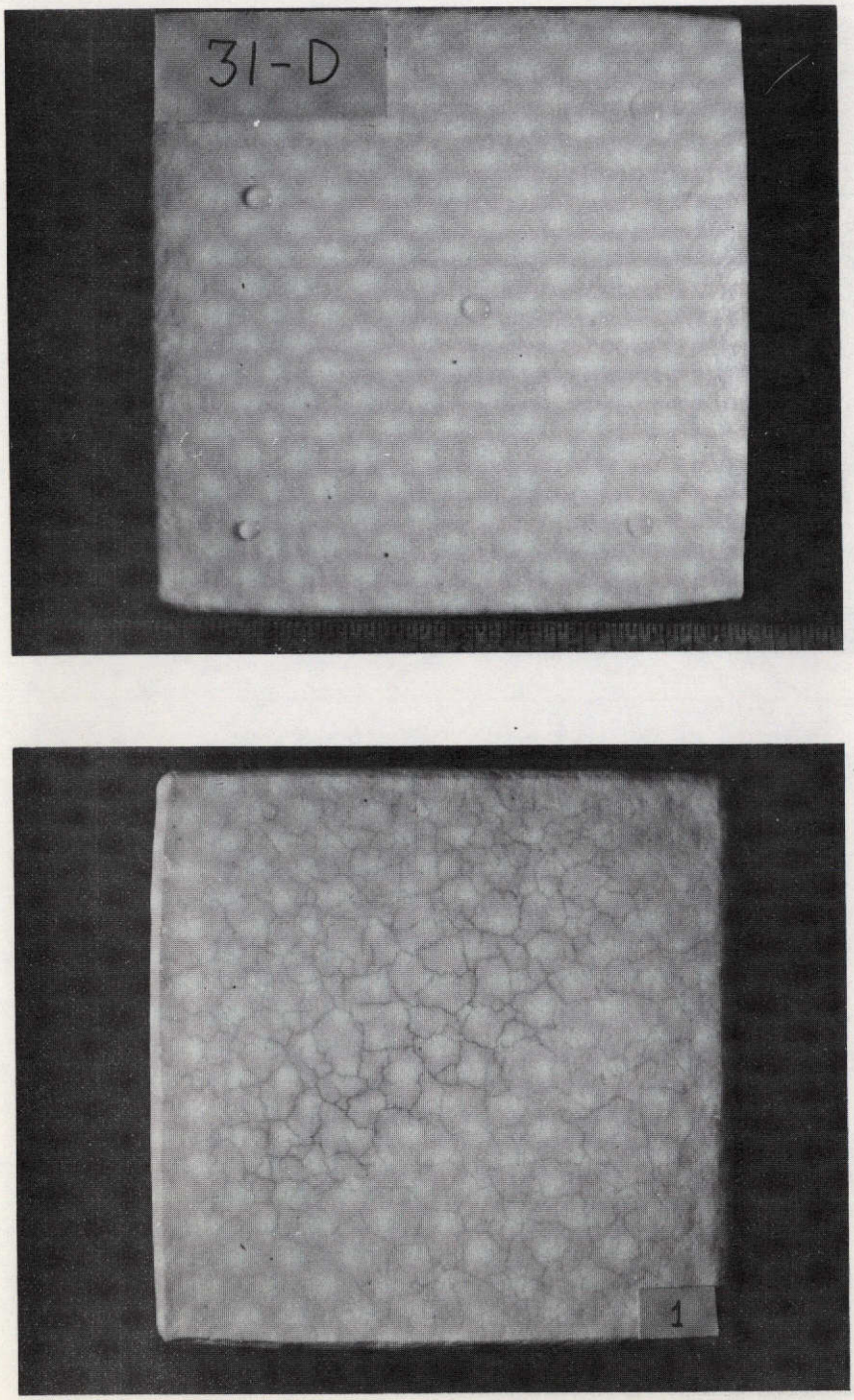

Figure 22. 31-D-U Surface of Re-entry Model No. 1 without Pigment, before and after G. E. Re-entry Simulator Exposure

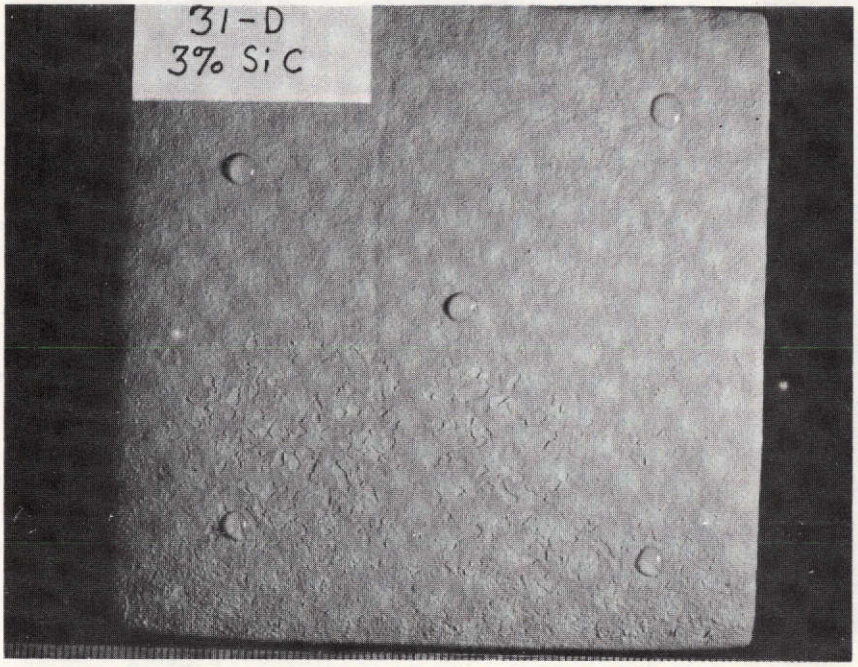

As Fabricated

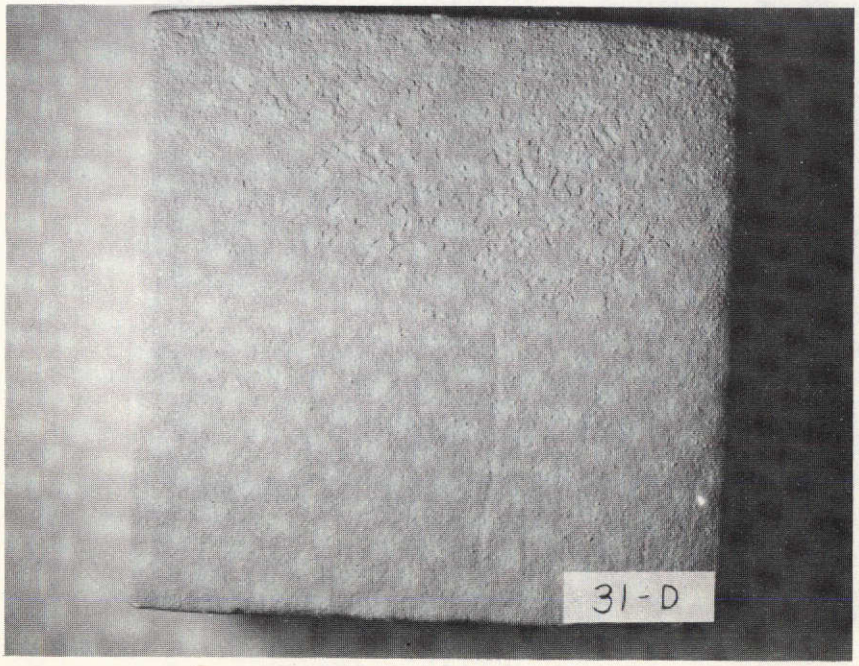

After 60 Cycles

Figure 23. 31-D-P Pigmented Re-entry Model No. 3 before and after Re-entry Simulator Exposure

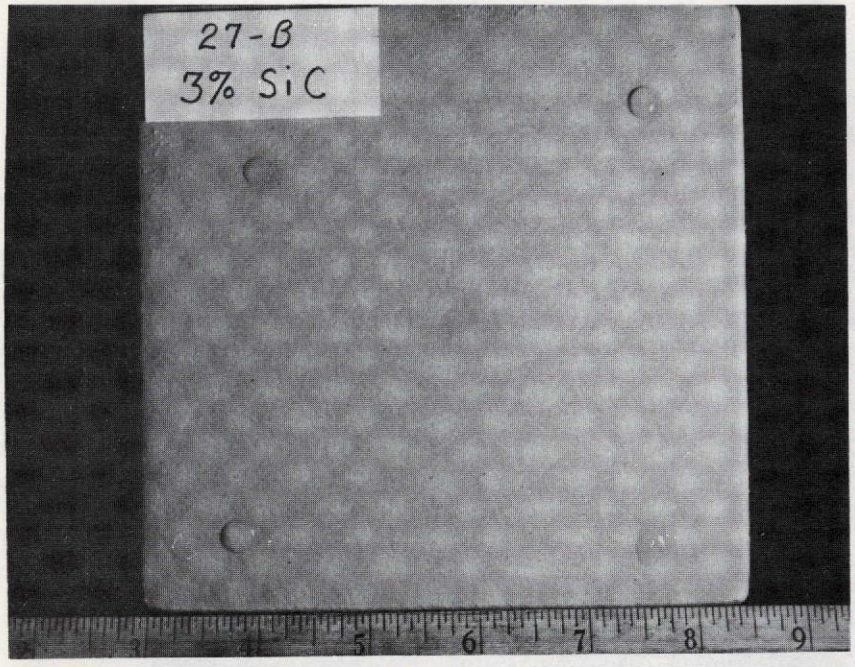

As
Fabricated

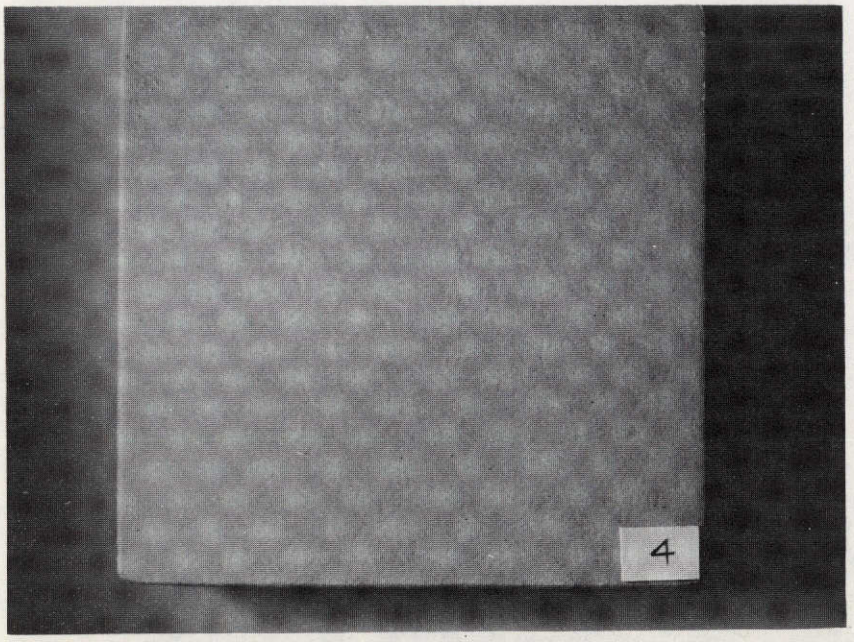

After
40
Cycles

Figure 24. 27B-P Pigmented Re-entry Model No. 4 before and after Re-entry Simulator Exposure

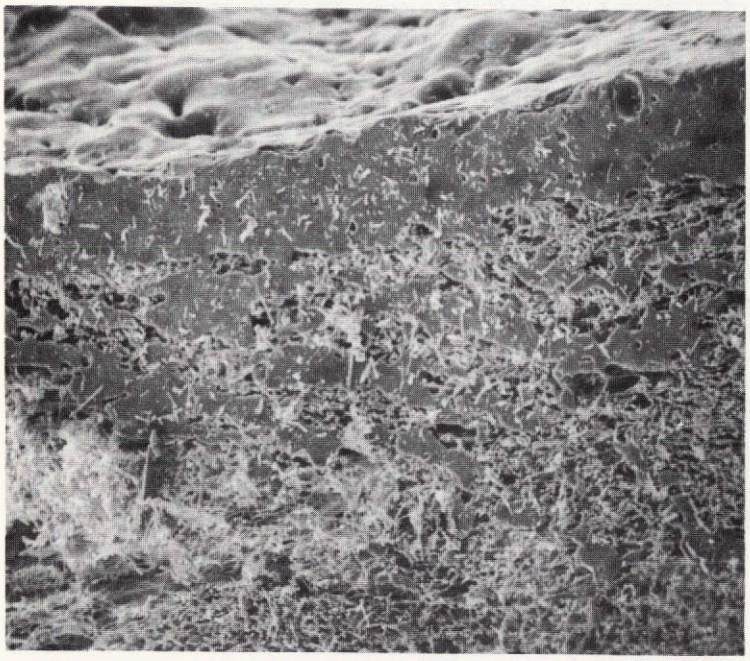

As Fabricated
(50X)

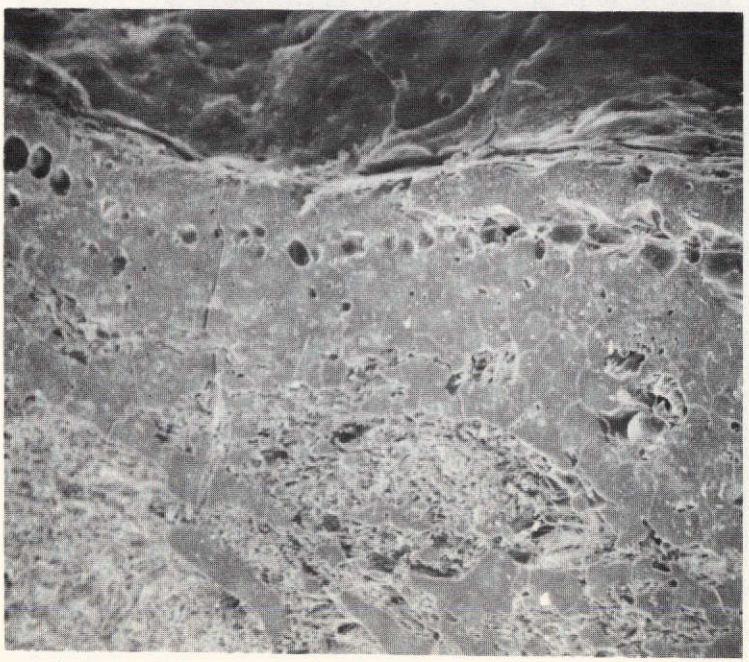

After 20 Cycles
(50x

Figure 25. SEM Photomicrographs of 27B-U Coating before and after Re-entry Simulator Exposure

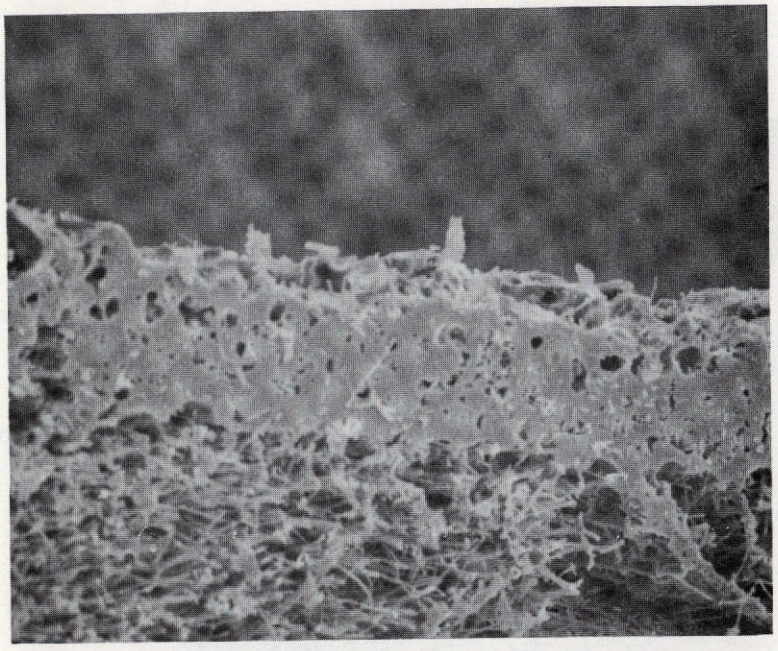

As Fabricated
(100X)

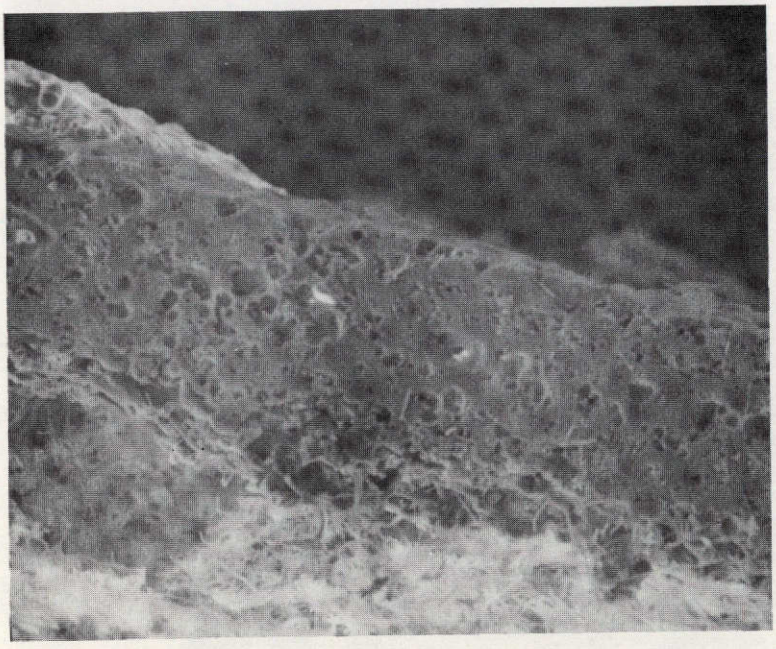

After 40 Cycles
(100X)

Figure 26. SEM Photomicrographs of 27B-P Coatings before and after Re-entry Simulator Exposure

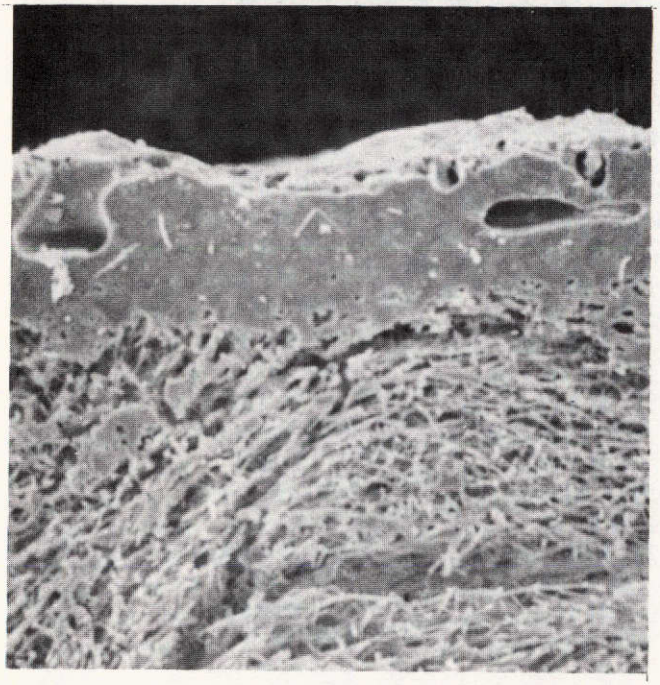

As Fabricated
(100X)

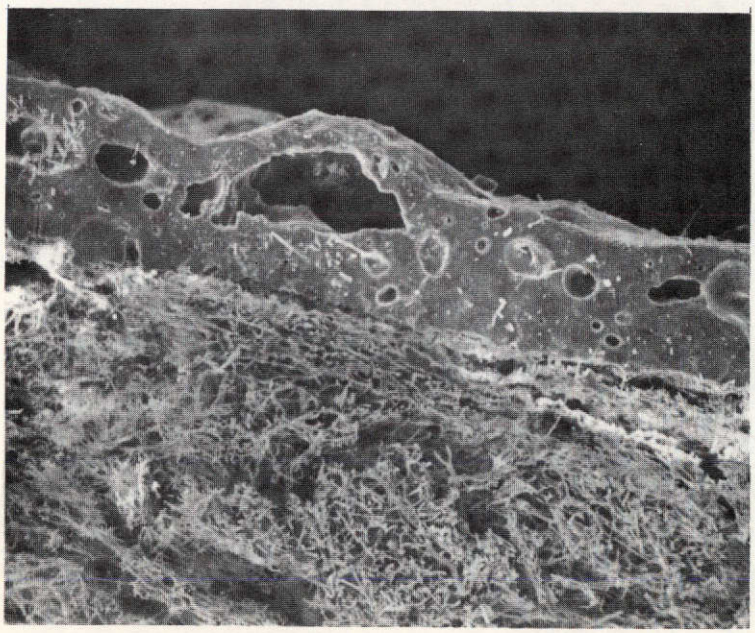

After 40 Cycles
(100X)

Figure 27. SEM Photomicrographs of 31-D-U Coating before and after Re-Entry Simulator Exposure

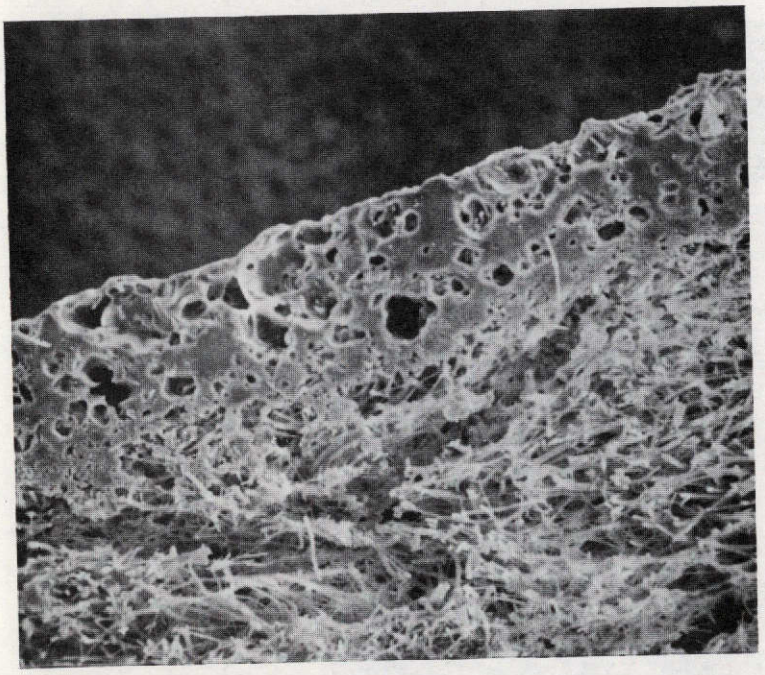

As Fabricated
(100X)

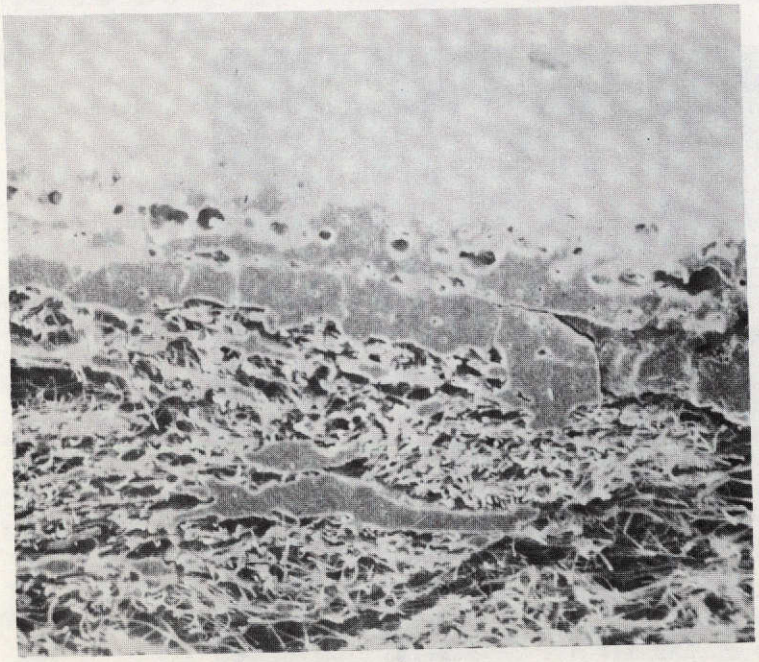

After 60 Cycles
(100X)

Figure 28. SEM Photomicrographs of 31-D-P Coating before and after Re-entry Simulator Exposure

TABLE VIII. RESULTS OF PRELIMINARY RE-ENTRY SIMULATION TESTS

Coating	Impact Strength (in-lbs)	Tensile Strength (psi)	Volume Percent Cristobalite	Thermal Conductivity Btu-in/ft^2-hr-°F	Moisture Permeability
27B-U	45	2600	0	8.29	Waterproof
Aged 2 hrs @ 2300°F	48	1280	65		Waterproof
After 20 cycles in Simulator			57		Cracked
27B-P	11	2510	Tr.	10.02	Slightly Porous
Aged 2 hrs @ 2300°F	13	882	49		Very Porous
After 40 cycles in Simulator			65		Cracked
31D-U	14	1930	0	7.26	Waterproof
Aged 2 hrs @ 2300°F	14	1100	44		Waterproof
After 40 cycles in Simulator			68		Cracked
31D-P	16	1880	0	9.02	Waterproof
Aged 2 hrs @ 2300°F	14	1063	49		Waterproof
After 60 Cyles in Simulator			69		Cracked

The thermal conductivity could not be measured directly on any of the coatings due to a non-favorable specimen configuration. It is doubtful that a significant change in this parameter would have been detected.

3.2 RE-ENTRY SIMULATION TESTING OF OPTIMIZED COATINGS

3.2.1 ARC TESTING

Cyclic exposures were conducted on ten models in the Battelle-Columbus (BCL) Aerothermal Research Facility to evaluate their thermal response to re-entry environmental conditions. The models were made to the configuration shown in Figure 29. They were coated on all but the back surface with the coatings identified in Table IX.

The test conditions were achieved using high-enthalpy, low-pressure arc heater with an 8-inch exit diameter convergent-divergent nozzle. Model stagnation pressures and heating rates were approximately 0.007 atm and 35 Btu/ft^2-sec, respectively, over 99 cycles and 0.009 atm and 68 Btu/ft^2-sec on the 100th cycle. The gas bulk enthalpy for 100 cycles was in the range of 3800 to 9000 Btu/lb.

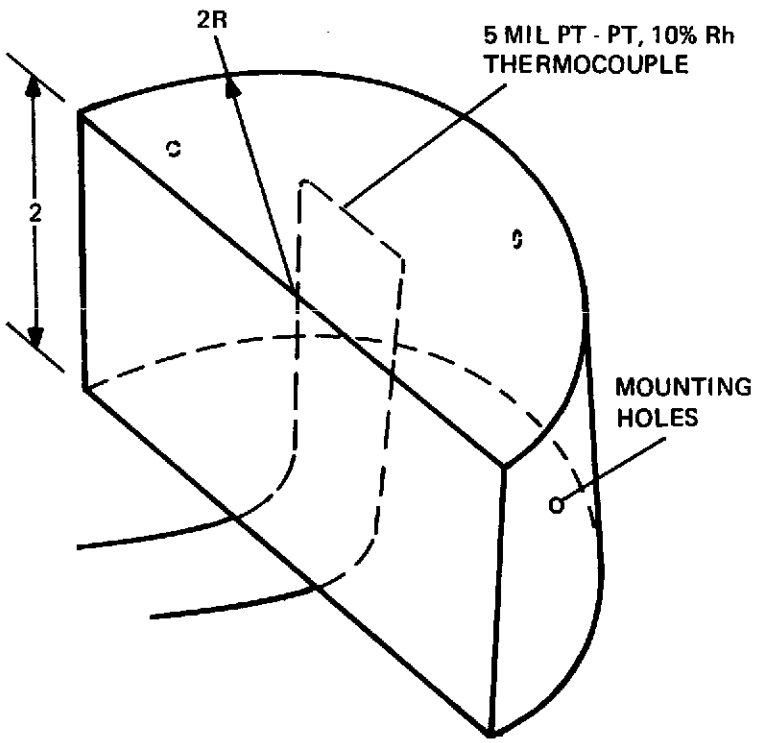

Figure 29. Arc Model Configuration

TABLE IX. IDENTIFICATION OF ARC MODELS

Model Number	Coating	Coating Weight	
		g/cm^2	lbs/ft^2
1	31D-LA	.030	.061
2	DD-3	.044	.090
3	DD-3	.048	.099
4	31D	.031	.063
5	31D	.024	.049
6	DD-3	.034	.069
7	31D-LA	.029	.060
8	31D-HE	.033	.067
9	31D-HE	.030	.061
10	PB-1	.053	.108

The Battelle Aerothermal Research Facility is designed and constructed to provide for performing experimental research in the areas of supersonic/hypersonic flows and hyperthermal environments. The facility and the environments are suited for the evaluation of materials' response at high pressures and temperatures, use and development of plasma diagnostic techniques, and fundamental research in heat transfer and gas dynamics. Figure 30 is a schematic showing the facility and its major components.

The arc heater, which was used during this program, operates with a reservoir pressure up to 2 atm and enthalpies up to 70,000 Btu/lb. Nozzles are available which allow consideration of model size and desired pressure and heat-transfer rate levels. A 1.0-inch-diameter throat, 8.0-inch-exit diameter, Mach 6.2 conical nozzle was used for this program.

The test chamber in the facility is approximately 3-feet wide, 5-feet high, and 6-feet in length and allows insertion of up to 7 models per run. The models are attached to water-cooled stings and, in turn, to radial arms which successively translate into the arc-heated gas along a radius perpendicular to the stream. Viewing ports are provided to permit monitoring of the test models with pyrometers and high-speed motion picture cameras.

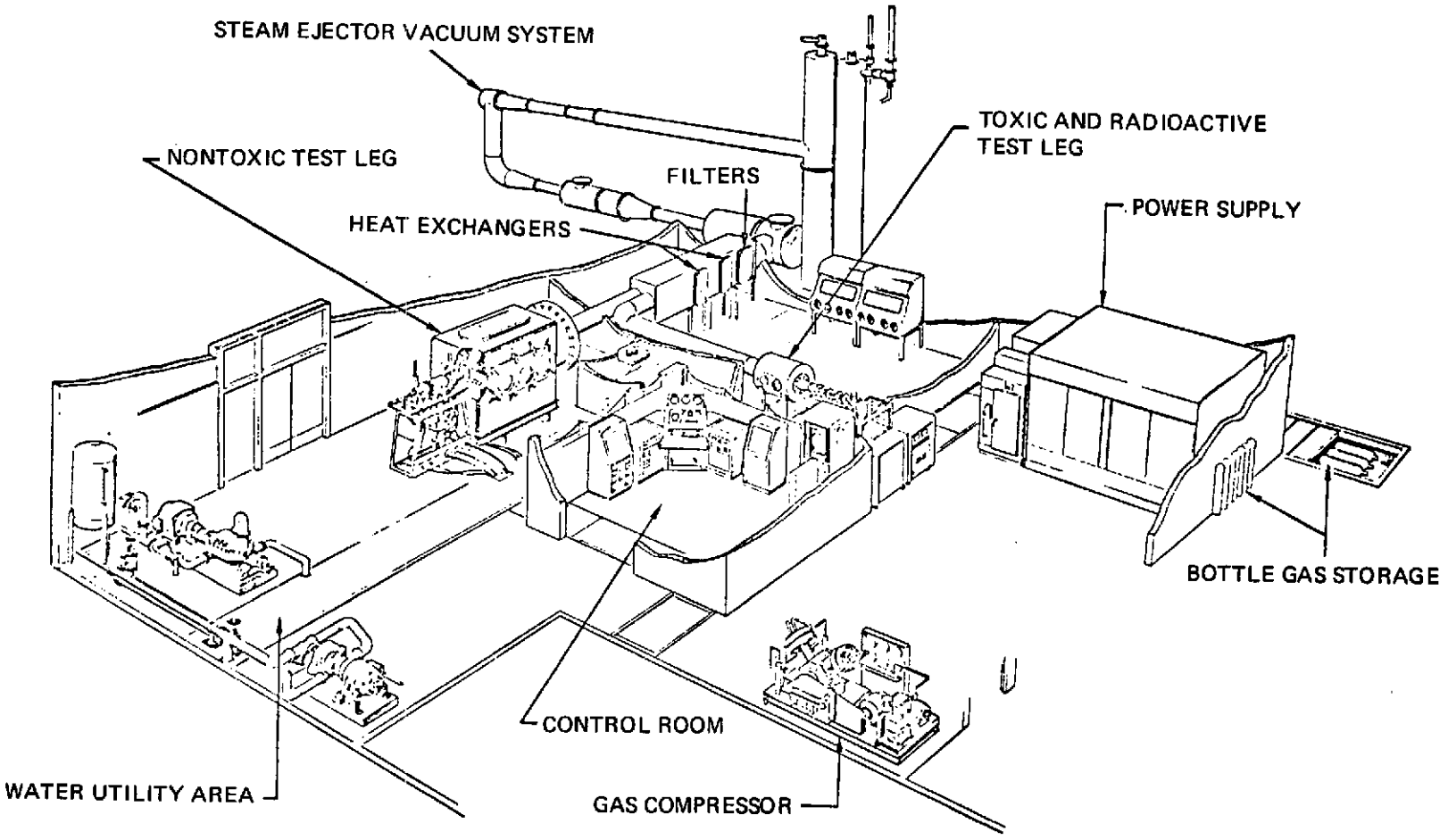

Figure 30. Aerothermal Research Facility at Battelle's Columbus Laboratories

Specimen surface temperatures were measured using two Infrared Industries TD-9H radiation thermometers. These pyrometers have a peak response of 0.80 μm with a filter half width of 0.03μm. The accuracy of the TD-9H pyrometers is 1 percent of the temperature span. Calibrations of the pyrometers were performed and recorded prior to the arc-jet runs. Different emittance settings were used for the pyrometers depending on the emittance of the specimen coating being tested.

The pyrometers were calibrated in place; therefore, signal attenuation due to the test-cabin window and reflecting optics (mirror) is accounted for. Previous calibration data for the test-cabin window attenuation were also used. The calibrations were performed by placing a body of known temperature and surface emittance in the optical path of the pyrometers at the specimen surface location.

Platinum versus platinum plus 10-percent rhodium thermocouples were fabricated into the front surface of the specimens to measure the specimen surface temperatures. A Joseph Kaye instrument was used as a 0°C reference junction for the thermocouples.

Two instrumented calorimeter models were used to measure the cold-wall heat flux and stagnation pressure prior to and following exposure of the CRSI specimens in the test gas. The calorimeter was used during the exposures for controlling the heater operating conditions to obtain the desired heat flux at the specimen surface, since the location of this calorimeter corresponded to that of the surface thermocouples in the specimens. Figure 31 shows the test set-up used.

The initial test plan was to control the arc conditions by monitoring the output of the thermocouple in the specimen. By gradually increasing the arc current until a temperature of 1260°C was registered the re-entry conditions of the GE simulator were to be duplicated. When this was attempted, neither the thermocouple or the optical pyrometers indicated 1260°C until a heat flux of 55 to 70 Btu/ft^2-sec was reached by the arc. At this heating rate several of the models were melted and destroyed. The explanation for this behavior probably lies in the extreme non-uniformity of the temperature generated by the arc. Even though the integrated temperature of the models was probably 1260°C, local areas at the center and edges were probably much hotter.

The remainder of the cycles were monitored by measuring the heat flux in the flow with the calorimeter only. The first 16 cycles were run at a heat flux of 25 to 30 Btu's/ft^2-sec. This was raised to about 35 Btu's/ft^2-sec for the remaining 84 cycles after it was found that the surface temperature was reaching only 870 to 980°C.

3.2.2 RESULTS OF ARC TESTS

A summary of the effects of arc testing on the various models is given in Table X. A description of the conditions encountered are given in Table XI. It was shown in this test that both the DD3 and PB-1 coatings were able to survive 99 cycles at a

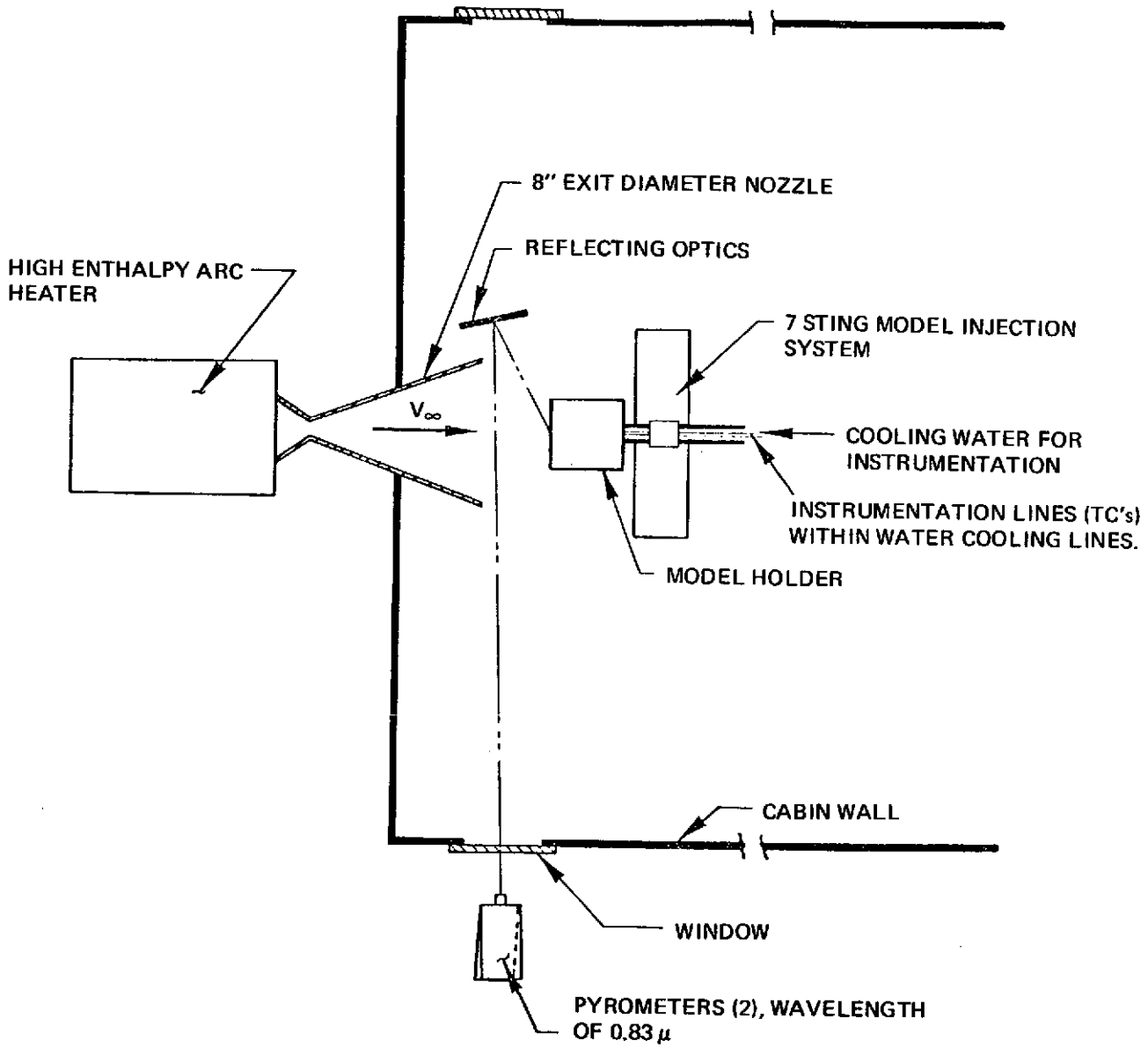

Figure 31. Schematic of Test Set-up

TABLE X. ARC TEST RESULTS

Model Number	Coating	Arc Environment Seen	Results
1	31-D-LA	Premature exposure 60 Btu/ft^2 Then 29 cycles to 30 Btu/ft^2	Cracked after 29 cycles
2	DD-3 Mod. 2	Not tested	
3	DD-3 Mod. 2	Premature exposure 60 Btu/ft^2 Then 29 cycles to 30 Btu/ft^2	Cracked after 29 cycles
4	31-D	Premature exposure 60 Btu/ft^2	Destroyed
5	31-D	Premature exposure 60 Btu/ft^2	Destroyed
6	DD-3 Mod. 2	99 cycles at 30 Btu/ft^2 1 cycle at 60 Btu/ft^2	Survived Waterproof & uncracked
7	31-D-LA	Premature exposure to 60 Btu/ft^2	Coating melted through
8	31-D-HE	Not tested due to faulty I. C.	
9	31-D-LA	Premature exposure to 60 Btu/ft^2	Coating melted through
10	PB-1	99 cycles at 30 Btu/ft^2 1 cycle at 60 Btu/ft	Survived Waterproof & Intact

TABLE XI. ARC CONDITIONS DURING TESTS

Cycle Numbers	Arc Heater Output (kw)	Heater Stagnation Enthalpy Btu/lb	Heater Stagnation Pressure (atm)	Surface Temperatures		Heating Rate Btu/ft^2-sec
				DD-3 (°C)	PB-1 (°C)	
1-16	90	4,000	.006	926	1031	25.5
17-99	134	7,000	.007	1015	1134	32.1
100	263	13,885	.0088	1221	1374	67.7

heat flux of 25-35 Btu's/ft^2-sec and 1 cycle at a heat flux of 60 Btu's/ft^2-sec. Figure 33 shows the time-temperature profile registered by the thermocouple in the DD-3 model during cycle number 17.

Figures 34, 35, 36, 37 and 38 show several of the models before and after cycling in the arc.

As shown in Figures 34 and 35 the behavior of the DD3 coating and the 31D-LA were very similar in the arc. Both coatings withstood an initial exposure to a heat flux of 65 Btu/ft and were then cycled 26 times at the 25-35 Btu level before cracking occurred. The PB-1 and DD-3 coated models that survived 100 cycles in the arc were not given this initial overshoot condition. These facts led to a general suspicion that the 31D coatings and the modified 0042 coatings (DD3 and PB1) were probably of equal resistance to devitrification. It was decided, therefore, that the two coatings that survived 100 re-entry cycles in the plasma arc should be tested in the GE re-entry simulator.

3.2.3 G. E. RE-ENTRY SIMULATOR TESTING OF THE DD-3 AND PB-1 COATINGS

Four 6" x 6" x 2" models were prepared and coated, two with DD-3 and two with the PB-1 coating. These models were installed in the GE re-entry simulator using the same time-temperature-pressure parameters used for the 31D and 27B systems tested earlier.

A set of flexure and impact specimens were made up along with the simulator models and these were aged at 1260°C for 16 hours to simulate the total time at maximum temperature in 100 cycles.

3.2.4 RESULTS OF THE G. E. RE-ENTRY SIMULATOR TESTS ON OPTIMIZED COATINGS

The DD-3 models both survived the initial 20 cycles in the simulator but cracked noticeably after 40 cycles as shown in Figures 39 and 40. These cracks and the crack pattern shown are similar to those found in the unpigmented 27B and 31D coatings being highly visible. The SEM photomicrographs of the DD-3 coating shown in Figure 41 show that there is no swelling or bloating of the coating. The cracks in the coating are much more numerous than indicated by the 100X image shown in Figure 41 and as the higher magnification (1000X) of Figure 42 shows, many cracks have begun to form at the coating fiber interface.

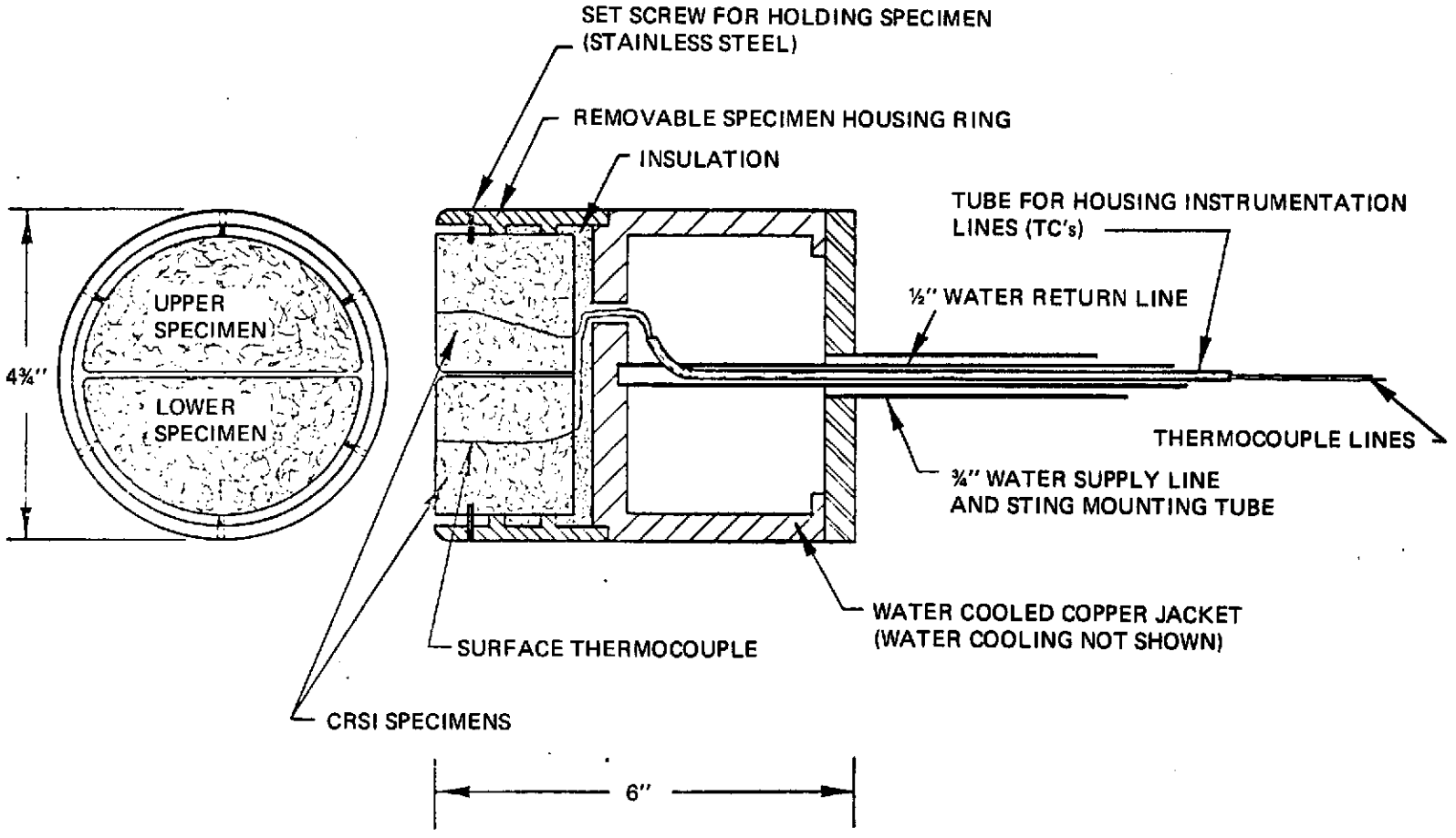

Figure 32. Specimen Holder

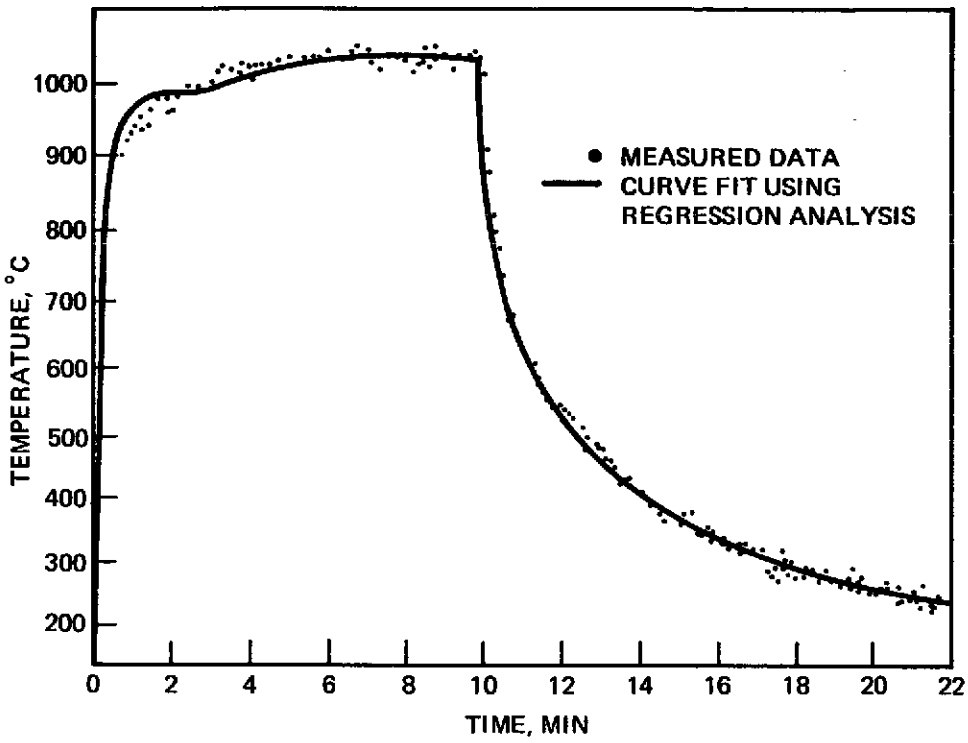

Figure 33. Time-Temperature Profile for DD-3 Model During Arc Cycle to 35 Btu/ft^2-Sec.

The PB-1 coatings began to shrivel noticeably after 20 cycles but did not crack until after 60 cycles in the simulator. Figures 43 and 44 show the appearance of the two models before and after cycling. The shriveling is very pronounced on both models after 60 cycles, however, the cracking is limited to a few hairline cracks. The uncracked areas on the coating are still waterproof as evidenced by the water droplets standing on the surface. The SEM photomicrographs shown in Figure 45 show that no bloating or bubbling of the coating has occurred after cycling and that most indications of cracking are isolated on the coating fiber interface. A higher magnification (1000X) of the coating-fiber interface after 60 cycles is shown in Figure 46. This shows that further cracking has started and would probably have generated further surface cracking if additional cycling had been performed.

Table XII shows the effect of aging or cycling on the properties of the coatings. The aged DD-3 flexure specimens were so badly cracked after aging that they could not be tested to give any meaningful data. As with the 31D and 27B coatings the effect of aging on impact strength is negligible.

The effect of aging is to devitrify the coating on the coating-fiber interface causing severe weakening and eventual cracking of both coatings.

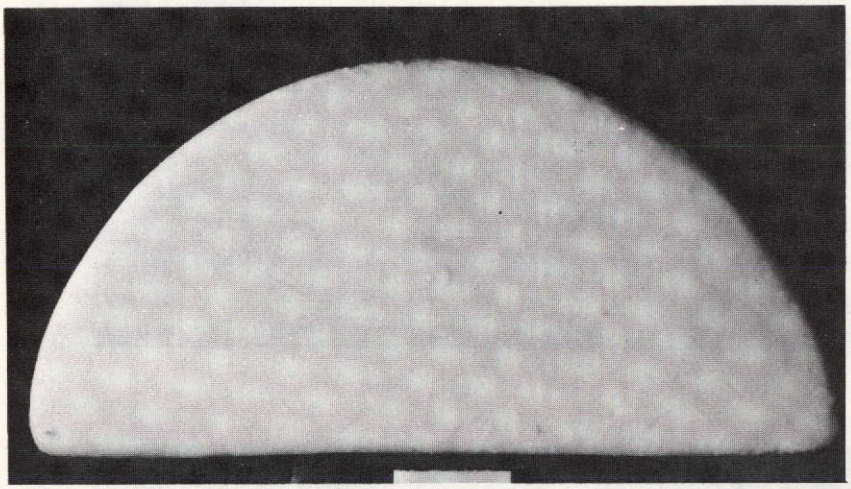

As Fabricated

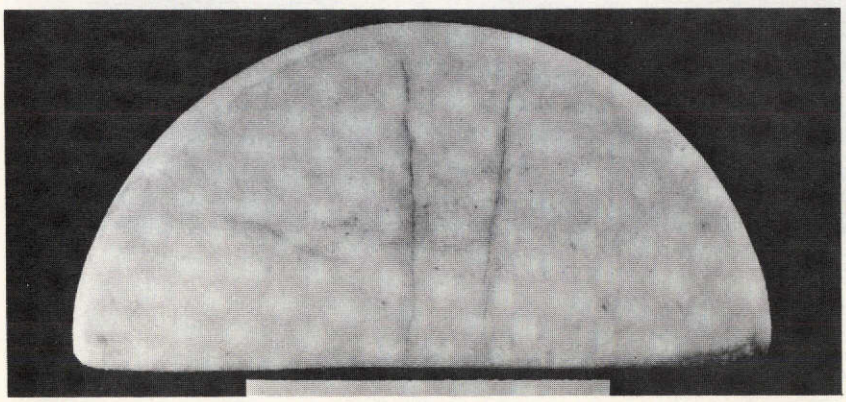

After 29 Re-entry
Cycles

Figure 34. Arc Model Number 1 as Fabricated and after 29 Re-entry Cycles

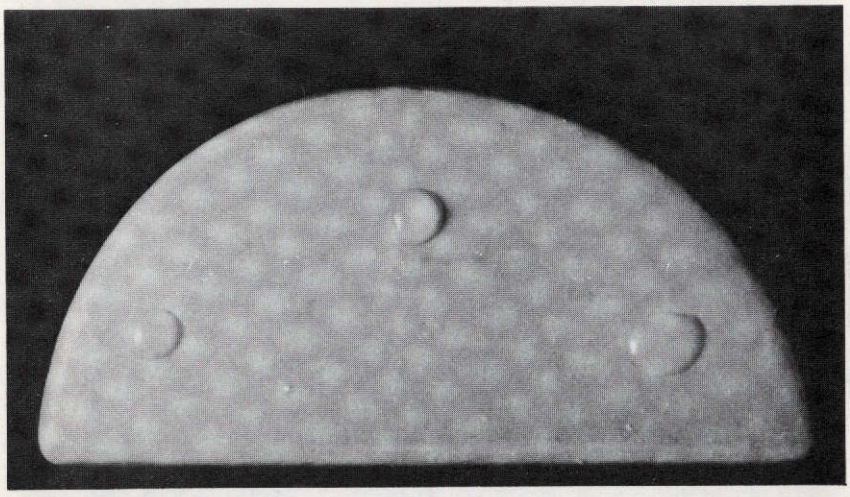

As Fabricated

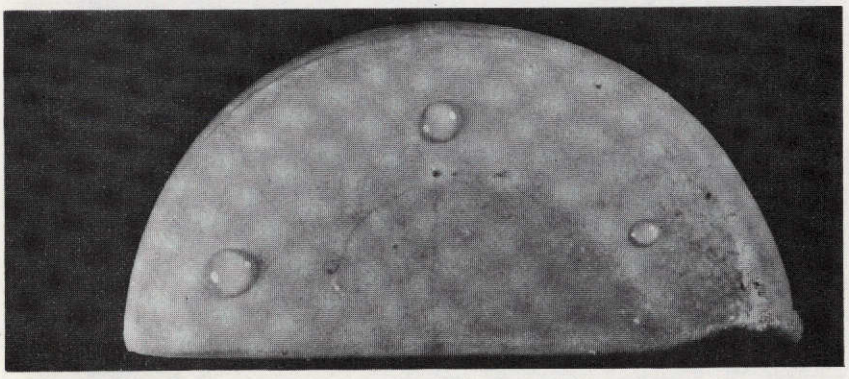

After 29 Cycles

Figure 35. Arc Model Number 3 as Fabricated and after 29 Re-entry Cycles

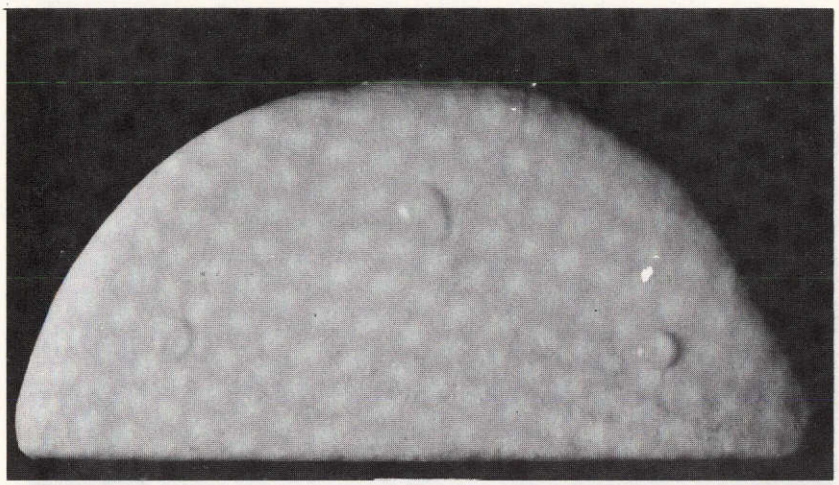

As Fabricated

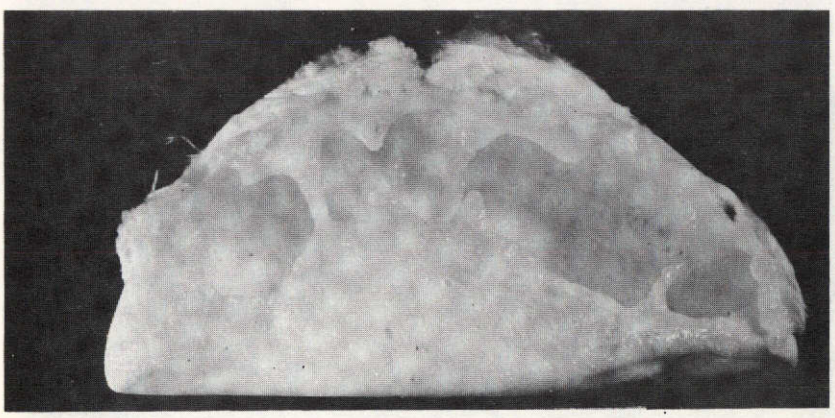

1 Cycle to 65 BTU/ft.^{2} sec

Figure 36. Arc Model Number 7 after a Single Exposure to 65 Btu/ft^2-sec Heat Flux. The thermocouple was destroyed and testing discontinued in under 5 minutes. Models 4, 5, and 9 were destroyed in a similar manner.

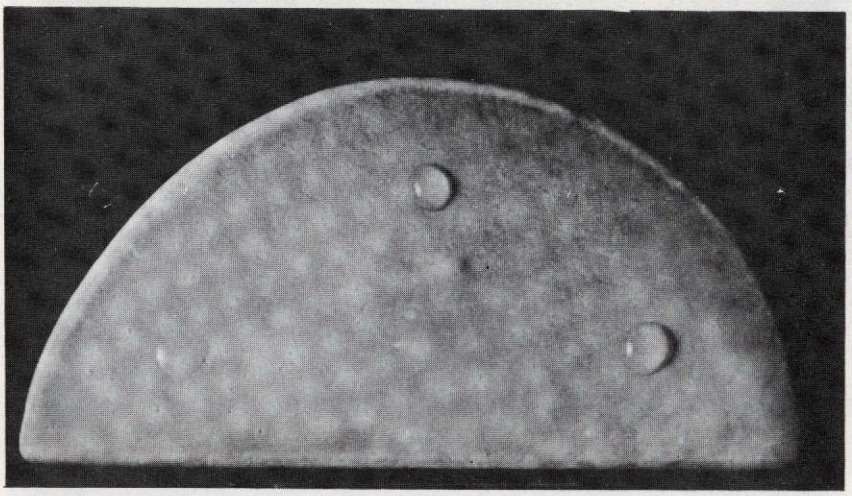

As Fabricated

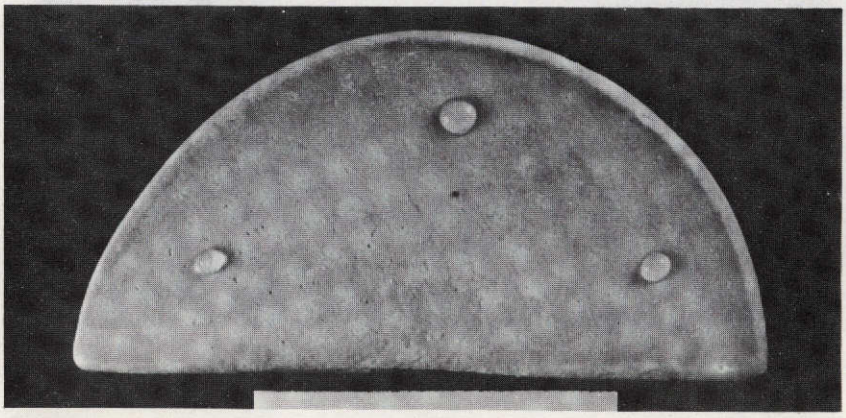

After 100 Cycles
to 30 BTU/ft.^{2} sec

Figure 37. Arc Model Number 6 as Fabricated and after 100 Reentry Cycles

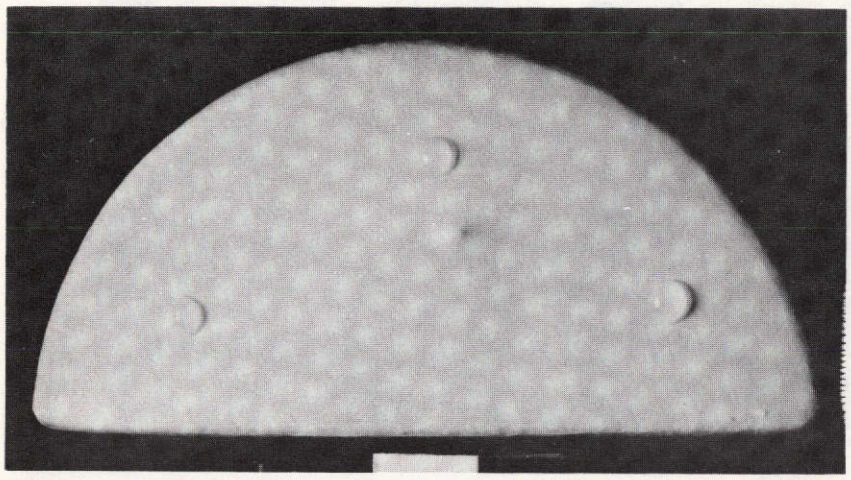

As Fabricated

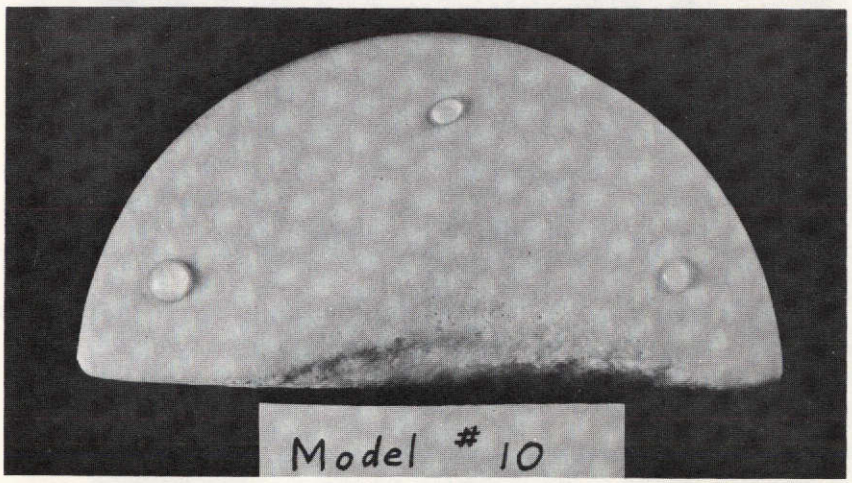

After 100 Cycles
to 30 BTU/ft.^{2} sec

Figure 38. Arc Model Number 10 as Fabricated and after 100 Re-entry Cycles

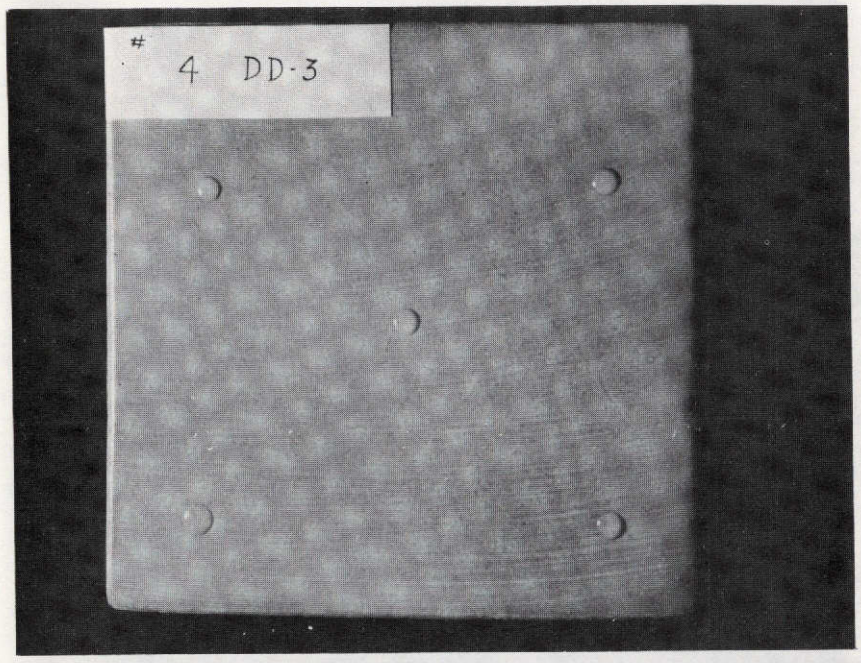

As Fabricated

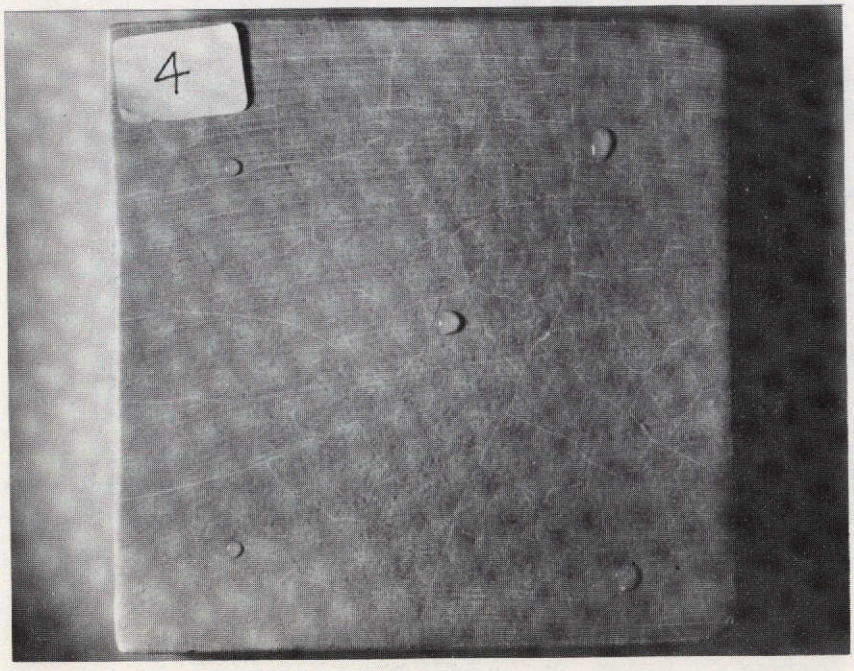

After 40 Cycles

Figure 39. Re-entry Simulator Model No. 2 DD-3 Coating before and after Cycling in G. E. Re-entry Simulator

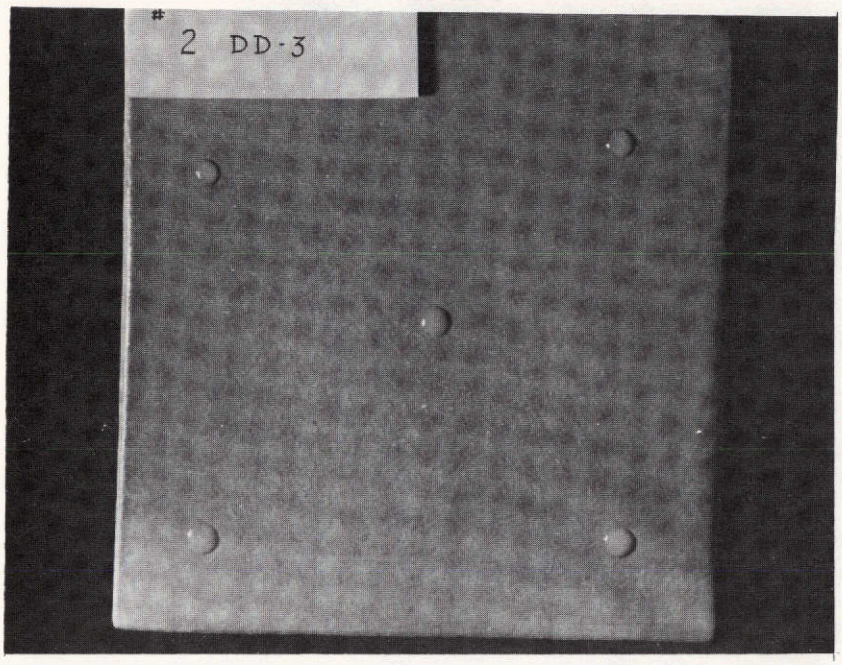

As Fabricated

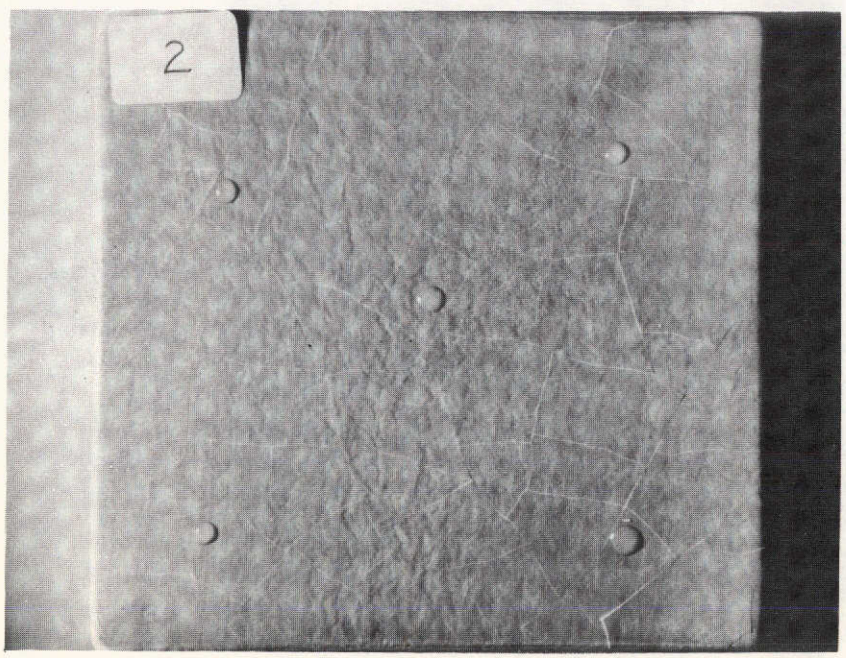

After 40 Cycles

Figure 40. G. E. Re-entry Simulator Model No. 4 DD-3 Coating before and after Cycling in G. E. Re-entry Simulator

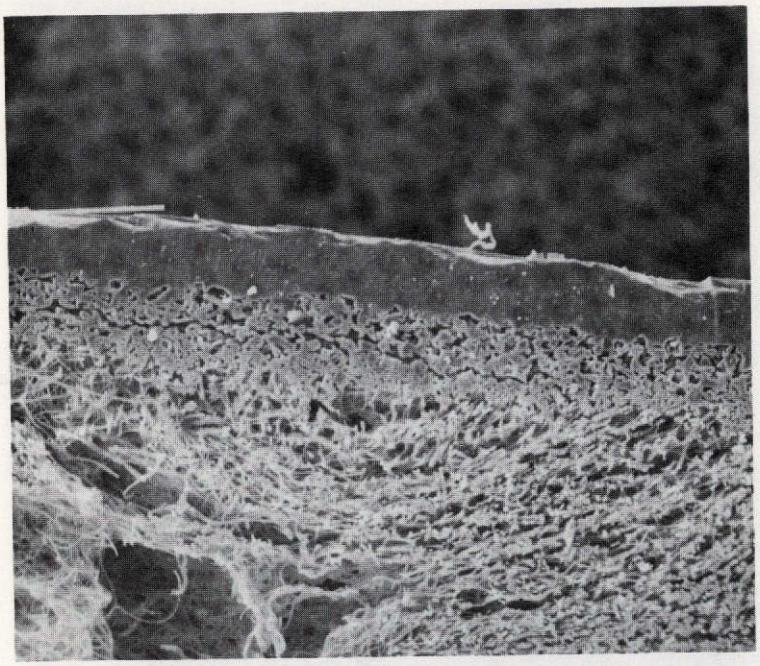

As
Fabricated
(100X)

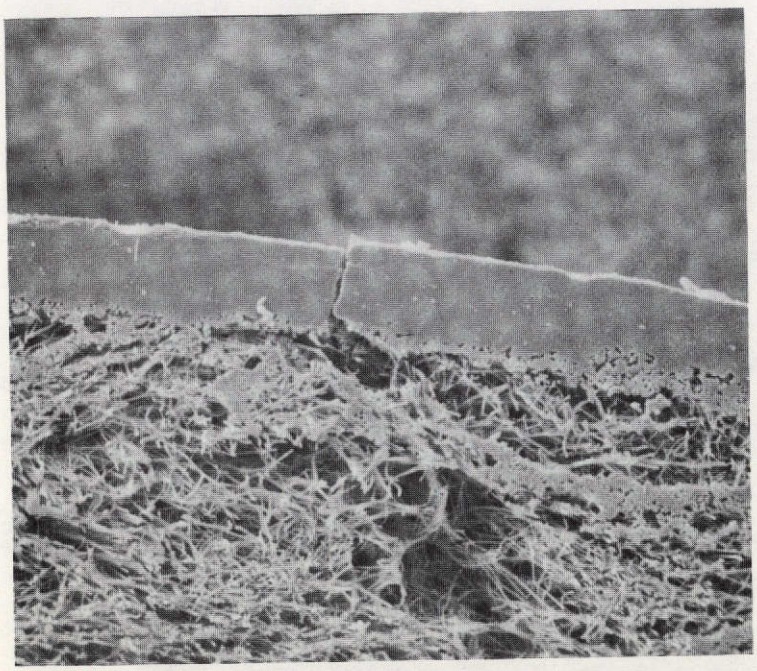

After
40 Cycles
in
Simulator
(100X)

Figure 41. SEM's of DD-3 Coating before and after Cycling in G. E. Re-entry Simulator

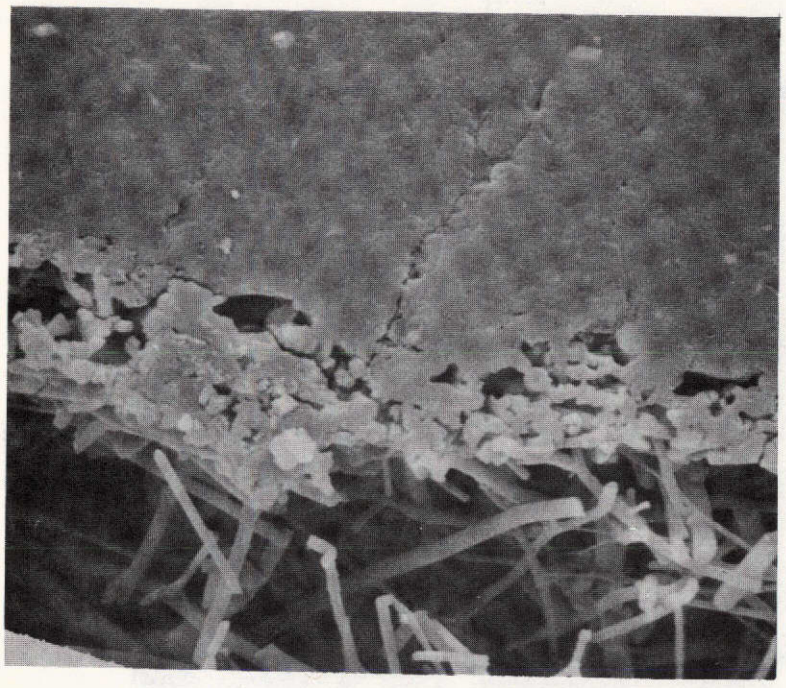

Figure 42. Coating-Fiber Interface of DD-3 Coating after 40 Cycles in Simulator (1000X)

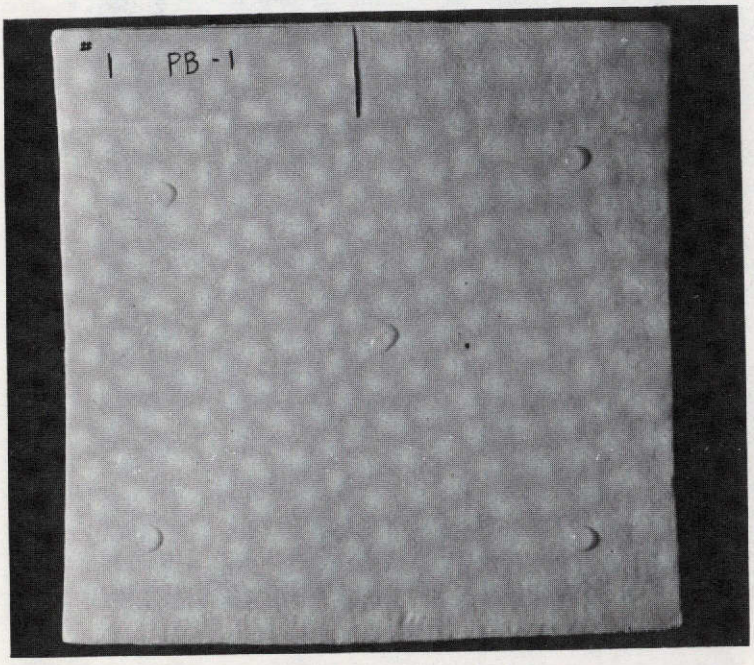

As
Fabricated

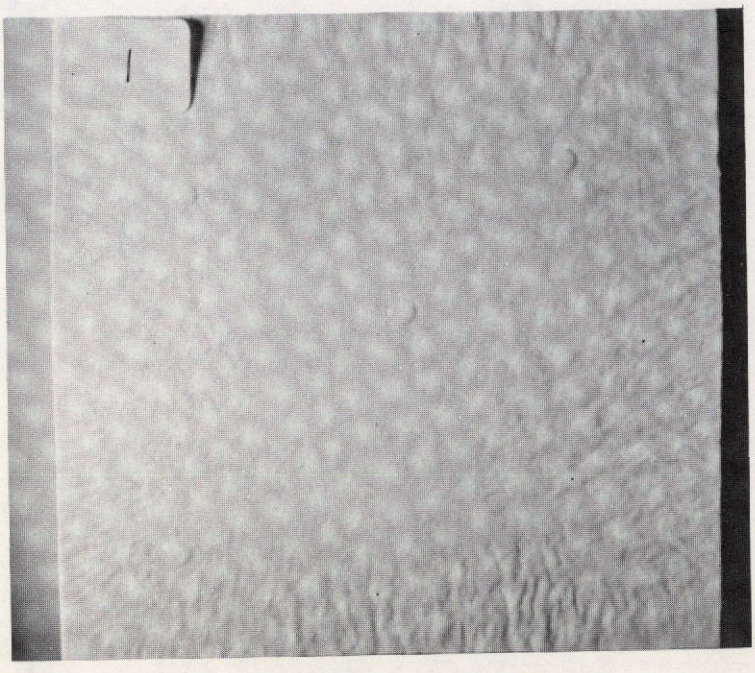

After
60
Cycles

Figure 43. Re-entry Simulator Model No. 1 PB-1 Coating before and after Cycling in G. E. Re-entry Simulator

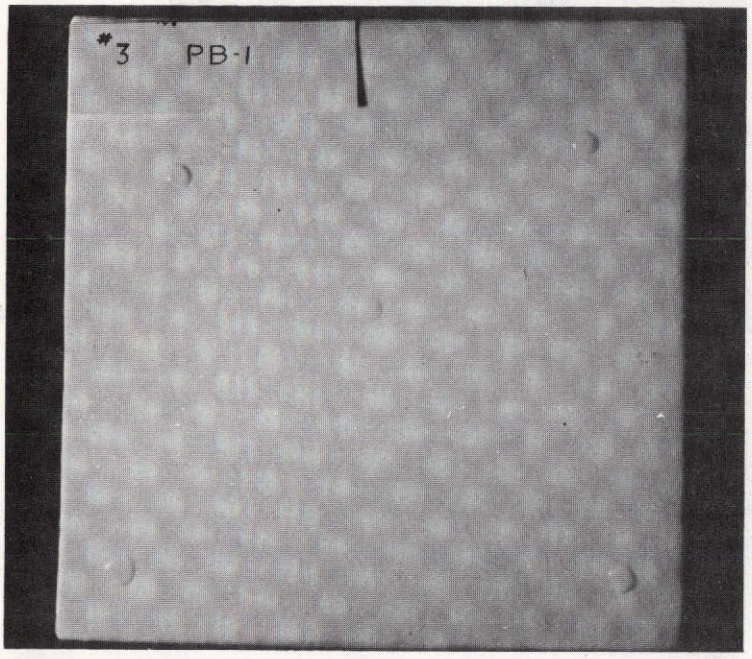

As
Fabricated

After
60
Cycles

Figure 44. G. E. Re-entry Simulator Model No. 3 PB-1 Coating before and after Cycling in G. E. Re-entry Simulator

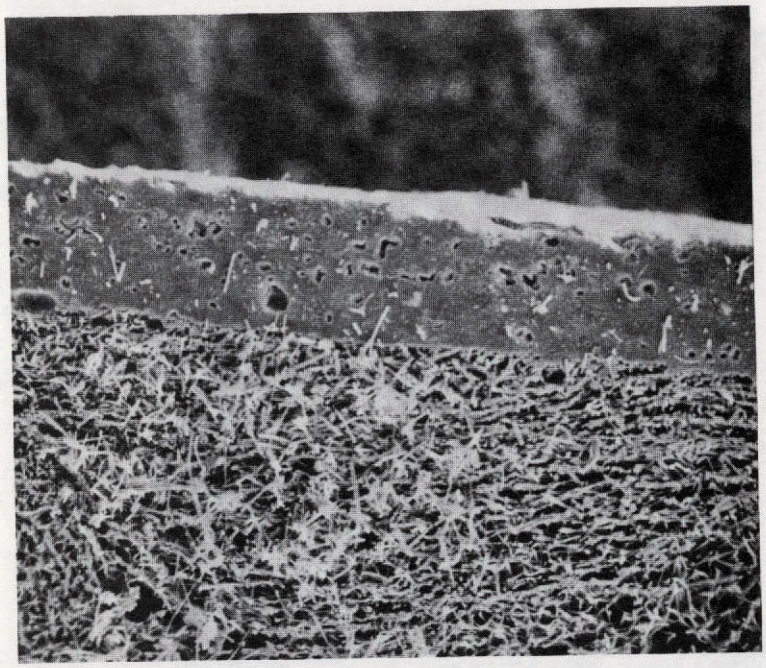

As
Fabricated
(100X)

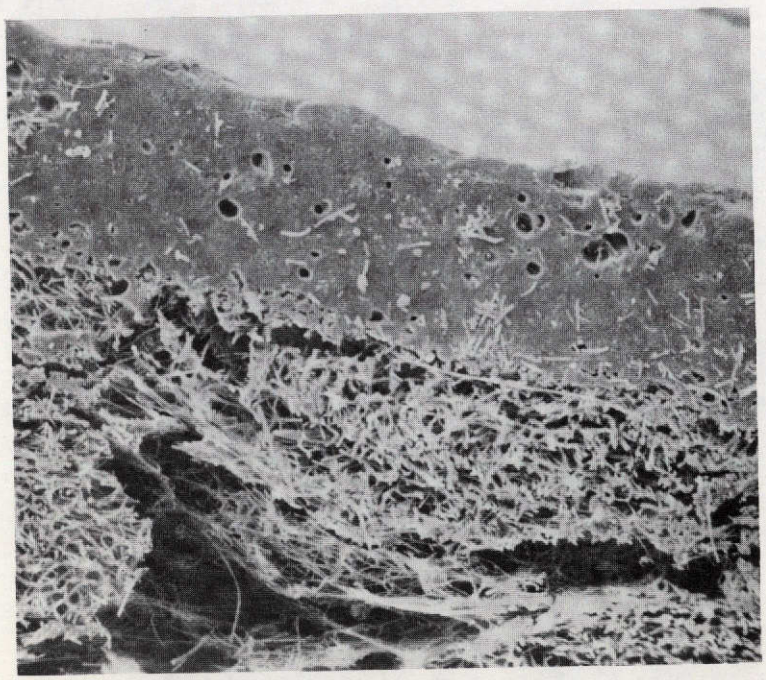

After 60
Cycles in
Simulator
(100X)

Figure 45. SEM's of PB-1 Coating before and after Cycling in G. E. Re-entry Simulator

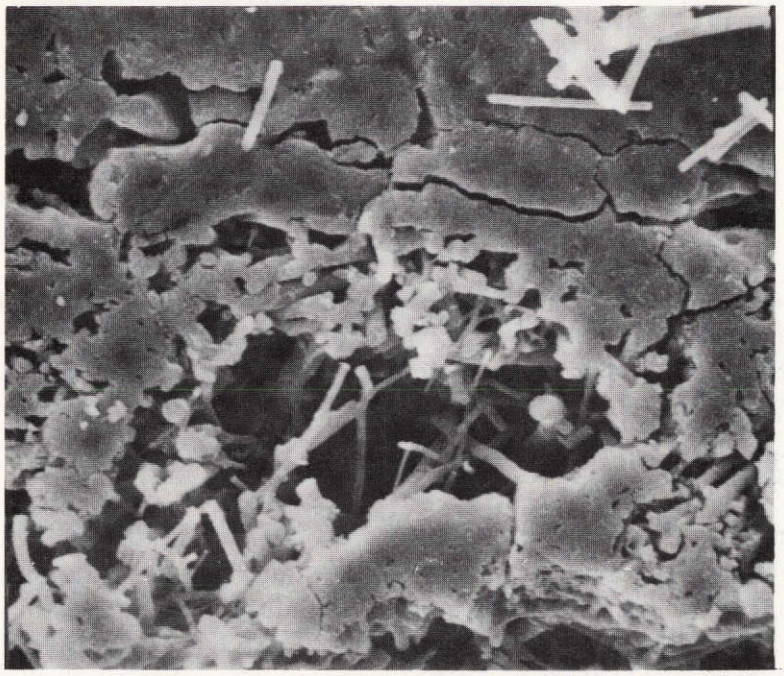

Figure 46. Coating-Fiber Interface of PB-1 Coating after 60 Cycles in G. E. Simulator (1000X)

TABLE XII. RESULTS OF G. E. RE-ENTRY SIMULATION TESTS ON OPTIMIZED COATINGS

Coating	Environmental Conditioning	Impact Strength	Tensile Strength	Volume Percent Cristo-balite	Moisture Permeability
DD-3	As-Fabricated	.61 Kg-m (40 in-lbs)	2.61×10^7 N/M^2 (3790 psi)	0	Waterproof
	Aged 16 hrs. @ 1260°C	.41 Kg-m (35.2 in-lbs)	Specimens Cracked	46	Cracked
	After 40 cycles in Simulator			36	Cracked
PB-1	As-Fabricated	.42 Kg-m (36.8 in-lbs)	3.35×10^7 N/M^2 (4860 psi)	0	Waterproof
	Aged 16 hrs. @ 1260°C	.41 Kg-m (35.6 in-lbs)	1.45×10^7 N/M^2 (2110 psi)	39	Waterproof
	After 60 cycles in Simulator			31	Cracked

SECTION 4

COATING PROPERTY DATA

The pre- and post-exposure test coating metallography, chemistry, and visual examinations are summarized previously in the report. The following discussions give the procedures and detailed data of the physical and mechanical property tests.

4.1 IMPACT STRENGTH

The impact strength of the models was run on a one-inch diameter load pad that was progressively impacted at 0.23 Kg-M (2 inch-lb) intervals until damage was visible on the coating surface. Twenty models were made with each coating, ten of which were thermally aged, the other ten were tested as fabricated. Table XIII shows the individual results for all the materials tested.

This data shows that thermal aging has little effect on the impact strength. This is to be expected since the impact strength is dependent on the modulus of the coating and substrate plus the compressibility of the substrate. The loss of tensile strength has little effect on the impact strength.

The unusually high strength of the 27B-U coating is due to the coating being unusually heavy. The coating is roughly twice as thick as the other specimens tested which accounts for the fourfold increase in impact strength.

4.2 TENSILE PROPERTY DETERMINATIONS

Tensile strength, elastic modulus and failure strain of coatings were determined from four point bending test results. The test specimen used for these tests, shown in Figure 47 is a symmetric (coated on both sides) beam. The equal coating thickness on both sides of the specimen results in the neutral plane of the beam being located at the center of the CRSI thickness. This configuration results in equal and opposite stresses in the two coating layers and greatly simplifies data reduction. Since the total CRSI thickness is large compared to the coating thickness, the coating tensile stress is reasonably uniform through its thickness and the four point loading configuration insures uniform stress between the two load application points. The large length-to-depth ratio was selected such that coating tensile failure would occur prior to CRSI shear failure.

TABLE XIII. IMPACT STRENGTH OF COATINGS

27B-U				27B-P			
As-Fabricated		Aged 2 hrs @ 1260° C		As-Fabricated		Aged 2 hrs @ 1260° C	
Kg-M	(psi)	Kg-M	(psi)	Kg-M	(psi)	KG-M	(psi)
.35	(30)	.65	(56)*	.13	(12)	.18	(16)
.60	(52)	.48	(42)	.12	(10)	.18	(16)
.46	(40)	.53	(46)	.12	(10)	.16	(14)
.71	(62)	.42	(36)	.14	(12)	.12**	(10)
.48	(42)	.71	(62)	.12	(10)	.12**	(10)
$\bar{X}$ .52	(45.2)	.56	(48.4)	.13	(10.8)	.15	(13.2)
SD .13	(10.9)	.11	(9.4)	.01	(1.0)	.03	(2.7)
31D-U				31D-P			
As-Fabricated		Aged 2 hrs. @ 1260° C		As-Fabricated		Aged 2 hrs @ 1260° C	
Kg-M	(psi)	Kg-M	(psi)	Kg-M	(psi)	Kg-M	(psi)
.12	(10)		(20)	.18	(16)	.16	(14)
.21	(18)		(12)	.23	(20)	.16	(14)
.16	(14)		(12)	.14	(12)	.14**	(12)
.14	(12)		(14)	.12	(10)	.12	(10)
.18	(16)		(14)	.18	(16)	.14	(12)
$\bar{X}$ .16	(14.0)		(14.4)	.17	(14.8)	.14	(12.4)
SD .03	(2.8)		(2.9)	.04	(3.5)	.02	(1.5)
DD-3				PB-1			
As-Fabricated		Aged 16 hrs @ 1260° C		As-Fabricated		Aged 16 hrs @ 1260° C	
Kg-M	(psi)	Kg-M	(psi)	Kg-M	(psi)	Kg-M	(psi)
.42	(36)	.32	(28)	.48	(42)	.32	(28)
.60	(52)	.51	(44)	.42	(36)	.53	(46)
.42	(36)	.42	(36)	.51	(44)	.44	(38)
.45	(39)	.46	(40)	.35	(30)	.35	(30)
.43	(37)	.30	(26)	.37	(32)	.42	(36)
$\bar{X}$ .46	(40.0)	.41	(35.2)	.42	(36.8)	.41	(35.6)
SD .07	(6.1)	.08	(6.7)	.06	(5.5)	.07	(6.4)

*Coatings were roughly twice as thick as the other specimens.
**Cracked from aging — Number indicates first additional damage from impact

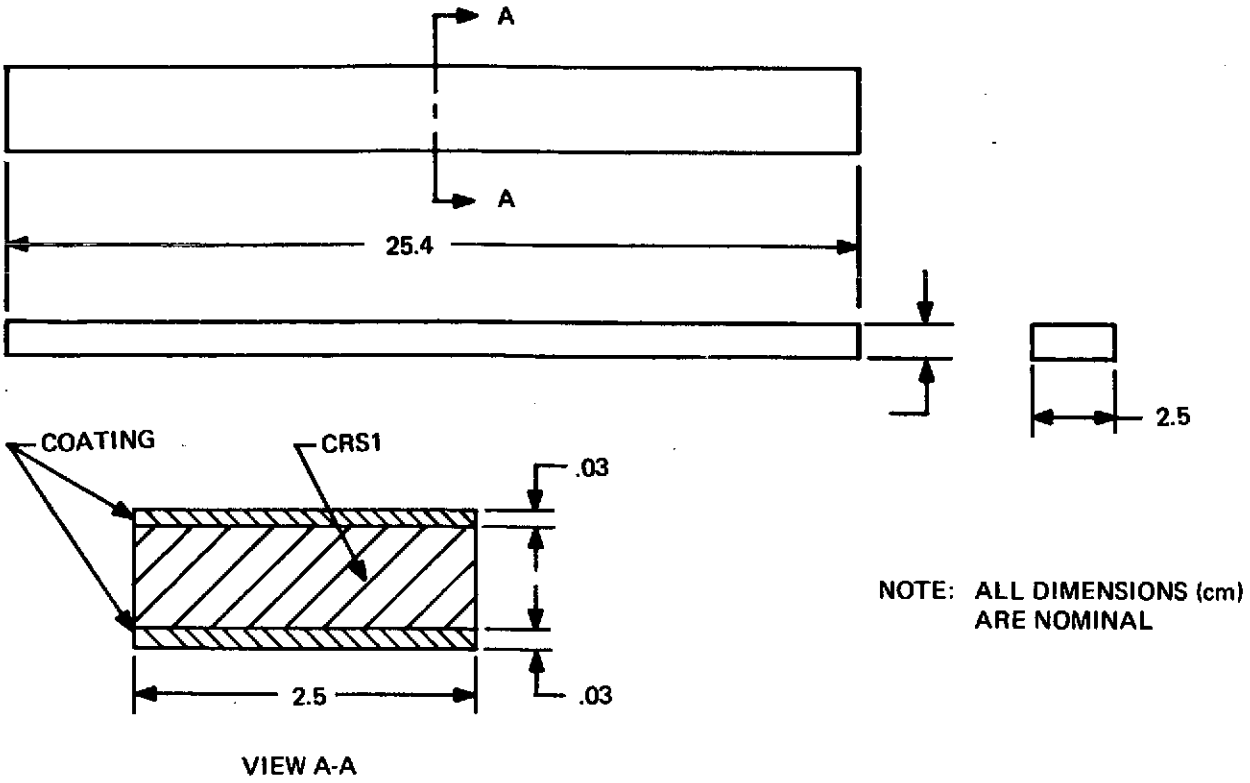

Figure 47. Bend Test Specimen for Coating Tensile Property Determinations

The test set-up used for these measurements is shown in Figure 48. Rubber pads 0.32 cm thick were used between the test specimen and the load and support points to avoid localized damage to the brittle coating. All tests were performed at a constant crosshead speed of 1.27 cm/min. This seemingly high testing speed was required to overcome deformation in the protective rubber pads.

One bonded, metal-foil strain gage was installed at the center of each coated face of each test specimen to obtain coating strain data directly. During test, the output of each strain gage was recorded, independently, as a function of applied load on XYY (dual pen) recorder.

Most of the tests were performed with 20.32 cm support span and a 10.16 cm load span. However, several of the test specimens were warped to the extent that a 10.16 cm support span was necessary in order to obtain a uniform test section. In these cases, a 5.08 cm load span was used.

Cross specimen thickness and width measurements were made prior to test. Coating thickness measurements on both the tension and compression faces of the beam were made after test at or near the point of failure with a filar eye piece microscope.

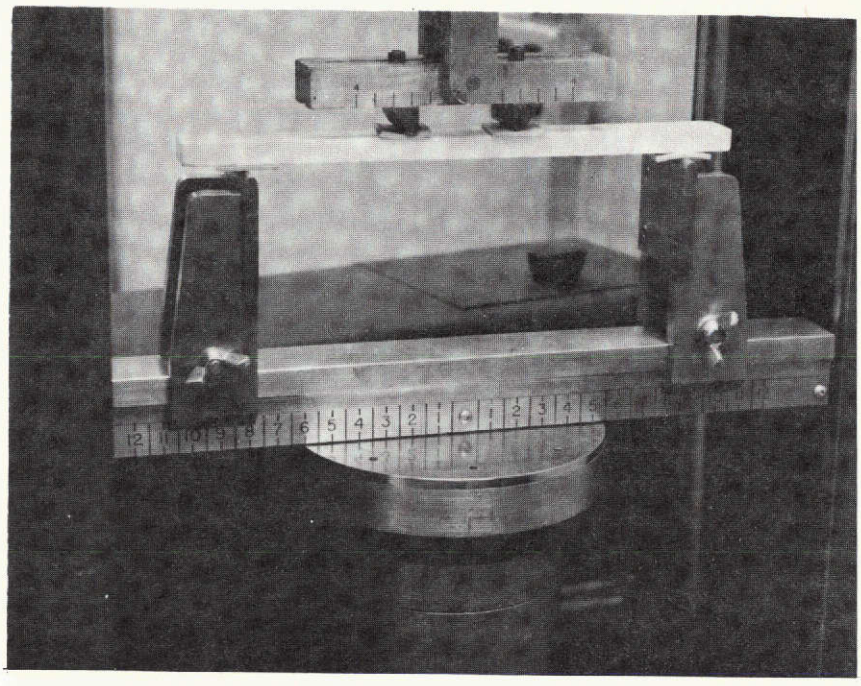

Figure 48. Bend Test Set-Up for Coating Tensile Property Determinations

(NOTE: 0.32 cm thick rubber pads between specimen and load support points)

Test loads were reduced to coating stress values using formulae derived from first principles of mechanics with the equal coating thickness assumption. Unfortunately, however, the post-test measurements showed that this assumption was not valid for many of the test specimens. The actual measured thickness values are reported with the reduced test data so that ultimate strength and elastic modulus data for test specimens where a significant coating thickness difference exists can be interpreted accordingly.

Failure strain measurements, on the other hand, are considered accurate since strain measurements were made directly using bonded strain gages.

All test results are presented in Table XIV including summary statistics for each group of test specimens.

The data shows that all of the coatings tested degrade on aging losing about half their strength. The DD-3 and PB-1 coatings have on initial coating strength of about 2.76×10^7 N/M^2 which is roughly twice the accepted value for JSC-0042.

TABLE XIV. COATING MECHANICAL PROPERTY DATA REDUCED FROM BEND TEST RESULTS

Coating	Specimen (No.)	Support Span (cm)	Coating Thickness, cm		Ultimate Strength ($N/M^2 \times 10^{-9}$)	Tensile Modulus ($N/M^2 \times 10^{-12}$)	Compression Modulus ($N/M^2 \times 10^{-12}$)	Failure Strain (%)
			Tension	Compression				
PB-1 (As-Fabricated)	7	20.3	.021	.018	29.3	1.35	1.10	.030
	8	20.3	.023	.023	43.9	1.33	.99	.048
	9	20.3	.019	.021	27.0	1.34	1.39	.021
	10	10.2	.024	.024	40.0	1.17	1.03	.040
	11	20.3	.023	.021	31.1	1.19	1.11	.028
	13	10.2	.023	.024	29.9	1.27	1.01	.028*
	$\bar{X}$				33.5	1.28	1.10	.032
	SD				6.7	.080	.015	.0098
PB-1 (Aged 16 hrs @ 1260°C)	1	10.2	.023	.027	15.7	.67	.54	.026
	12	10.2	.021	.021	13.3	.68	.74	.020
	$\bar{X}$				14.5	.68	.64	.023
	SD				1.7	.017	.14	.0042
DD-3 (As-Fabricated)	2	20.3	.010	.010	19.4	1.18	**	.016
	3	20.3	.008	.009	30.5	1.50	1.29	.021
	4	10.2	.010	.010	22.3	1.30	1.16	.020
	5	10.2	.010	.009	26.6	**	.79	.041*
	6	20.3	.008	.009	31.8	1.42	1.70	.020
	$\bar{X}$				26.1	1.35	1.23	.023
	SD				5.3	.14	.38	.011
31-D Unpigmented (Aged 90 min. @ 1260°C)	17	20.3	.012	.013	12.6	.42	.48	.035
	30	20.3	.018	.013	11.6	.57	.71	.0231
	35	20.3	.017	.013	12.9	.59	.51	.028
	39	20.3	.010	.010	11.7	.45	.45	.068
	40	20.3	.010	.013	17.9	.38	.33	.047
	$\bar{X}$				13.3	.48	.50	.040
	SD				.26	.09	.14	.018

TABLE XIV. COATING MECHANICAL PROPERTY DATA REDUCED FROM BEND TEST RESULTS (Continued)

Coating	Specimen (No.)	Support Span (cm)	Coating Thickness, cm		Ultimate Strength ($N/M^2 \times 10^{-9}$)	Tensile Modulus ($N/M^2 \times 10^{-12}$)	Compression Modulus ($N/M^2 \times 10^{-12}$)	Failure Strain (%)
			Tension	Compression				
	1	20.3	.013	.015	8.4	.29	.21	.034
31-D	5	20.3	.020	.018	10.7	.24	.20	.050
Unpigmented	11***	20.3	.017	.023	7.4	.31	.18	.026
	21	20.3	.023	.015	5.9	.17	.42	.053
(Aged 90 min.	26	20.3	.030	.030	3.6	.09	.09	.045
@ 1260°C)	$\overline{X}$				7.6	.21	.17	.015
	SD				4.6	.09	.065	.0353
	15	20.3	.020	.019	9.4	.48	.50	.026
31-D	19	20.3	.033	.026	13.7	.38	.39	.040
3% SiC	28	20.3	.028	.030	12.5	.34	.26	.003
	32	20.3	.023	.023	12.6	.52	.49	.024
(As Fabricated)	37	20.3	.027	.030	16.6	.46	.48	.0162
	$\overline{X}$				13.0	.44	.42	.0218
	SD				2.6	.08	.10	.0136
	2	20.3	.024	.027	7.0	.15	.12	.030
31-D	6	20.3	.024	.018	2.5	.06	.11	.059
3% SiC	7	20.3	.023	.013	6.9	.12	.23	.062
	10	20.3	.018	.026	8.1	.25	.15	.036
(Aged 90 min.	25	20.3	.019	.023	7.6	.29	.21	.027
@ 1260°C)	$\overline{X}$				7.3	.23	.17	.028
	SD				.46	.08	.07	.0022
	16	20.3	.015	.012	16.5	.53	.84	.030
27-B	20	20.3	.012	.012	28.0	.58	.54	.050
Unpigmented	29	20.3	.015	.013	15.4	.66	.67	.026
	33	20.3	.012	.011	15.9	.58	.71	.029
(As-Fabricated)	38	20.3	.010	.013	14.1	.70	.61	.022
	$\overline{X}$				18.3	.63	.63	.0318
	SD				6.5	.06	.07	.0125

TABLE XIV. COATING MECHANICAL PROPERTY DATA REDUCED FROM BEND TEST RESULTS (Continued)

Coating	Specimen (No.)	Support Span (cm)	Coating Thickness, cm		Ultimate Strength ($N/M^2 \times 10^{-9}$)	Tensile Modulus ($N/M^2 \times 10^{-12}$)	Compression Modulus ($N/M^2 \times 10^{-12}$)	Failure Strain (%)
			Tension	Compression				
	3	20.3	.013	.068	11.0	.27	.20	.042
27-B	9	20.3	.015	.019	7.2	.26	.18	.030
Unpigmented	13	20.3	.019	.015	7.2	.17	.27	.048
(Aged 90 Min.	24	20.3	.020	.017	8.2	.20	.17	.060
@ 1260°C)	34	20.3	.016	.012	7.5	.23	.39	.037
	$\overline{X}$				8.8	.25	.19	.044
	SD				2.0	.04	.02	.015
	14	20.3	.010	.015	9.4	.48	.50	.026
27-B	18	20.3	.006	.008	25.9	.56	.45	.046
3% SiC	31	20.3	.008	.011	13.2	.71	.20	1.45
(As-Fabricated)	36	20.3	.013	.011	16.6	.46	.48	.0160
	$\overline{X}$				17.3	.50	.48	.029
	SD				8.2	.053	.03	.0153
	4	20.3	.013	.010	5.9	.14	.17	.038
27-B	8	20.3	.011	.018	8.9	.17	.15	.047
3% SiC	12***	20.3	.012	.013	5.3	.21	.07	.018
	22	20.3	.013	.017	6.3	.12	.10	.052
(Aged 90 min.	23***	20.3	.015	.010	4.7	.10	.20	.0425
@ 1260°C)	$\overline{X}$				6.2	.15	.11	.045
	SD				1.6	.04	.06	.0089

* Approximated by linear extrapolation
** Strain Gage Failure
*** Specimen visibly cracked before testing

4.3 MOISTURE PERMEABILITY

The moisture permeability of the coatings was tested by placing a drop of distilled water on the surface of the coating and allowing it to stand for 5 minutes. If the water did not spread of soak into the coating after 5 minutes it was considered waterproof. All of the flexure test bars, impact specimens, re-entry simulator models, and arc test models were tested for moisture permeability before and after aging tests. These results are shown along with the other tests corresponding to the appropriate data. Except for occasionally underfired individual specimens, all the coatings discussed in this report were waterproof.

4.4 THERMAL CONDUCTIVITY

Due to the difficulty in making an appropriate specimen it was not possible to measure thermal conductivity before and after thermal aging. The measurements were made on 2.54 cm diameter specimens which were made by mixing dry powders with approximately 20 weight percent parafin binder. This mixture was dry pressed into a 3.2 cm diameter by 1.3 cm thick pellet which was subsequently calcined at 760°C for one hour and fired at 1370°C for 30 minutes. Thermal conductivity curves for coatings 27-B and 31-D are shown in Figure 49.

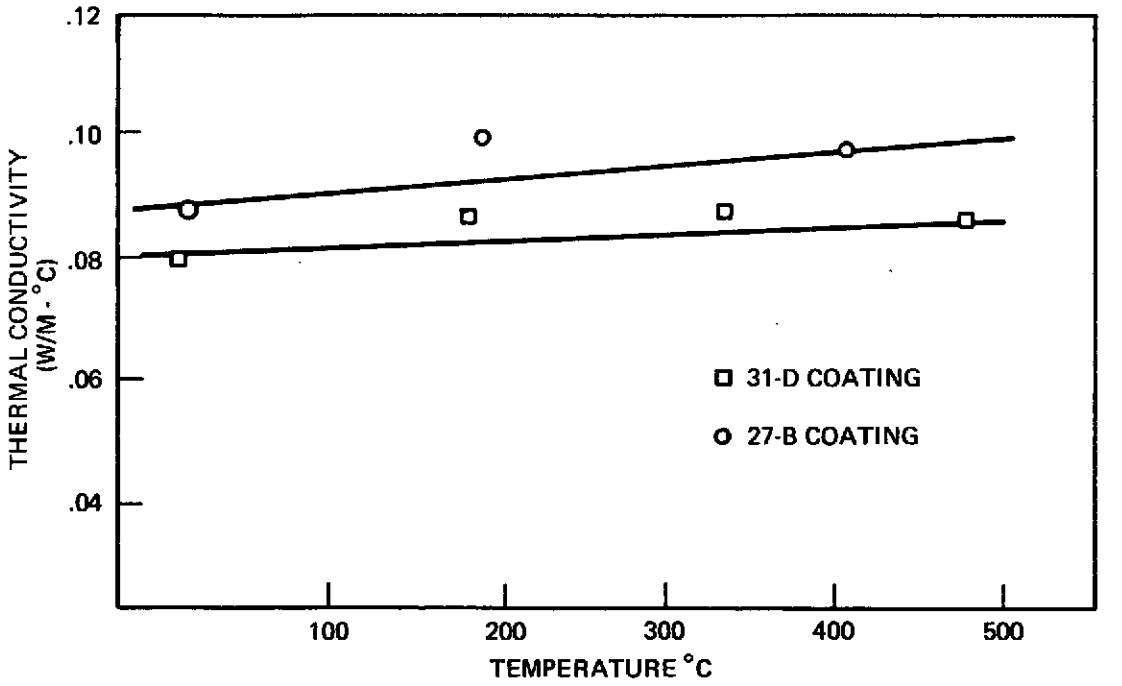

Figure 49. Thermal Conductivity of 27B and 31D Coatings

The measurements were performed on the one inch diameter comparator cut-bar facility in its short stack mode, using 1.3 cm thick heat meter thermal conductivity standards of Corning 7740 Pyrex glass.

The data points fit a straight line to well within 10%, characteristic of an amorphous (glassy) ceramic whose thermal conductivity function is dominated by short range boundary scattering. No radiation transmission effects are apparent in the data, which is the anticipated result since the materials are formulated to have high infrared emittance, therefore low transmittance.

4.5 THERMAL EXPANSION

In order to measure thermal expansion a specimen 5.1 x .3 x .6 cm had to be fabricated. Since all of the coatings were graded with a high boron layer, a densifier and a final coat, there was no practical way of making a representative sample. The individual bodies that make up the coating and tiles were measured by pressing a 5.5 x 2.5 cm diameter pellet from the precursor powders using a paraffin binder. The pellets were fired at 1370°C for 30 minutes and then machined into test bars 5.1 x .3 x .6 cm. These bars were tested in a quartz tube dilatometer.

The thermal expansion curve for the 31-D formulation is shown in Figure 50. The thermal expansion coefficients of various other low expansion high silica bodies is shown in Figure 51.

4.6 OPTICAL PROPERTIES

The solar absorptance of all of the coatings was measured using an Absolute Directional Integrating Sphere Reflectometer. The solar absorptance is calculated from the spectral reflectance using the following relationship:

$$\alpha_s = 0.002 \Sigma (1 - \rho_i)$$

where:

α_s is the solar absorptance

ρ_i is the spectral reflectance at intervals corresponding to two percent of the solar spectrum

The room temperature emittance was determined using a heated cavity reflectometer. The emittance is calculated for specific temperatures based on the expected reflectance of a perfect blackbody at that temperature.

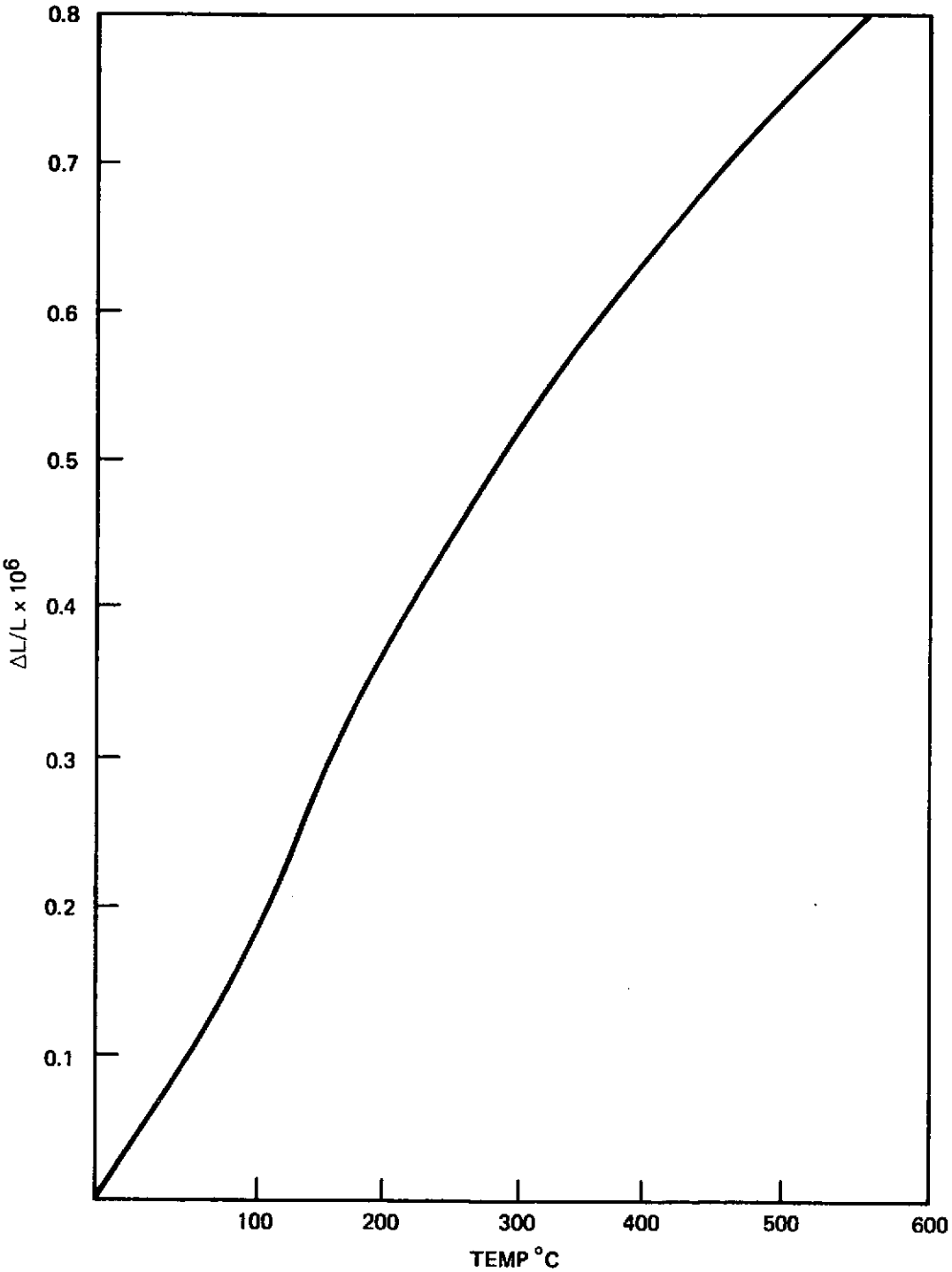

Figure 50. Thermal Expansion of Formulation 31-D

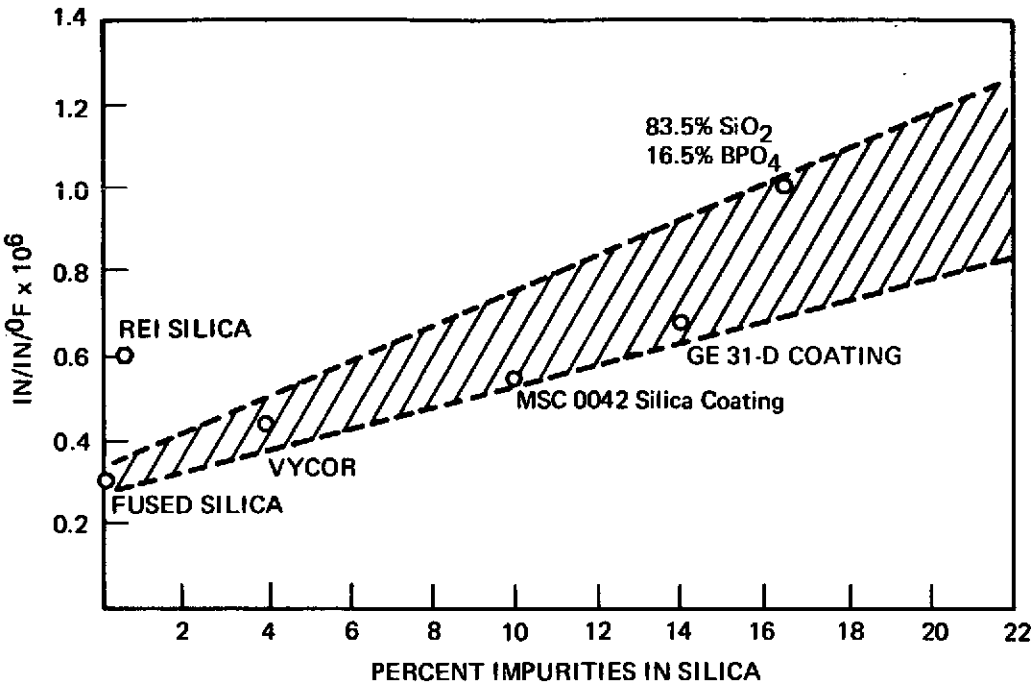

Figure 51. Thermal Expansion of High Silica Bodies

The emittance at 1100°C was determined from the total reflective data and also by measuring the total emitted radiation directly in a push rod comparator. This technique utilizes a radiometer to view a specimen along the axis of a cylindrical furnace. The specimen is mounted on a push rod, which is used to move the specimen from the center of the furnace. During measurements the output of the radiometer is plotted as a function of time with an oscillograph recorder as the sample is quickly moved from the position at the center of the furnace to the position at the end. The radiometer observes blackbody radiation, a radiant power level of E_{BB}, from the sample when the sample is at the center of the long tube furnace, regardless of the emittance of the sample because the furnace core and sample plug constitute a blackbody cavity. When the sample is moved to the end of the furnace, the radiant power observed by the radiometer drops to a value of ϵ_N. E_{BB} since only the self-emitted power from the sample is then observed. Hence, the total normal emittance of the sample, ϵ_N, is the ratio of the radiometer output with the sample at the end of the furnace to the radiometer output with the sample at the center of the furnace. The ϵ_H is calculated from ϵ_N by the observed empirical relationship between those material properties.

The radiometer used is a specially designed and modified Leeds and Northrup type 8891-C high speed "Ray O-Tube" total radiation pyrometer. The front window of the pyrometer is replaced with a calcium fluoride window in order to increase the transmitted wavelength band to the required limit.

4.7 SCANNING ELECTRON MICROSCOPE (SEM) ANALYSIS

Top and side views of the various coatings evaluated were made with a scanning electron microscope. The top views were made with little sample preparation necessary. The side views, however, required tedious preparation to obtain an undisturbed cross section. The coating samples were cut from the model to be analyzed with about 0.5-1.0 cm of fibers still attached. The sample was then immersed in a vial of methyl methacrylate monomer, catalyzed with 3 wt. percent benzoyl peroxide. The vial was sealed and the methacrylate allowed to cure for several days at room temperature. The now impregnated sample was then cut to about 0.6 cm thick and the surfaces ground and polished using standard metallographic techniques.

Since the scanning electron microscope cannot see through the methyl methacrylate, the polished section was heated in a closed retort to burn the resin out. The specimens were then coated with a gold-palladium coating and inspected in the SEM. These procedures were used to produce all of the photomicrographs shown in the reentry simulation discussions.

No significant results were observed from examination of any of the top views. They all looked essentially like the view shown in Figure 52.

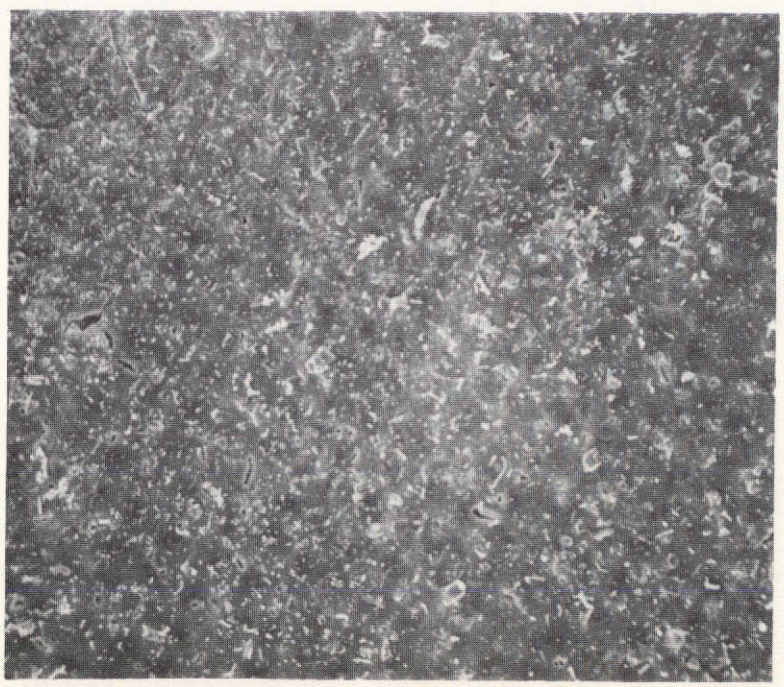

Figure 52. SEM Photomicrograph of 31-D Coating. Top View (100X)

4.8 X-RAY DIFFRACTION ANALYSIS

The x-ray diffraction analysis used to evaluate the coatings was designed to determine the cristobalite content at the coating-fiber interface. The coatings were cut into 2.5 cm square specimens and the fibers were removed from the back surface with 600 grit sandpaper. If the coating was too weakened by aging or cycling to be made into a free standing slab, it was glued onto an aluminum plate prior to removing the fibers. This specimen was mounted into the sample holder of a diffractometer with the back surface exposed to the x-ray beam.

The x-ray source was a copper x-ray tube using a nickel filter and scintillation counter detector. The amount of cristobalite present was determined by measuring the linear intensity of the Bragg reflection off the $<111>$ crystal plane of cristobalite ($d = 7.04$ Å). This intensity was compared to a 100% cristobalite standard, which was made by soaking the fibers in a 5% sodium chloride solution and firing at 1430°C for one hour. All x-ray data given in the coating formulation and re-entry simulation sections of this report was obtained in this manner.

SECTION 5

DISCUSSION OF RESULTS

The results of the coating exposure tests show that there are some anomalies in the coating systems. It is interesting to note that the unpigmented 31-D and 27-B coatings did not crack when they were aged in the vacuum furnace while the coatings pigmented with SiC cracked frequently. When these coatings were cycled in the G.E. re-entry simulator however, it was the pigmented coatings that evolved as the most stable. The silicon carbide pigment, therefore, has both a beneficial and a deleterious effect on the coatings, i.e., the bloating and expanding of the glassy matrix caused by its reaction with silicon carbide during aging causes the general deterioration of the coating. The beneficial effect of the pigment is its ability to absorb a great deal of the radiant energy of the re-entry simulator thereby reducing the temperature of the coating-fiber interface where all the cracking appears to occur.

Another anomaly from the coating exposure tests is the surprisingly high level of devitrification of the coatings when aged at 1260°C and at reduced pressure. During the coating formulation studies it was found that aging the unpigmented coatings in air at 1260°C for 16 hours produced little or no devitrification. Aging in vacuum or reduced pressure caused a much more rapid devitrification rate than aging in air.

The impact strength studies on all of the coatings except the double thick 27-B coating show that aging effects in the coating cannot be detected by a change in the impact strength.

The tensile strengths of the various coatings were all degraded by aging in a vacuum. The aged tensile properties of the DD-3 coating are not given due to an accidental loss of these specimens during their removal from the furnace. Note that the tensile strength of both the DD-3 and PB-1 coatings is about twice the published value of 13.8×10^6 N/M^2 for JSC-0042.

The x-ray diffraction results of the 27-B and 31-D coatings after thermal aging in reduced pressure show that the degree of devitrification in these coatings is much higher than that of the DD-3 or PB-1 coatings. The tensile strength data on these aged coatings shows that both underwent a similar degree of degradation. This indicates that the effects of devitrification on the physical properties of the 31-D and 27-B coatings may not be as severe as for the DD-3 and PB-1 system. This possibility has been expressed by Horn and Hummel (Ref. 1) who have indicated that the volume expansion of the alpha-to-beta cristobalite transition can be reduced by substituting BPO_4 into the cristobalite lattice.

The results of the plasma arc test indicate that the DD-3 and PB-1 coatings are fairly stable in the environment which they encountered. A 25 Btu/ft^2-sec heat flux is expected to heat a fully catalytic surface to a temperature of 1260° C. The fact that the surface temperatures indicated by the model thermocouple and the optical pyrometers were significantly below 1000° C at this heat flux level shows that both surfaces are non-catalytic. The effective emittances of the PB-1 and DD-3 coatings were 0.6 and 1.0 respectively. Figure 53 shows the re-entry cycle that was originally established by NASA/Lewis to verify the capability of these coatings. Time and budget considerations, however, made the alternate square wave cycling profile far more practical to run. As the Figure shows, the alternate exposure generates in less time and in fewer cycles the equivalent to 100 anticipated cycles because with each cycle it produces both longer times at higher temperatures and a more severe thermal shock than the anticipated re-entry cycle. This indicates that both the DD-3 and PB-1 coatings may have withstood 100 of the originally proposed re-entry cycles.

Although a plasma arc test is designed to give the most realistic simulation possible of the heat and flow conditions during re-entry, it is an extremely sophisticated and expensive technique which goes far beyond the scope of this study. Due to the extremely limited resources available for this program only existing hardware (nozzles, model holders, calorimeters, etc.) could be used. It was, therefore, not possible to establish a uniform temperature of 1260° C on the surface of the models in the arc. The best nozzle available gave a gradient of 22 percent in the absolute temperature across the face of the model. This accounts for the melting of several of the models when the arc was being monitored by the surface temperature alone. Local heating at the edges of the model probably exceeded 1600° C at the heat flux levels that were experienced. The decision was made to run the arc at 25 Btu/ft^2-sec as this is the heat flux anticipated in re-entry. After cycling the models for 15 cycles at this level and obtaining surface temperatures well below 1000° C the arc current was raised to bring the heat flux to 35 Btu/ft^2-sec bringing the surface temperature closer to the 1260° C temperature desired for coating exposure evaluation.

The early destruction of most of the arc models prevented any comparative data from being generated on the various coatings in the arc. Considering these factors it is not possible to draw any definite conclusions from the arc tests run and all data given in this or the Battelle report (Ref. 2) should be considered as extremely preliminary.

The tests did point out several important considerations which should be considered for further testing to make any future test results truly meaningful:

1. Careful design of an appropriate arc nozzle, expansion chamber and model configuration should preclude any testing to assure front face temperature uniformity to within ±2% maximum.

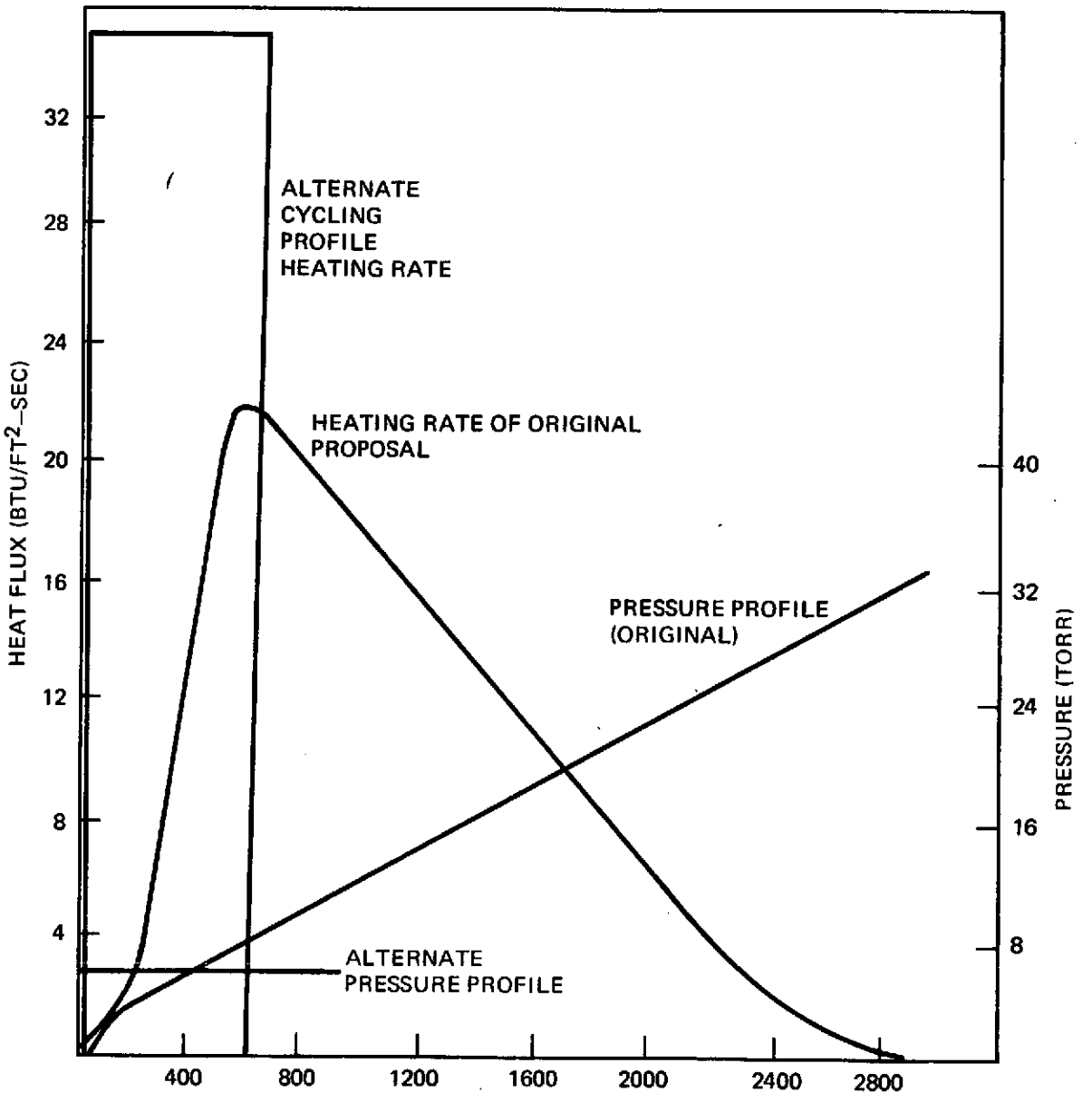

Figure 53. Proposed and Actual Time-Temperature-Pressure Profiles

2. Comparative testing of a baseline material should be run on several models so that a material's behavior in the arc can be compared to a known material.

3. A procedure for running the test should be standardized and fully checked out on standard materials before any attempt is made to evaluate an experimental material.

4. In order to use the arc as a truly useful developmental tool, it should be used continuously during coating development activity as a means of measuring the progress of coating evolution. A program of at least three and preferably four separate test series is essential to truly understand a material's behavior in the arc and be able to tailor its properties to perform properly.

5. If the arc is to be used as a proof positive test to show that a coating is completely developed and ready for application to prime hardware, a complete specification should be prepared for the test describing the details of the equipment to be used, the size and shape of the models, the specific test parameters and the exact criteria for passage or failure of the coating.

A limiting problem exists with the present attempts to stabilize silica based coatings with oxide impurities. The silica fibers used to form the tiles are essentially pure silica and any diffusion of these oxide impurities into the fibers will undoubtedly create a situation of unfavorable stoichiometry. This situation will eventually cause inevitable devitrification. A possible approach to the problem would be to use fibers in the tile which are of the same composition as the coating. It has been shown in Section 2.3 of this report that a number of materials exist which are more resistant to devitrification than pure fused silica. Figure 54 shows fibers made from the 31-D coating slip indicating that it is possible to make both coatings and fibers from materials in the SiO_2-B_2O_3-BPO_4 ternary system.

The G.E. re-entry simulator results shown in Tables VII and XI are significant when compared to the results of GE's space shuttle proposal efforts on the 0042 coating (Ref. 3). The original 0042 coating when applied by GE in accordance with the JSC specification (Ref. 4) was not able to survive 5 cycles in the GE re-entry simulator. Figure 55 shows one of these tiles, a later version of the 0042 coating was, therefore formulated in which the 7940 silica used for the densifier was replaced with Vycor (Corning 7913). This modification produced a coating capable of withstanding 20 cycles in the simulator. Figure 56 shows one of these tiles after 20 cycles. Simply treating the surface with boric acid prior to coating, replacing the Vycor with a 96% 7940 - 4% B_2O_3 slip, and eliminating the silicon carbide from the coating formulation, a coating (PB-1) capable of withstanding 40 cycles in the GE re-entry simulator has been made.

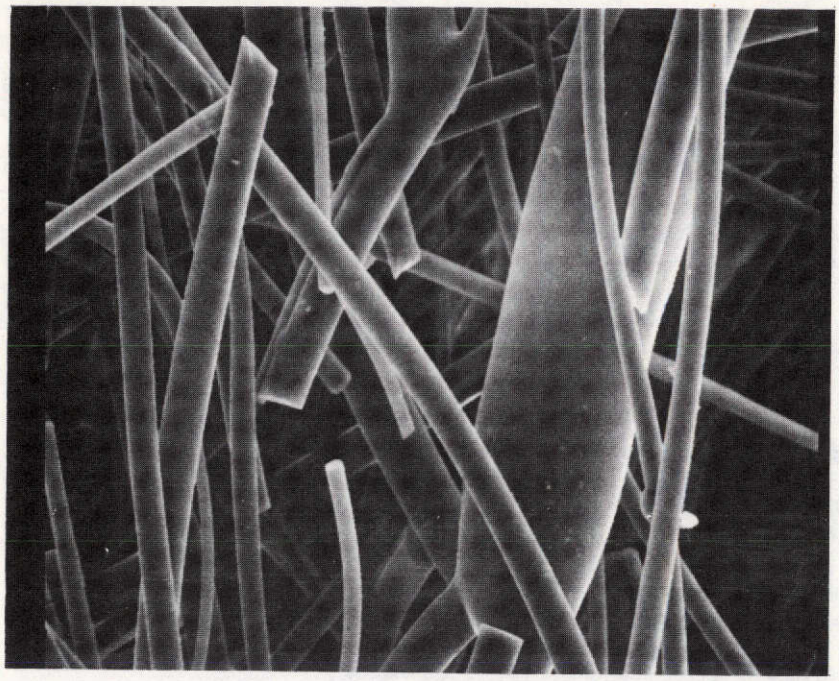

Figure 54. Fibers Blown from #31-D Coating Slip (300 X)

The fact that the PB-1 coating behaved similarly to the 31-D-P coating in the G.E. re-entry simulator indicates that the PB-1 body formed from the two commercial glasses (Corning Codes 7913 and 7740) is inherently resistant to devitrification. This indicates that even though the PB-1, DD-3, and 0042 coatings contain small amounts of alkalies and alkaline earth oxides they may still be as resistant to devitrification as the 31-D system which contains no alkalies whatever. Table XIV shows the comparative chemical compositions of the various coatings.

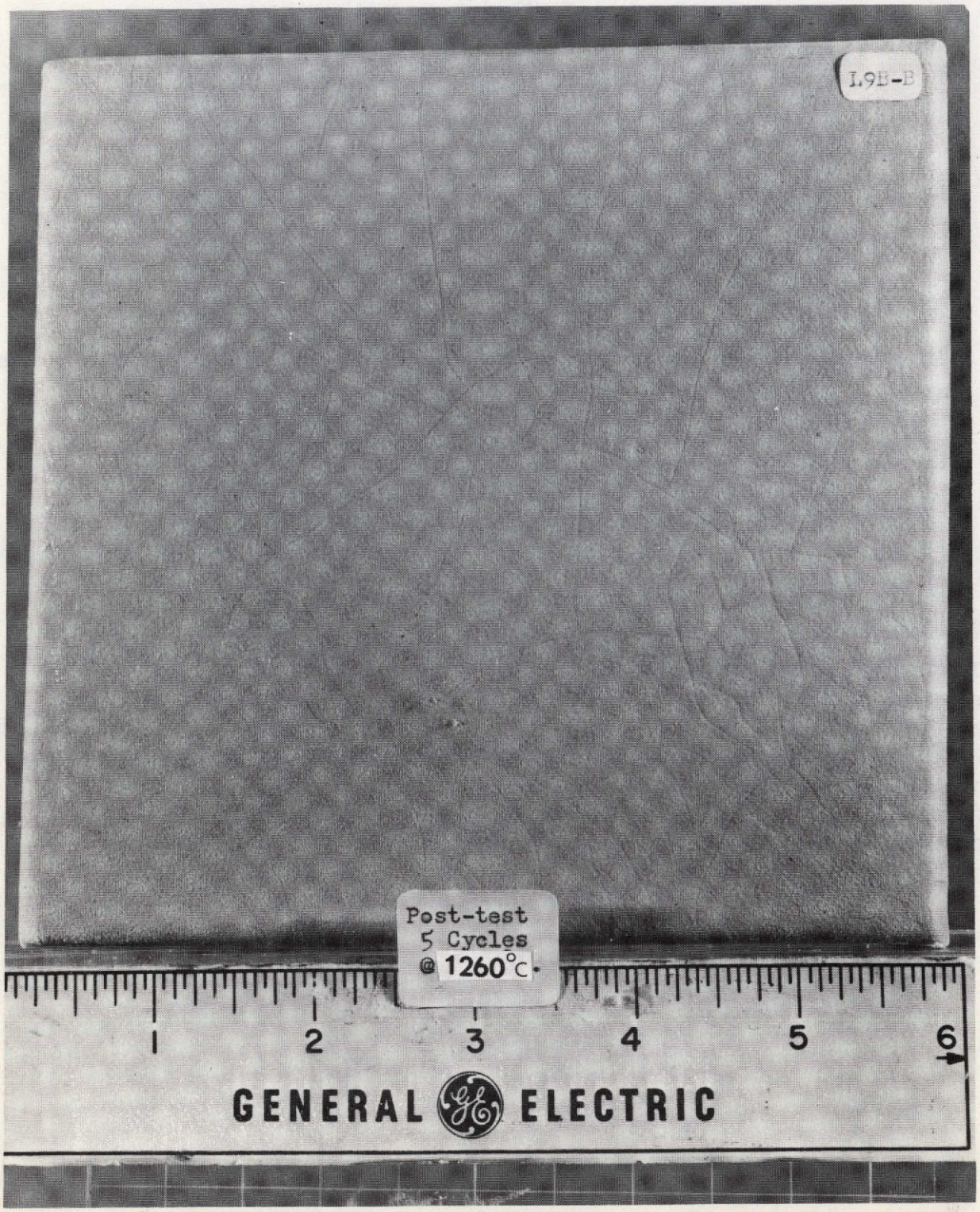

Figure 55. Original 0042 Coatings after 5 Cycles in the G.E. Re-entry Simulator

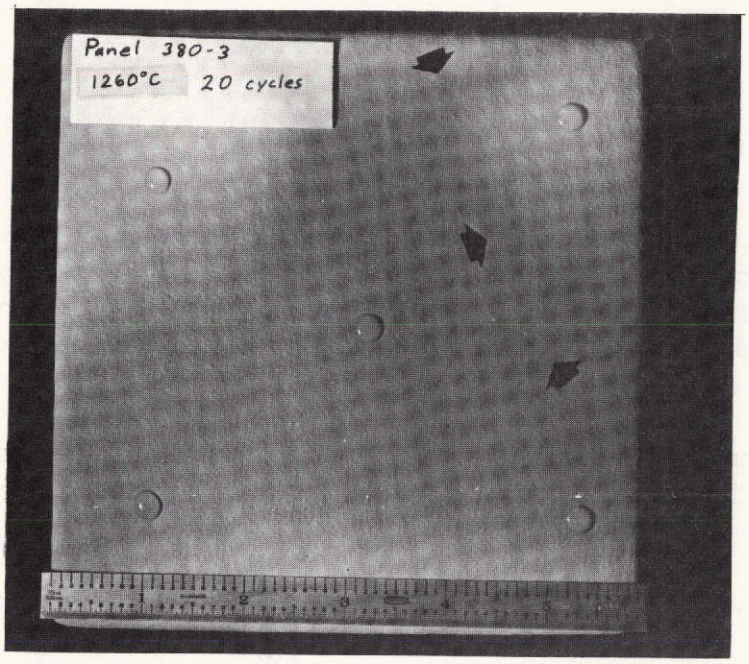

Figure 56. 0042 with Modified Densifier after 20 Cycles in G.E. Re-entry Simulator

TABLE XIV. COATING COMPOSITIONS, %

	SiO_2	B_2O_3	BPO_4	Al_2O_3	MgO	Na_2O	K_2O	Sic	CeO_2	HfB_2
0042	91.0	4		0.2	0.1	0.15	0.1	4.75		
31-D	86	5	9	Tr						
31-D-P	83.5	5	8.6	Tr				2.9		
31-D-HE	70.2	4.1	7.3	Tr				0.9	17.5	
31-D-LA	78.3	4.5	8.2	Tr						9
27-B	90	6	4	Tr						
DD-3 Mod. 2	91.0	4		0.2	0.1	0.15	0.1			4.75
PB-1	91	4		0.2	0.1	0.15	0.1		3.15	1.6

SECTION 6

CONCLUSIONS

1. Of all the coatings developed and tested in this study the PB-1 coating came the closest to meeting all of the program objectives. It is environmentally more stable and stronger than the G.E. produced 0042 coating. It also approaches the objectives of high emittance at 1100°C, low solar absorptance, and a low absorptance to emittance ratio at low temperature (40°C).

2. The addition of B_2O_3, BPO_4, and Al_2O_3 to fused silica will significantly reduce the devitrification rate at 1260°C. The most stable compounds have the following impurity levels:

    1. B_2O_3 2-4%
    2. BPO_4 8-12%
    3. Al_2O_3 0.1-1.0%

3. The degradation of a high silica coating on CRSI during thermal exposure occurs at the coating-fiber interface. Devitrification of the silica in this boundary initiates further devitrification throughout the coating which results in weakening and eventual failure.

4. Treating the surface of CRSI tile with boric acid prior to coating helps to retard devitrification at the coating fiber interface. Subsequent densification of the tile surface with a 96% SiO_2-4% B_2O_3 slip also helps.

5. Both the 31-D-P and the DD-3 coatings have improved stability to thermal aging over the G.E. produced 0042 coating. The chemical compositions of these coatings are given in Table XV.

6. Coatings with a high emittance at 1100°C and low solar absorptance are definitely possible and emittances as high as 0.8 with a white coating can be produced with an appropriate engineering effort.

7. Cerium oxide is an effective high emittance pigment when combined with the proper amounts of darkening agents such as SiC or HfB_2.

8. Hafnium diboride is a preferred darkening pigment over silicon carbide because it gives a high emittance with a slightly lower solar absorptance. More important, the HfB_2 does not react with the coating matrix to cause bloating as the SiC does. By eliminating the bloating a more dense body is formed with nearly twice the strength of a SiC pigmented coating.

9. Thermal aging of CRSI coatings at 1100°C is more severe in a vacuum than in air.

10. The G.E. re-entry simulator test has shown that definite progress has been made toward improving the thermal stability of CRSI coatings.

11. The Battelle arc tests have shown that both the PB-1 and the DD-3 coatings can withstand 100 cycles to 25-35 Btu/ ft^2-sec heat flux levels in a hypersonic flow environment. The chemical compositions of these coatings are given in Table XV.

SECTION 7

RECOMMENDATIONS FOR FUTURE WORK

1. Far more work is needed on evaluating various combinations of pigments such as CeO_2-HfB_2, CeO_2-B_2O_3, and CeO_2-HfB-B_2O_3 in a coating matrix to find a truly optimum combination of darkeners and color modifiers for the coating.

2. A fairly rigorous study of the buffering effect of boric acid on the devitrification rate of silica fibers should be undertaken. The devitrification rate of silica fibers in contact with various impurities should also be studied to gain a better understanding of how to control devitrification. A study similar to the one run in this program in Section 2.3 using fibers instead of coating precursors could be easily done and well worth the investment.

3. The possibility of making a more devitrification resistant glass should be explored. As a starting point, the chemical compositions of 31-D, JSC-0042, and Vycor glass are all known to be extremely resistant to devitrification. The 31-D material has already been fiberized from a viscous slip. Vycor could be fiberized on a commercial quartz yarn making facility, and JSC-0042 could probably be fiberized by either of these processes. A more stable fiber which is less sensitive to additional impurities than pure silica could be the solution to a great number of problems which are, no doubt, plaguing the present efforts to design a reliable CRSI system.

SECTION 8

REFERENCES

1. W. F. Horn, F. A. Hummel, "A Study of the System SiO_2-B_2O_3-P_2O_5-Al_2O_3", PhD Thesis, The Pennsylvania State University, 1973.

2. R. G. Luce, and I. M. Grinberg, "Data Summary Report on Cyclic Exposure Tests of Space Shuttle CRSI Materials", Data Report from Battelle Columbus Laboratories, February 1974.

3. "Shuttle Orbiter High Temperature Reusable Surface Insulation", GE-RESD Proposal N-72915, March 14, 1973.

4. "Improvement of Reusable Surface Insulation Material", Addendum to Final Report LMSC D266204, Process Specification for Application of Coating to Lightweight Thermal Insulation, March 1972.

The End
Sept 24, 1974